ABSTRACT

AVCI, UTKU. Electron Microscopy Complements Genetic Manipulation for Understanding Xylem Development. (Under the direction of Dr. Candace H. Haigler).

Availability of genome sequences, and gene-specific mutant collections has made genetic approaches, including gene knockout and over-expression, faster and easier ways to characterize functions of genes related to specific biological processes. Among the methods used towards identification of gene functions, electron microscopy, which requires a dedicated person and special skills, is generally neglected. This research mainly utilized electron microscopy techniques and proved how this approach can reveal key results, otherwise impossible to observe. Sample preparation of Arabidopsis for electron microscopic observation was aided by fast microwave-assisted processing of whole seedlings. This method: (a) yielded good ultrastructural preservation even with mild fixation to retain protein antigenicity in immunolabeling protocols; and (b) minimized potential artifacts of specimen handling and movement of soluble proteins.

The research focused on tracheary elements (TEs), which are the principal conductive cells of the xylem. Tracheary elements, including vessels and tracheids, function to deliver water throughout plant parts and give mechanical strength to the plant body. Tracheary elements are differentiated from procambium or vascular cambium through cell changes including secondary wall synthesis, cell suicide and autolysis. This research revealed key results in many aspects of above-mentioned differentiation process. Ultrastructural observations reported here showed the details of tonoplast implosion and a new final stage of TE autolysis. Ultrastructural details of cells and cell walls were determined upon over-expression of a transcription factor and a cellulose synthase gene.

Genetic manipulations related to three aspects of vascular cell differentiation were analyzed. First, the cellular roles of two xylem-specific cysteine proteases from *Arabidopsis thaliana*, XCP1 and XCP2, were analyzed in root primary xylem. These proteases have been hypothesized to be involved in TE autolysis, a process essential to the creation of hollow water-conducting xylem vessels. This research provided direct support for this hypothesis and new insights into TE autolysis and the cellular behavior of cysteine proteases. XCP1 and XCP2 were only detected in the cytoplasm until a late stage of differentiation when they were visualized within the central vacuole along with cellular components destined to be degraded there. Analysis of T-DNA lines showed that *xcp1* and *xcp1xcp2* TEs had cellular remnants that persisted after wild type TEs had fully cleared. Therefore, XCP1 degrades particular cellular components during TE autolysis, and, as suggested by the different appearance of cellular remnants in *xcp1* vs. *xcp1xcp2* TEs, XCP2 is likely to have a related but distinct role.

Second, the cellular role of Xylem NAC Domain1 (XND1), a transcription factor, was investigated during Arabidopsis primary xylem differentiation. XND1 is highly expressed and regulated in xylem. Over-expression of XND1 in Arabidopsis resulted in extreme dwarfism and blocked xylem differentiation. Electron microscopy showed that the incipient xylem cells failed to deposit patterned secondary walls, and they did not undergo autolysis. The phloem cells in XND1 over-expressors proliferated and had highly thickened cell walls that appeared as an exaggeration of the phloem wall structure seen in the control plants. These dwarf plants also had unusual poorly developed plastids that were frequently seen in the cortex cells.

Third, cellulose synthases (CesAs) are major, highly regulated players in cellulose biosynthesis although their exact biochemical role is still unknown. Over-expression in aspen of a previously cloned CesA gene from aspen (PtrCesA1) resulted in reduction in the amount of stem cellulose as determined chemically elsewhere. Through light and electron microscopic observations, this research showed collapse in the overall tissue of secondary xylem in over-expressors as well as reduced secondary wall birefringence in the polarizing microscope. Changes in the middle lamella and layering in the secondary wall were also detected.

ELECTRON MICROSCOPY COMPLEMENTS GENETIC MANIPULATION FOR UNDERSTANDING XYLEM DEVELOPMENT

By

UTKU AVCI

A dissertation submitted to the Graduate Faculty of

North Carolina State University

In partial fulfillment of the

Requirements for the degree of

Doctor of Philosophy

Crop Science

Raleigh, NC

2007

APPROVED BY:

Dr. Candace H. Haigler (Chair of advisory committee)	Dr. Randy Wells
Dr. Richard L. Blanton	Dr. Ralph E. Dewey

DEDICATION

I would like to dedicate this dissertation to my family for their endless support and love.

BIOGRAPHY

Utku AVCI was born in Trabzon, TURKEY on April 6th, 1979. He was raised in this small, beautiful town of the Black Sea coastline, which is located at the northeast corner of TURKEY. He earned his Bachelor of Science degree in Biology at Karadeniz Technical University in the same town in 2000. During the master education in the same department, he was offered to join Dr. Candace Haigler's lab as a PhD student. In January 2003, he started his PhD in the Department of Biological Sciences at Texas Tech University in Lubbock, TX. After one semester, he relocated to North Carolina State University with Dr. Candace Haigler and pursued his PhD degree in the Department of Crop Science.

ACKNOWLEDGMENTS

I would like to sincerely thank Dr. Candace H. Haigler, my advisor, for her guidance, and patience throughout my presence in the United States. I learned quite a lot of things from her that I will always remember and appreciate. I also wish to thank my committee members, Drs. Richard L. Blanton, Randy Wells, and Ralph Dewey. I would also like to thank our collaborators, Drs. Eric Beers at Virginia Tech and Chandrashekhar Joshi at Michigan Technological University and their labs for their great contributions.

There are a number of others I wish to thank. I am indebted to Dr. Mark Grimson at Texas Tech, manager of EM Lab, for his constant patience, support, and mentoring. He taught me the basics of electron microscopy and helped me to develop the skills that made this dissertation possible. I greatly appreciate my lab members, Drs. Bir Singh and Deshui Zhang, for their friendship and help during my education.

I would like to thank my family, my father, mother, and younger brother, for their unending support, guidance and love.

Finally, I wish to thank for financial support the NSF grant (IBM-0131386 to E.P.B. and C.H.H), and the Department of Crop Science. I would like to extend my appreciation to people who work in the Phytotron, CMIF, and Center for Electron Microscopy at North Carolina State University. During the last year of this research, the NCSU Center for Electron Microscopy also contributed instrument time free-of-charge through its small grant program.

TABLE OF CONTENTS

LIST OF TABLES

Chapter 2. Microwave-assisted Processing of Plant Samples for Electron Microscopy

LIST OF FIGURES

Chapter 2. Microwave-assisted Processing of Plant Samples for Electron Microscopy

Chapter 3. Roles of XCP1 and XCP2 Cysteine Proteases in Tracheary Element Differentiation in *Arabidopsis thaliana*

ABBREVIATIONS

cDNA	Complementary DNA
CesA	Cellulose Synthase
ER	Endoplasmic Reticulum
GUS	Beta-glucuronidase
HMGa	High-mobility Group A protein
MALDI-TOF	Matrix Assisted Laser Desorption/Ionization Time-of-Flight
mL	Milliliter
MW	Microwave
PCD	Programmed Cell Death
PCR	Polymerase Chain Reaction
rER	Rough Endoplasmic Reticulum
Rubisco	Ribulose Bisphosphate Carboxylase/Oxygenase
TB	Tris Buffer
TBS	Tris Buffered Saline
TBST	Tris Buffered Saline plus 0.05% (v/v) Tween 20
TE	Tracheary Element
TEM	Transmission Electron Microscopy
TF	Transcription Factor
W	Wattage
XCP1	Xylem-specific Cysteine Protease 1
XCP2	Xylem-specific Cysteine Protease 1
xcp1	T-DNA mutant of XCP1

xcp2	T-DNA mutant of XCP2
xcp1xcp2	Double knockout of XCP1/XCP2
XND1	Xylem NAC Domain 1
T-DNA	Transferred-DNA

CHAPTER 1

Introduction

Plant vascular system

Plant vascular tissue is a vital, continuous network of cells to transport water, minerals, and nutrients throughout the plant body. It is a complex tissue including many cell types. Xylem and phloem are major components of this system. Xylem is composed of conducting tracheary elements (TEs) and non-conducting elements such as xylem parenchyma, and it functions to store and transport water, minerals and plant hormones. Tracheary elements consist of vessels and tracheids, which are dead at maturity with thick secondary walls. Phloem is composed of conducting sieve elements and non-conducting companion cells, phloem parenchyma, and fibers, and it functions to transport solutes and the products of photosynthesis from mature leaves to sink tissues.

Vascular tissue in plants differentiates from meristematic cells of procambium and vascular cambium. During primary growth, primary xylem and primary phloem are produced from procambium cells, which are derived from root and shoot apical meristems. Plants that undergo secondary growth form secondary xylem and secondary phloem by the action of vascular cambium.

Vascular tissue represents a system to study cell specification, cell elongation, cell wall biosynthesis, pattern formation, and programmed cell death (Ye, 2002). Mechanisms involved in each area of interest are very complex and challenging. Elucidation and understanding of these mechanisms is of great importance in terms of understanding fundamental biology and economic utility of plants. For example, there is an increasing interest in alternatives to fossil fuels, gasoline and diesel. Cellulose, one of the major carbon sinks on earth, is a renewable biological material, and it is being used in bio-ethanol production through enzymatic degradation and fermentation. However, there are obstacles

and inefficiencies in this process, which requires more effective enzymes to make the process more efficient and less costly. Therefore, identification of biological mechanisms underlying cell wall biosynthesis might help solve such problems. Further, plant stress limits crop productivity, which gives rise to big economic losses. Better understanding of water, hormone, and mineral transport mechanisms facilitated by xylem might eventually lead to create solutions for crop stresses such as water stress, salt stress, and nitrogen deficiency. Enhancing mineral content in food crops would be another beneficial outcome of more research in this area.

Wood formation

Trees are characterized by the ability to form wood (secondary xylem), which is the most important natural renewable source of energy on earth and one of the most important commodities for world trade to supply material such as timber, fuel, pulp, and paper. Moreover, wood is a major sink to prevent global warming by reducing excess atmospheric CO_2. Considering the overall significance, understanding wood development is very important, but this is a demanding research area that is far from complete.

Wood is a vascular tissue to conduct water and to give mechanical strength to woody plants. It is originated from vascular cambium, a lateral meristem responsible for the formation of secondary xylem and phloem. Mainly, there are two types of cells in woody tissue: (1) fibres for mechanical support; and (2) tracheary elements, composed of tracheids (found in both gymnosperms and angiosperms) and vessels (not found in gymnosperms) for transporting water and minerals throughout the plant. As for primary xylem, cells are formed by a cascade of four major steps, which includes cell division, cell expansion, deposition of secondary walls (biosynthesis of cell wall polysaccharides, such as cellulose, and lignin), and

programmed cell death (Plomion et al., 2001). These are complex processes that are controlled by interaction of factors that are both exogenous (environmental conditions) and endogenous (hormones, genetic control mainly at the transcriptional level) (Demura and Fukuda, 2007; Plomion et al., 2001).

Research of interest

Arabidopsis provides a model for primary xylem formation and also secondary xylem formation since a true vascular cambium develops when Arabidopsis is grown at a low density and all emerging inflorescences are removed repeatedly (Busse and Evert, 1999; Dolan and Roberts, 1995; Zhao et al., 2000). Arabidopsis also has advantages of having a fully sequenced genome, small size, high fecundity with short life cycle, and easy transformation. However, it is questionable that Arabidopsis can be used as a model for a tree that fundamentally differs from herbaceous plant species. Arabidopsis has proved to be useful in this role in terms of presence of homologous genes to pine (Allona et al., 1998) and similarity of anatomical characteristics to secondary xylem in poplar (Chaffey et al., 2002). Our collaborator (Dr. Eric Beers at Virginia Tech, VA) is one of the researchers using Arabidopsis as a model system for xylem differentiation. Successful isolation of xylem and bark tissues led them to identify many xylem and phloem specific genes (Zhao et al., 2000; Zhao et al., 2005). Effects of selected candidate genes among those will be discussed in detail in Chapter 3 and Chapter 4.

Completion of the *Populus* (commonly known as poplars including aspens and cottonwoods) genome sequence attracted interest of researchers to accept *Populus* as a model woody plant in recent years. Poplar was chosen as a model tree due to its relatively small genome size (450-550 Mbp), the ease of transformation, and the ability to regenerate and

analyze transformants in a sufficiently short time (Brunner et al., 2004). Poplar also provides a woody plant model to complement resources being developed in Arabidopsis, which will bring important insights into many mechanisms in plants including wood development. Moreover, comparative biology between species will help reveal functional diversity in higher plants (Jansson and Douglas, 2007). Another collaborator (Dr. Chandrashekhar Joshi at Michigan Technological Univeristy, MI) is using aspen to study wood formation, focused on cellulose biosynthesis and production (Joshi, 2003; Bhandari et al., 2006). I studied the effect of one of the cellulose synthase genes that is over-expresssed in aspen based on microscopy techniques, which will be discussed in Chapter 5.

Electron microscopy

Availability of genome sequences and gene-specific mutant collections has made forward and reverse genetics faster and easier ways to characterize functions of genes to specific biological processes. Among the potential methods applicable to the identification of gene functions, electron microscopy, which requires dedicated person and skills, has generally been neglected. The reason is that main focus in this area was on identification of genes and their expression patterns in recent decades. Reduced interest in using electron microscopy caused fewer persons to be trained and many electron microscopy laboratories at universities to be closed. Also, typical individual research grants with relatively small budgets could not support hiring an electron microscopist. Staff in electron microscopy labs generally lacks knowledge in the specific area of research that needs to be well understood in order to interpret the results that are obtained. With the new era of stepping into identifying protein function and analyzing mutant phenotypes, development of resources with the new advanced techniques to generate reliable results in the area of transmission electron

microscopy (TEM) has become necessary to allow researchers to access this powerful and unique tool in order to understand gene and protein function in the cellular and developmental context. Cryogenic fixation and microwave-assisted chemical fixation methods appeared as new advanced techniques with great usefulness (Newman and Hobot, 1993; Giberson and Demaree, 2001). Therefore, poor fixation quality and elimination of artifacts that occurs during conventional chemical fixation (Heumann, 1992) are no longer a problem. Optimization of microwave-assisted chemical fixation and processing methods for TEM helped observe cell structure and protein localization in a reliable manner. Utilization of electron microscopy techniques proved how electron microscopy could reveal key results, otherwise impossible to be unveiled with the other approaches.

References

Allona I, Quinn M, Shoop E, Swope K, Cyr SS, Carlis J, Riedl J, Retzel E, Campbell MM, Sederoff R, Whetten RW (1998) Analysis of xylem formation in pine by cDNA sequencing. Proceedings of the National Academy of Sciences of the USA 95: 9693–9698.

Bhandari S, Fujino T, Thammanagowda S, Zhang D, Xu F, Joshi CP (2006) Xylem-specific and tension stress-responsive coexpression of KORRIGAN endoglucanase and three secondary wall-associated cellulose synthase genes in aspen trees. Planta 224: 828-837.

Brunner AM, Busov VB, Strauss SV (2004) Poplar genome sequence: functional genomics in an ecologically dominant plant species. Trends in Plant Science 9: 49-56.

Busse JS, Evert RF (1999) Pattern of differentiation of the first vascular elements in the embryo and seedling of *Arabidopsis thaliana*. Int J Plant Sci 160: 1-13.

Chaffey N, Cholewa E, Regan S, Sundberg B (2002) Secondary xylem development in *Arabidopsis*: a model for wood formation. Physiol Plant 114: 594-600.

Demura T and Fukuda H (2007) Transcriptional regulation in wood formation. Trends in Plant Science 12: 1360-1385.

Dolan L, Roberts K (1995) Secondary thickening in the roots of *Arabidopsis thaliana*: anatomy and cell surfaces. New Phytol 131: 121-128.

Giberson RT, Demaree RS (2001) Microwave techniques and protocols. Humana Press, New Jersey.

Heumann, HG (1992) Microwave stimulated glutaraldehyde and osmium tetroxide fixation of plant tissue: ultrastructural preservation in seconds. Histochemistry 97: 241-347.

Jansson S, Douglas CJ (2007) *Populus*: a model system for plant biology. Annu Rev Plant Biol 58: 435-458.

Joshi CS (2003) Xylem-specific and tension stress-responsive expression of cellulose synthase genes from aspen trees. Appl Biochem Biotechnol 105:17-26.

Newman GR, Hobot JA (1993) Resin microscopy and on-section immuno-chemistry. Springer-Verlag, NY, p. 7-14.

Plomion C, Leprovost G, Stokes A (2001) Wood formation in trees. Plant Physiol 127: 1513-1523.

Ye ZH (2002) Vascular tissue differentiation and pattern formation in plants. Annu Rev Plant Biol 53: 183-202.

Zhao C, Johnson BJ, Kositsup B, Beers EP (2000) Exploiting secondary growth in Arabidopsis. Construction of xylem and bark cDNA libraries and cloning of three xylem endopeptidases. Plant Physiol 123: 1185-1196.

Zhao C, Craig JC, Petzold HE, Dickerman AW, Beers EP (2005) The xylem and phloem transcriptomes from secondary tissues of the Arabidopsis root-hypocotyl. Plant Physiol 138: 803-818.

CHAPTER 2

Microwave-assisted Processing of Plant Samples for Electron Microscopy

Introduction

Fixation

One of the most important steps towards observing a given sample under the microscope is killing and preserving the tissue in its native state as much as possible. Fixation can occur in two ways: (1) stabilization of tissues by chemical cross-linking with use of chemical fixatives; and (2) immobilization of tissues by freezing, which is called cryofixation. Chemical fixation, cryofixation, and microwave-assisted chemical fixation are the main methods used in today's microscopic research and each fixation method has its limitations and advantages.

Chemical fixation

Chemical fixation, the oldest and most commonly used fixation method, requires fixatives to diffuse through tissue and stabilize cell components. For example, glutaraldehyde is known as a strong protein cross-linker and is desirable for structural analysis. However, high concentration of glutaraldehyde often destroys antigenicity (Newman and Hobot, 1993). All chemical fixatives have disadvantages in preserving the tissue: (1) cross-linking of cellular components may reduce or remove antigenicity; and (2) extraction of soluble components and damage to membranes may occur (Newman and Hobot, 1993). All these changes can lead to distortion of cellular structure and movement of proteins from their original location.

Cryofixation

Cryotechniques, which are methods to prevent the above-mentioned problems in chemical fixation, are used to freeze tissues rapidly. Because of nearly instant freezing that minimizes ice crystal formation, structure and antigenicity can be preserved very well.

However, the downside is that tissue samples to be fixed should be much smaller and thinner compared to chemical fixation (Newman and Hobot, 1993). Even though cryogenic methods provide excellent results, they require dissection of tissues, are slow, often rely on expensive equipment, and are not applicable to cells deep within tissues because of the limited depth of fast freezing, which is up to 50 micrometers with plunge freezing (Galway et al., 1995) and up to 200 micrometers with high pressure freezing (Moor, 1987).

Microwave-assisted fixation and processing of plant samples

Microwaves (MWs) are a form of non-ionizing radiation with the standard frequency of 2.45 GHz and a wavelength of 12.2 cm. Microwave-based fixation, which is often used in the medical sciences, occurs through synergistic action of: (a) the brief pulse of microwave energy that makes polar molecules oscillate at about a billion cycles per second; (b) the effects of mild heating (generally 25-45 °C); and (c) increased chemical diffusion rates. This method has been used with excellent results in animals and also significantly reduces the processing time in plant systems and tissues compared to traditional methods (Giberson and Demaree, 2001).

Specimen preparation techniques for electron microscopy are always a critical step in obtaining good quality samples worthy of analysis. Plant material is known to be especially hard to fix and process compared to that of animals since most plants have a protective epidermis that is often waxy, intercellular air spaces, and cells with thick walls; all of these factors slow the penetration of fixative into tissue (Russin and Trivett, 2001). Plant cells also usually have a vacuole and plastids containing appreciable volume of fluid. Thus, release of their contents during processing can also affect fixation by locally diluting the fixative solution and shifting pH. The plant vacuolar membrane is easily disrupted by chemical

fixation (Heumann, 1992; Haigler and coworkers, unpublished). Traditional chemical fixation and embedding usually result in distortion of *in vivo* ultrastructure and substantial movement and extraction of soluble components (Mersey and McCully, 1978; Gilkey and Staehelin, 1986; Benhamou et al., 1991). Such changes would likely allow soluble proteins to diffuse into the cytoplasm or out of the cell, which is an unwanted situation for any kind of study.

In contrast, plant materials fixed in the presence of microwave energy have shown excellent structural preservation and also exhibited greater antigenicity in tissues used for immunolocalization (Giberson and Demaree, 2001). It has been shown that microwave-based chemical fixation reduces vacuolar rupture, preserves the location of soluble proteins and small peptides, and increases the intensity of immunolabeling (Benhamou et al., 1991; Giberson and Demaree, 2001; Leria et al., 2004; Kok and Boon, 1992; Jamur et al., 1995). Because of increased diffusion rates during brief microwave exposure, blocks ready to section can be prepared from live material within a couple of hours using microwave-assisted protocols for fixation, dehydration, and embedding. Therefore, many sequential tests to optimize protocols are possible in a short time. In addition, tissue blocks up to 1 cm thick can be fixed with good quality (Kok and Boon, 1992), so specimen dissection can be minimized or eliminated. The results reported here show, after optimization of the microwave-assisted protocol, good ultrastructural and antigenic preservation within Arabidopsis seedlings that were fixed intact immediately after removal from their growing environment.

Materials and Methods

Microwave-assisted chemical fixation

Except for results in Chapter 5, all other results in this dissertation were based on microwave-assisted chemical fixation. All steps that require microwave (MW) energy for processing were aided by a PELCO Biowave, Model 34700, MW system (Redding, CA), which is characterized by a high level of control of MW energy via true variable wattage control, an integrated vacuum system, and a probe to be inserted into the sample to restrict sample temperature. This system permits precise temperature control, which prevents any heat related damage to the samples under investigation. Protocols for both immunocytochemistry and ultrastructural observations were optimized as shown in Table 1 and Table 2, respectively. Required times in each step can be adjusted for any tissue depending on its thickness and cellular characteristics.

The PELCO ColdSpot accessory was always in use during microwave processing. This device serves as the water load and processing surface for the samples inside the microwave. Water is circulated between the PELCO ColdSpot and the Load Cooler that is an integrated part of the microwave to cool down the water. The water load dissipates the microwaves evenly throughout oven and prevents development of any hot spots.

The dedicated laboratory-grade microwave also allows temperature to be regulated during microwave exposure, which avoids “cooking” the specimen. In this research, temperature was restricted to 30°C during fixation steps and 37°C during infiltration steps. For this purpose, the integrated temperature probe was inserted in a blank sample during fixation and infiltration steps so that if the temperature set was exceeded, the magnetron was

turned off automatically. Due to low microwave time in dehydration and wash steps, the use of temperature probe could be omitted during those procedures.

The PELCO Microwave Vacuum Chamber was used during fixation and infiltration. It was set to 20 inches of Hg. The vacuum applied along with microwave energy reduced fixation and resin infiltration times. Vacuum is generally applied to remove air in intercellular spaces of plants in order to ease fixation. In infiltration steps, the vacuum helps the resin penetrate into tissue more quickly and uniformly.

Ice may be used in fixation and infiltration steps, but no significant difference was observed in terms of quality of fixation. In the case of increase in microwave time for the fixation of thicker tissues, ice might be helpful to hinder the temperature from rising above the temperature set point during microwave exposure.

For small samples such as Arabidopsis seedlings, 2 mL microcentrifuge tubes were used with about 600 µl volume of each solution. For bigger samples, 20 mL glass scintillation vials could be used with a solution volume sufficient to cover samples. Many samples can be processed in parallel within the size limit of the vacuum chamber, with the exact number depending on what kind of vessel is in use for holding samples. Caps of tubes and vials were removed during microwave exposure.

Plant material

Seeds of *Arabidopsis thaliana* (Columbia) were incubated on moist filter paper in Petri dishes (24 h, 4°C) then germinated and grown for 1.5-2 d (continuous fluorescent light, 25°/20°C, and 16h/8h day/night cycle). Some cold-treated (3-4 d, at 4°C in distilled water) seeds are transferred onto soil (Pro-Mix, Premier Horticulture Inc., PA) and grown at approximately 200 µmol m^{-2} s^{-1} light intensity with a 16h/8h day/night cycle at 20 – 22 °C.

Leaves from 1 month-old plants were harvested and processed for immunolabeling of Rubisco.

Over 10 wild-type samples were sectioned for the purpose of observing TE differentiation in Arabidopsis. Many (over 100) sequential sections were taken from the root of each sample. Figures that show the progression of TE differentiation in this chapter are representatives of repetititons and same stages were similarly observed in repetition.

Immunocytochemical labeling

For immunolabeling studies, the use of osmium and high concentration of glutaraldehyde was avoided due to loss of antigenicity. Small amounts of glutaraldehyde (0.2% v/v) added to formaldehyde resulted in better tissue integrity without reducing immunolabeling density. Addition of 1.5% potassium ferricyanide to the secondary osmium fixation resulted in better contrast of membranes. After infiltration in resin (Spurr's for ultrastructure and LR White for immunolocalization), samples were flat-embedded between two slides coated with the liquid releasing agent (Salnikov et al., 2003). Spurr's was heat-polymerized (50°C, overnight) and LR White was polymerized by UV light (4°C, 2 d). Sections were made with a diamond knife on an ultramicrotome (MT2-B, Sorvall), and then stained with 2% uranyl acetate (aq. or in 70% ethanol for immunolabeling and ultrastructure, respectively) for 15 minutes and lead citrate (Reynolds, 1963) for 4 minutes in humid Petri dishes (including sodium hydroxide pellets to trap CO_z during lead citrate staining) before observation in the transmission electron microscope (JEOL 100S). Negatives were scanned at high resolution (Epson 4870 scanner) and Canvas 9 software was used for the preparation of digital plates.

Basic solutions used were: Tris buffer (TB) that refers to 20 mM Tris-buffer, 0.02% azide, pH 8.2; Tris buffered saline (TBS; TB plus 150 mM NaCl, pH 7.5); and TBST (TBS plus 0.05% (v/v) Tween 20). TB was used to minimize gold aggregation and background. Thin sections collected on nickel grids were: (a) blocked (30 min, RT, high humidity chamber) in TBST plus 5% normal goat serum (Sigma S-2007) and 0.1 M Glycine; (b) incubated (overnight, 4°C) in TBST with 5% goat serum and primary antibody, either 1:10 anti-HMGa antisera or 1:1000 Rubisco antibody; (c) washed 3x by dipping grids in TBS; (d) incubated (1 h RT) in TB plus 0.06% bovine serum albumin and 1:50 goat anti-rabbit secondary antibody coupled to 10 nm colloidal gold (AuroProbe, Amersham Biosciences, Piscataway, NJ) for Rubisco and 15 nm gold for HMGa; and (d) washed in TB then distilled water. Anti-HMGa antisera (donated by Dr. Steven Spiker, North Carolina State University, Raleigh) was used to localize a nuclear protein (Spiker and Everett, 1987). Anti-Rubisco was donated by Dr. James Moroney, Louisiana State University (Borkhsenious et al., 1998).

Results and Discussion

Advantages and quality of microwave-assisted processing

The microwave-assisted methods allowed us to significantly reduce processing times compared to chemical fixation methods, which can take days, along with the good preservation of cellular structure and antigenicity.

Experience with all Arabidopsis organs showed that good quality results could be achieved most of the time (over 90%) in all tissues except in the differentiation zone behind the root tip. This zone consists of many cells with different natures that are destined for special tasks. Assuming each cell has its own properties, fixative and buffer concentrations should be optimized for the specific cell of interest. Fixative and buffer concentrations used

here gave good results in differentiating TEs, which was the target of the research. However, other cells within the differentiating stele sometimes (less than 30%) showed signs of plasmolysis or lack of good preservation. Adjusting the osmotic concentration of the fixative and buffer is expected to overcome such problems when they occur.

Cytoskeletal elements such as microtubules and Golgi stacks are difficult to fix while retaining their native structure. The microwave-assisted ultrastructural method yielded intact, straight, clearly defined microtubules with similar quality (Fig. 1 a) to those observed with the cryofixation technique (Fig. 1 b) (Salnikov et al., 2003). Golgi stacks were observed with closely stacked cisternae (Figure 1 c), and again their quality was similar to ones processed through cryofixation (Fig. 1 d).

Figure 2 shows images from several tissues of Arabidopsis processed with the microwave-assisted method allowing immunocytochemistry. Overall, all samples were preserved with great quality. Vacuolar integrity (as shown by its rounded profile) and plastids (with no distortion and swelling) were well demonstrated in a cotyledon (Fig. 2 a). There was no sign of plasmolysis (as indicated by separation of the cytoplasm and cell wall), and the intercellular space and vacuolar membranes were undistorted (Fig. 2 b). Even cells with very thick walls could be fixed with success, which can be seen in a cross section of trichome with interesting cell wall architecture (Fig. 2 c). A chloroplast and the nucleus showed good internal detail in a 1-month Arabidopsis leaf (Fig. 2 d), confirming the overall quality of the microwave-assisted protocol in different tissues.

Immunolabeling efficiency of the method

The standard methods of tissue fixation for post-embedding immunocytochemical localization recommend avoiding osmium tetroxide as a secondary fixative. High

concentration of glutaraldehyde is also not recommended for soluble proteins because of the ability of the fixative to modify secondary structure of proteins (Newman and Hobot, 1993). Glutaraldehyde and secondary fixation step with osmium can be eliminated for immunocytochemical studies (Giberson and Demaree, 2001). In place of glutaraldehyde, formaldehyde is the choice for a fixative that does not prevent access of antibodies to epitopes of interest. The downside of the use of formaldehyde is that preservation of tissues is not as good as in tissues fixed with glutaraldehyde or a high concentration glutaraldehyde plus formaldehyde mixture. On the other hand, addition of low concentration of glutaraldehyde (0.1-0.2% v/v) to formaldehyde helped to better preserve tissue integrity without affecting antigenicity. Figure 3 shows the success of the microwave-assisted technique for immunolabeling of two proteins: (a) HMGa, a nuclear protein; and (b) Rubisco, an enzyme in the Calvin cycle, which catalyzes the first major step of carbon fixation. Both proteins were localized at their original sites.

New findings on differentiating tracheary elements by use of microwave-assisted fixation and processing

Microwave-assisted processing of Arabidopsis seedlings made interesting observations possible on TE differentiation. As seen in Figure 4, fixation quality was good, revealing microtubules (arrowheads in Fig. 4), known to be hard to preserve. Two central vacuoles in the process of merging showed intact tonoplasts. Dividing mitochondria above vacuoles and a multivesicular body (arrow) can also be seen in Figure 4.

Details of TE differentiation will be discussed in the next chapter. Figures 5 through 12 show TE differentiation captured in several stages from an incipient TE to a dead TE. Microwave-assisted processing allowed us to observe each developmental stage and to

compare them with the known information in the literature. The progression of TE differentiation in young Arabidopsis roots had similarities and differences compared to reports in the literature as detailed in Table 3. Our observations, summarized in the column 'Arabidopsis *in vivo*', were compared to the data obtained in *Zinnia elegans in vitro* and a variety of other plants previously studied *in vivo*. The *Zinnia* in vitro system perhaps has some unique characteristics since it is a culture system where mesophyll cells are induced to trans-differentiate into TEs in the presence of phytohormones. Our observations mainly coincide with the ones made on corn and pine TEs. Increase in the number of organelles such as endoplasmic reticulum (ER), mitochondria and Golgi was seen in the very early stages of TEs (Fig. 5 and 6). Many Golgi vesicles and small vacuoles in the cytoplasm have been observed. In later stages, the big central vacuole, which arises from fusion of smaller ones, occupied most of the cell (Fig. 7). At the onset of bulk autolysis, the vacuole collapsed inward and the tonoplast broke down (Fig. 8), resulting in all the cell contents mixing together. ER and Golgi were swollen, and mitochondria and ER persisted longest (Fig. 10). Autolysis of cell contents ended with fine fibrous material occupying the entire cell before the TE becomes completely empty (Fig. 11). Finally, the empty TE was functional for water transport (Fig. 12).

In *Zinnia*, rapid collapse of the vacuole (inward) was observed after completion of secondary wall synthesis (Groover et al., 1997). However, this observation was not based on electron microscopy and was also not mentioned in other *in vivo* studies. In this research, implosion of the vacuole was captured and inward collapse of the tonoplast membrane was observed (Fig. 8). Fibrous material, which was seen just before empty TEs appeared, should be a new stage of TE differentiation in plants and not be specific to Arabidopsis since all

other stages were previously discussed in the literature. Similar fibrous material was observed in differentiating xylem of minor veins of *Mimosa pudica* L. leaf, where fibrous material is attributed to being the product of dilated ER cisternae without much information related to progression of TE differentiation (Esau, 1975). However, it is known that dilated cisternae occur as a result of virus infection (Lynn, 1975; Nagano et al., 2005; Zechmann et al., 2005), and plant stress (Matsushima et al., 2002). Moreover, dilated ER cisternae were not observed during TE differentiation in our research. Similarly, neither fibrous material nor dilated cisterane during TE differentiation were observed in other studies (Srivastava and Singh, 1972; Cronshaw and Bouck, 1965).

Therefore, we believe that this is the first time that fibrous material in the autolyzing TE has been authentically associated with the progression of normal TE differentiation. Microwave-assisted chemical fixation, which allowed us to fix and process tissues quickly with minimal disturbance and handling, might be one of the reasons that we observed this last event. In addition, the relatively small Arabidopsis root allowed us to take many serial sections passing through all stages of TE differentiation, which might be impractible or very hard in other plants studied such as corn and pine (Srivastava and Singh, 1972; Cronshaw and Bouck, 1965). We hypothesize that this fibrous material could be a product of final primary cell wall degradation in the TE, which should be further investigated.

Summary

In the functional genomics era, it is important to have an efficient and accurate means of determining the location of proteins within cells at high resolution. Chemical specimen preparation methods for immunolocalization in the electron microscope are time-consuming and often result in poor ultrastructural preservation and substantial movement and extraction

of soluble proteins. In contrast, the results reported here demonstrate that MW-assisted processing of whole plant tissues, requiring approximately 35 min processing time for immunolabeling (Table 1), allows successful localization of antigens, and that those antigens were retained in their original cellular locations.

The results obtained with microwave-assisted fixation approached the quality of those from cryofixation. High quality cryofixation for immunolabeling is limited to cells near the tissue surface, and the subsequent freeze substitution and embedding can require up to 3 weeks to achieve good infiltration of plant tissues (Moor, 1987). Another advantage of the MW protocols is that many variations of fixation can be tested over a short time and very small quantities of chemicals can be used.

References

Benhamou N, Noel S, Grenier J, Asselin A (1991) Microwave energy fixation of plant tissue: an alternative approach that provides excellent preservation of ultrastructure and antigenicity. J Electron Microsc Tech 17: 81-94.

Borkhsenious ON, Mason CB, Moroney JV (1998) The intracellular localization of ribulose-1,5-bisphosphate carboxylase/oxygenase in *Chlamydomonas reinhardtii*. Plant Physiol 116: 1585-1591.

Burgess J, Linstead P (1984a) *In-vitro* tracheary element formation: structural studies and the effect of tri-iodobenzoic acid. Planta 160: 481-489.

Cronshaw J, and Bouck GB (1965) The fine structure of differentiating xylem elements. J Cell Biol 24: 415-431.

Dolan L, Janmaat K, Willemsen V, Linstead P, Poethig S, Roberts K, Scheres B (1993) Cellular organization of the *Arabidopsis thaliana* root. Development 119:71-84.

Esau K (1975) Dilated endoplasmic reticulum cisternae in differentiating xylem of minor veins of *Mimisa pudica* L. leaf. Ann Bot 39: 167-174.

Galway M, Heckman J, Hyde G, Fowke L (1995) Advances in high pressure and plunge freeze fixation. In: Methods in Cell Biology, Vol 49. Methods in Plant Cell Biology, Part A. DW Galbraith, HJ Bohnert and DP Bourque, eds. Academic Press, New York, pp 3-19.

Giberson RT, Demaree RS (2001) Microwave techniques and protocols. Humana Press, New Jersey.

Gilkey JC, Staehelin LA (1986) Advances in ultrarapid freezing for the preservation of cellular ultrastructure. J Electron Microsc Tech 3: 177-210.

Groover A, DeWitt N, Heidel A, Jones A (1997) Programmed cell death of plant tracheary elements differentiating in vitro. Protoplasma 196: 197-211.

Heumann, HG (1992) Microwave stimulated glutaraldehyde and osmium tetroxide fixation of plant tissue: ultrastructural preservation in seconds. Histochemistry 97: 241-347.

Jamur MC, Faraco CD, Lunardi LO, Siraganian RP, Oliver C (1995) Microwave fixation improves antigenicity of glutaraldehyde-sensitive antigens while preserving ultrastructural details. J Histochem Cytochem 43: 307-311.

Kok LP, Boon ME (1992) Microwave cookbook for microscopists: Art and Science of Visualization 3rd edition. Columb Press Leyden: Leiden. 432 pp.

Leria F, Marco R, Medina FJ (2004) Structural and antigenic preservation of plant samples by microwave-enhanced fixation, using dedicated hardware, minimizing heat-related effects. Microsc Res Tech 65:86-100.

Lynn LH (1975) Tubules in dilated cisternae of endoplasmic reticulum of *Thlaspi arvense* (Cruciferae). Amer J Bot 62: 756-760.

Matsushima R, Hayashi Y, Kondo M, Shimada T, Nishimura M, Hara-Nishimura I (2002) An endoplasmic reticulum-derived structure that is induced under stress conditions in Arabidopsis. Plant Physiol 130:1807-1814.

Mersey B, McCully ME (1978) Monitoring of the course of fixation of plant cells. J Microsc 114: 49-76.

Moor H (1987) Theory and practice of high-pressure freezing. In: Cryotechniques in Biological Electron Microscopy, eds Steinbrecht R A and Zierold K, pp. 175–191 (Springer-Verlag, Berlin).

Nagano AJ, Matsushima R, Hara-Nishimura I (2005) Activation of an ER-body-localized beta-glucosidase via a cytosolic binding partner in damaged tissues of *Arabidopsis* thaliana. Plant Cell Physiol 46: 1140-1148.

Newman GR, Hobot JA (1993) Resin microscopy and on-section immuno-chemistry. Springer-Verlag, NY, p. 7-14.

Reynolds ES (1963) The use of lead citrate at high pH as an electron-opaque stain in electron microscopy. J Cell Biol 17: 208-212.

Russin WA, Trivett CL (2001) Vacuum-microwave combination for processing plant tissue for electron microscopy. In: Microwave Techniques and Protocols, R.T. Giberson and R.S. Demaree Jr, eds., Humana Press: Totowa, NJ, p. 25.

Salnikov V, Grimson MJ, Seagull RW, Haigler CH (2003) Localization of sucrose synthase and callose in freeze substituted, secondary wall stage, cotton fibers. Protoplasma 221: 175-184.

Spiker S, Everett KM (1987) Blotting Index of Dissimilarity: Use to study immunological relatedness of plant and animal high mobility group (HMG) chromosomal proteins. Plant Mol Biol 9:431-442.

Srivastava LM, Singh AP (1972) Certain aspects of xylem differentiation in corn. Can J Bot 50: 1795-1804.

Zechmann B, Muller M, Zellnig G. (2005) Effects of different fixation and freeze substitution methods on the ultrastructural preservation of ZYMV-infected Cucurbita pepo (L.) leaves. J Electron Microsc 54: 393-402.

Table 1. Microwave-assisted method for immunolocalization

Step	Time	Wattage (W) (±5%)	Vacuum[b]
1. Formaldehyde fixation[a]	3 min on/1 min off (3x) 20 s on/20 s off (6x)	150 650	Yes Yes
2. Buffer Rinse	1 min (3x)	250	No
3. Dehydration (30, 50, 70, 90, 100% Ethanol)	40 s each	250	No
4. Resin Infiltration 1:1 LR White:ethanol 100% LR White	 3 min 3 min (3x)	 250 250	 Yes Yes
Total time	~ 35 min		

[a]4% or 2% EM-grade formaldehyde (v/v) (LADD research) plus 0.2% glutaraldehyde (optional) in 20 mM sodium cacodylate buffer, pH 7.2.
[b]Vacuum was 67537 Pascal supplied by the microwave oven.

Table 2. Microwave-assisted method for ultrastructural observations

Step	Time	Wattage (W) (±5%)	Vacuum[b]
1.Primary fixation[a]	3 min on/1 min off (3x) 20 s on/20 s off (6x)	150 250	Yes Yes
2. Buffer Rinse	1 min (3x)	250	No
3. Secondary fixation[b]	2 min on/2 min off (3x)	150	No
4. Buffer Rinse (Optional)	1 min (2x)	250	No
5. Dehydration (30, 50, 70, 90, 100% Acetone)	40 s each	250	No
6. Resin Infiltration 1:3 Spurr's resin: acetone 1:1 Spurr's resin: acetone 3:1 Spurr's resin: acetone 100% Spurr's resin	 3 min 3 min 3 min 3 min (3x)	 250 250 250 250	 Yes in all steps
Total time	~ 1 hour		

[a]2.5% glutaraldehyde (v/v) in 50 mM sodium cacodylate buffer, pH 7.2.
[b]1% osmium and 1.5% potassium ferricyanide (w/v) in the same buffer.
[c]Vacuum was 67537 Pascal supplied by the microwave oven.

Table 3. Comparison of TE differentiation

	Zinnia *in vitro*	**Arabidopsis *in vivo***	**Other *in vivo***
Young TEs with no secondary walls	Highly vacuolated with chloroplasts containing starch. Not much cytoplasmic specialization (Burgess and Linstead, 1984a).	Increase in the rER, mitochondria and Golgi. Many Golgi vesicles have been observed. Small vacuoles in cytoplasm have been observed. In the later stages, big central vacuole occupies most of the cell as a result of fusing small vacuoles into the big one as indicated on other systems.	Incipient TEs are marked by many small vacuoles, proliferating mitochondria, increase in ER, polyribosomes and Golgi with numerous vesicles (Cronshaw and Bouck, 1965, Srivastava and Singh, 1972). Fusion of small vesicles to form a large vacuole is one of the earliest changes in TEs (Srivastava and Singh, 1972). Many Golgi vesicles with two types of vesicles are observed. Young xylem cells have several small vacuoles that expand as the cell differentiate and finally may fuse together to form a large vacuole (Cronshaw and Bouck, 1965).
TEs with ongoing secondary wall deposition	The cytoplasm becomes less dense in appearance, most likely through the action of confined hydrolysis by small vesicles called autophagic vacuoles (Groover et al., 1997).	High Golgi activity continues with many vesicles. Several mitochondria have been observed. ER is swollen. The vacuole occupies most of the cell. Clearing of the cytoplasm was not seen prior to vacuole collapse, dense cytoplasm persists before vacuole collapse.	High Golgi activity and vesicle production continues (Srivastava and Singh, 1972). The amount of ER and Golgi increase during the deposition of cell wall. The cellulose thickenings appear to have reached their full dimension before any degeneration of cytoplasm occurs (Cronshaw and Bouck, 1965).
Vacuole Collapse And Final Events	Rapid collapse of the vacuole (inward) occurring after completion of secondary wall synthesis, which leads to complete degradation of cytoplasmic components involving swelling and rupture of organelles (Groover et al., 1997).	Vacuole collapse happens and the tonoplast breaks down. All cell contents mix together. Golgi swell. Mitochondria and ER persist longest. Mitochondria degeneration can be observed in its matrix. Autolysis of cell contents ends with fine fibrous material occupying the entire cell. Finally TEs become empty and functional for water transport.	Following the deposition of secondary wall, degeneration of the cytoplasm starts with a breakdown of the vacuolar membrane. The last components to persist are the cisternae of rER and the mitochondria. Disorganization of mitochondria and breakdown of ER into vesiculate structures before their loss was reported (Cronshaw and Bouck, 1965).

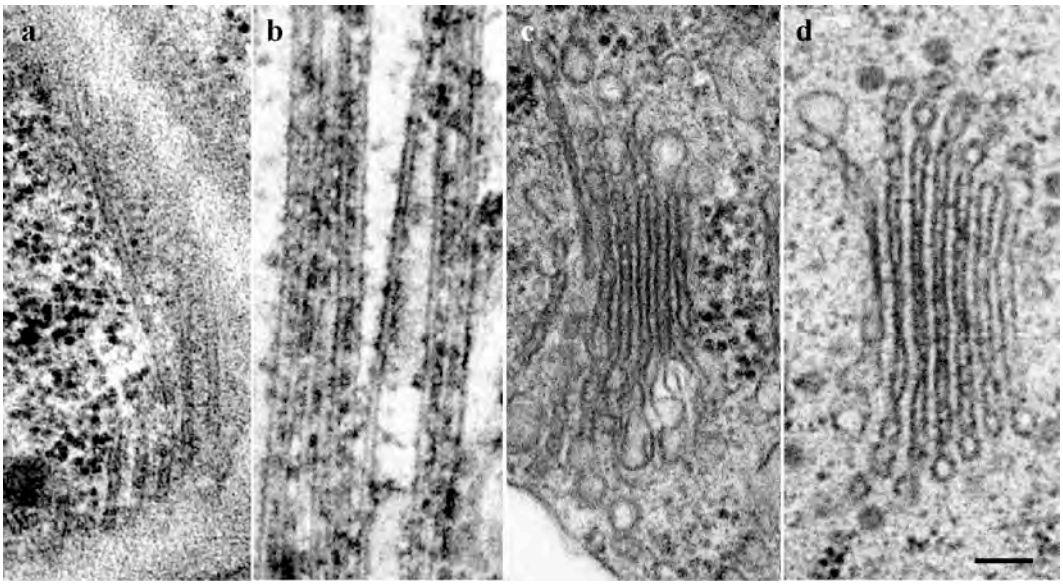

Figure 1. Transmission electron micrographs comparing microwave-assisted chemical fixation (ultrastructural protocol) and cryofixation. Results of microwave-assisted chemical fixation of Arabidopsis (a,c) are shown for the corner of a TE cell in (a) and a part of central root tip cell in (c). Published results for cryofixation of cotton fiber are shown in (b, d) (Salnikov et al., 2003). Non-collapsed microtubules are visible in both (a) and (b), and well-organized Golgi with closely stacked cisternae are visible in both (c) and (d). Therefore, microwave-assisted protocols can produce ultrastructural results similar to cryofixation. Bar = 100 nm for all images.

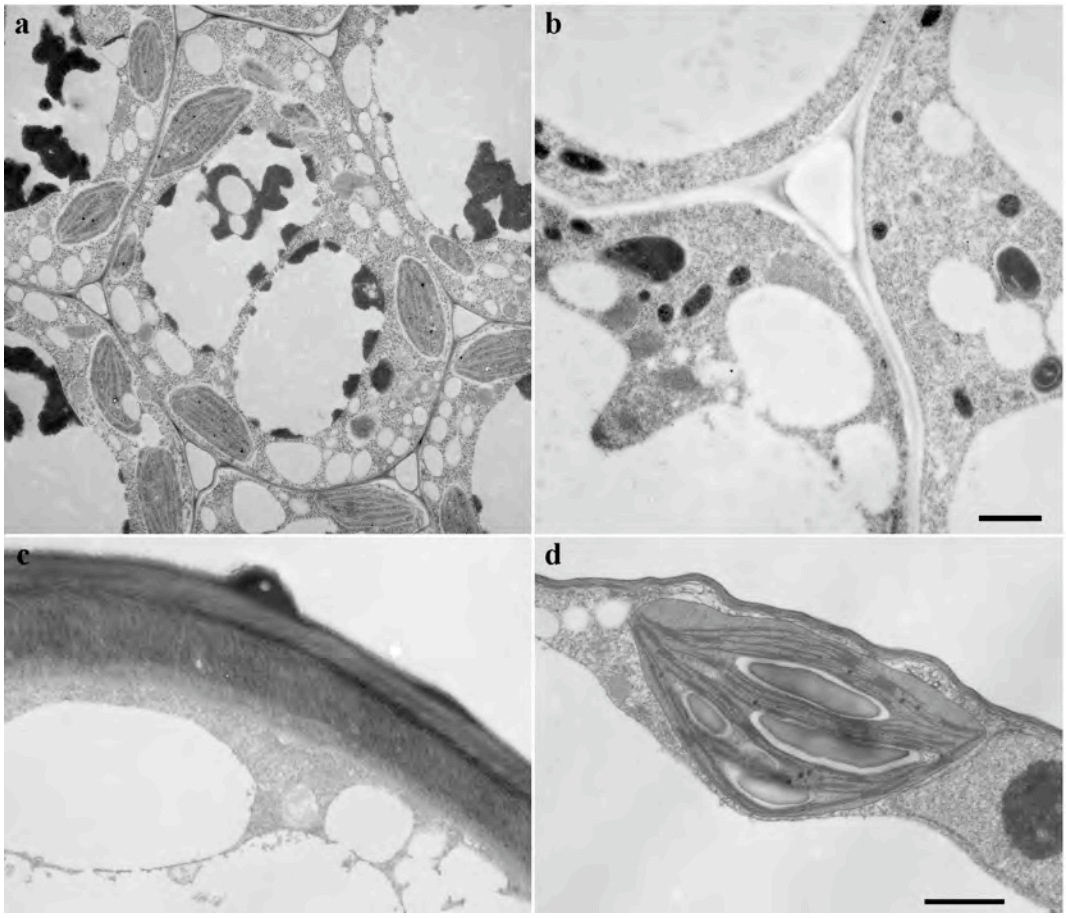

Figure 2. Transmission electron micrographs obtained after microwave-assisted processing for immunochemistry (a, b) and ultrastructure (c, d) in several tissues of Arabidopsis. A cotyledon cell (a) showed well-preserved vacuoles, plastids, and overall cell integrity. In the cortex of the root, an intercellular space, and the middle lamella separating three cells (b) were well-preserved. There was no plasmolysis and the rounded vacuoles reflected their living turgid state. A cross-section of a trichome in a newly emerging leaf showed interesting cell wall characteristics (c). In a mature leaf, a chloroplast and nucleus were well-preserved. All bars = 1 μm and bars in (b) and (d) also apply to (a) and (c), respectively.

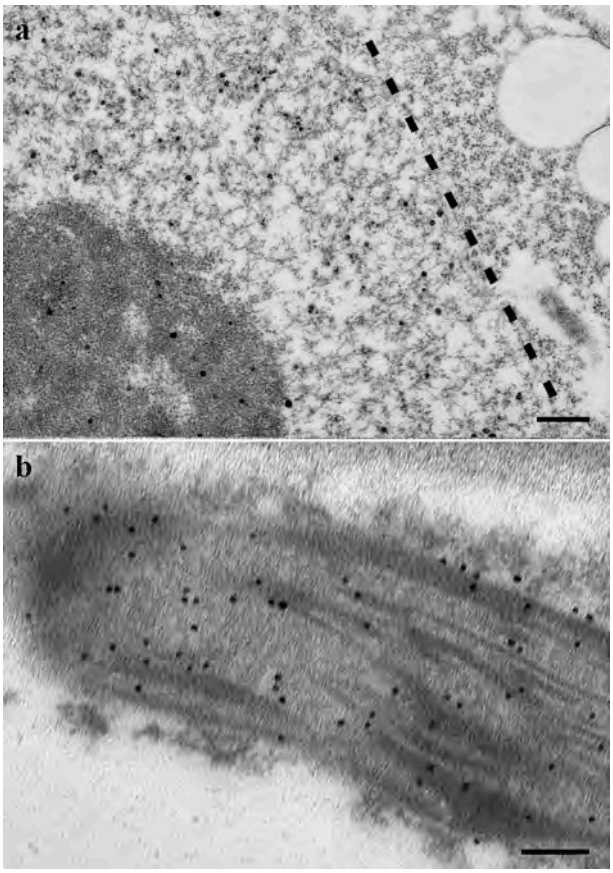

Figure 3. Transmission electron micrographs demonstrated that microwave-assisted chemical fixation led to good ultrastructural preservation, retention of native protein compartmentalization, and high immunolabeling efficiency of control proteins in Arabidopsis tissues. (a) High mobility group (HMGa) nuclear protein was distributed throughout the nucleus of a root cell, but not labeled in the cytoplasm. The position of the nuclear envelope is highlighted by dashes. (b) Rubisco was distributed within the chloroplast of a leaf cell without any artefactual redistribution to the cytoplasm. Bars = 100 nm for both micrographs.

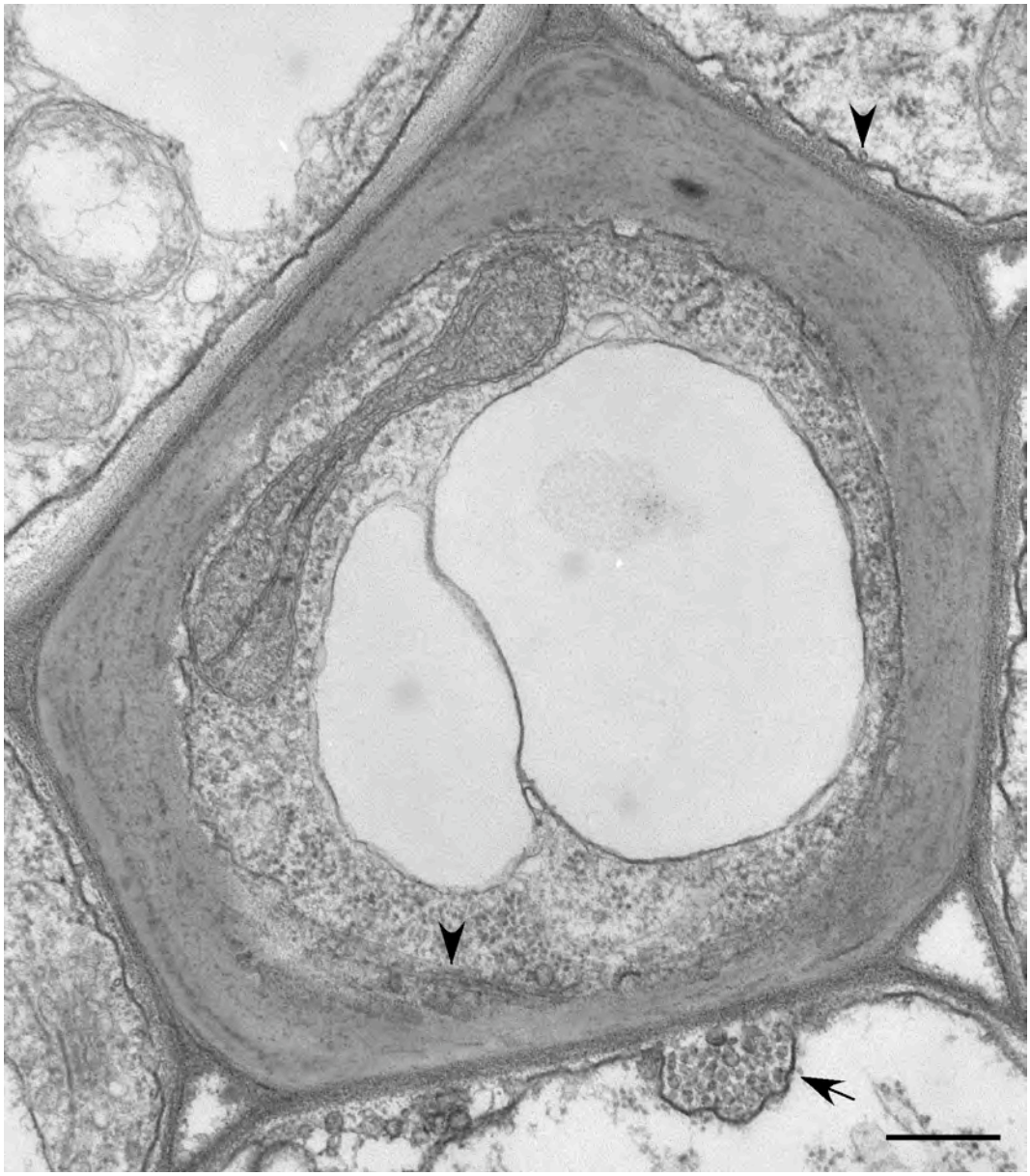

Figure 4. A well-preserved, late-stage, differentiating TE. Arrowheads indicate microtubules (longitudinal sections in one case, cross section in the other), which are well-known as being difficult to preserve. The arrow shows a multivesicular body fusing with the plasma membrane. There are two big vacuoles in the center and a mitochondrion above them. Bar = 500 nm.

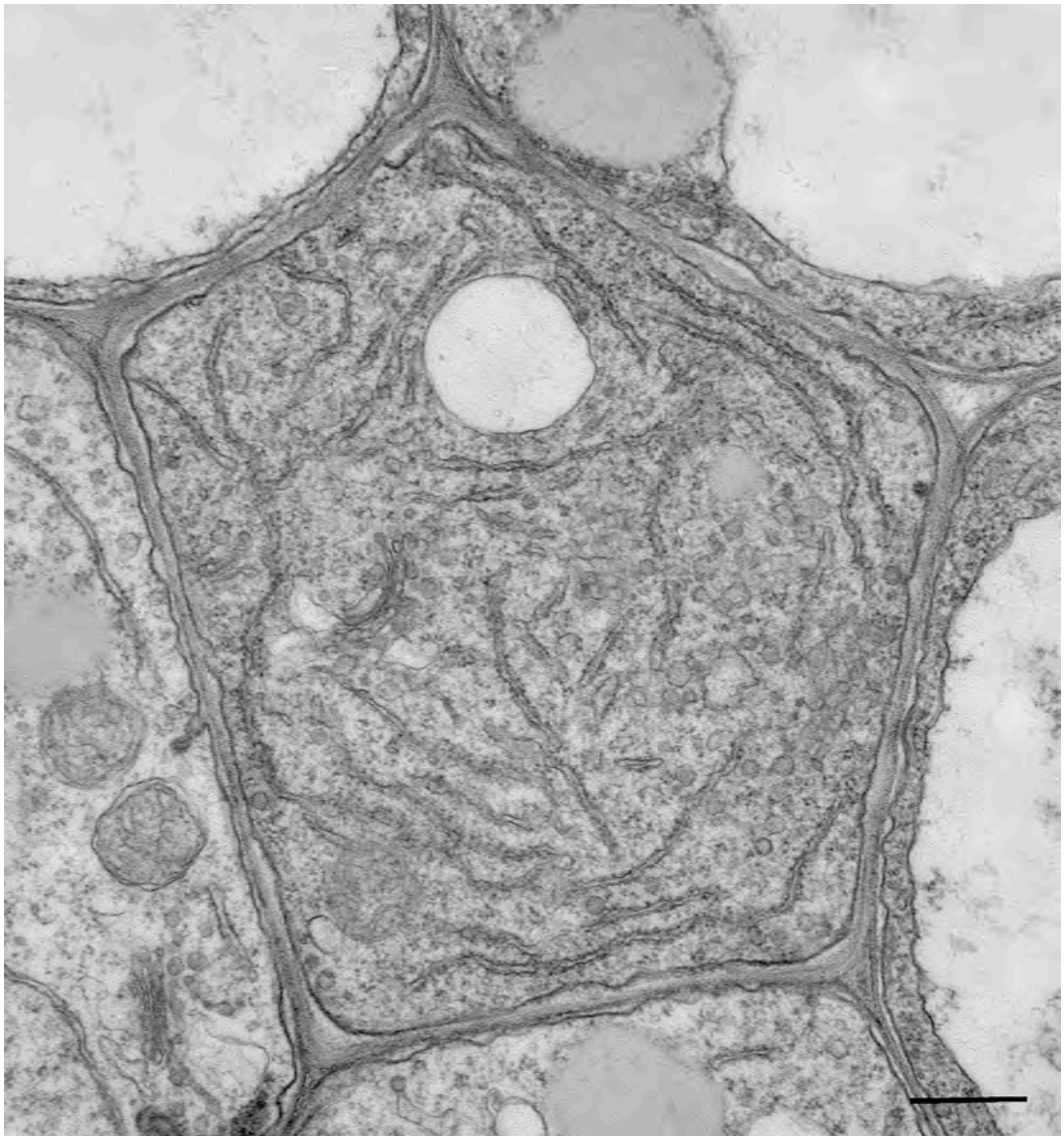

Figure 5. Early stage of TE differentiation prior to the synthesis of thick secondary walls. Many vesicles and endoplasmic reticulum cisternae can be seen. Early stages of TEs could be distinguished by their staining darker than adjacent cells because of their comparatively dense cytoplasm. However, the exact cross-sectional placement within the Arabidopsis diarch stele could be determined by observing adjacent pericycle and endodermis cells (Dolan et al., 1993). Bar =500 nm.

Figure 6. Mid-stage TE with many organelles. Increase in the number of organelles indicates high-level cellular activity. Bar = 500 nm.

Figure 7. A late-stage TE before vacuolar implosion. Bar = 500 nm.

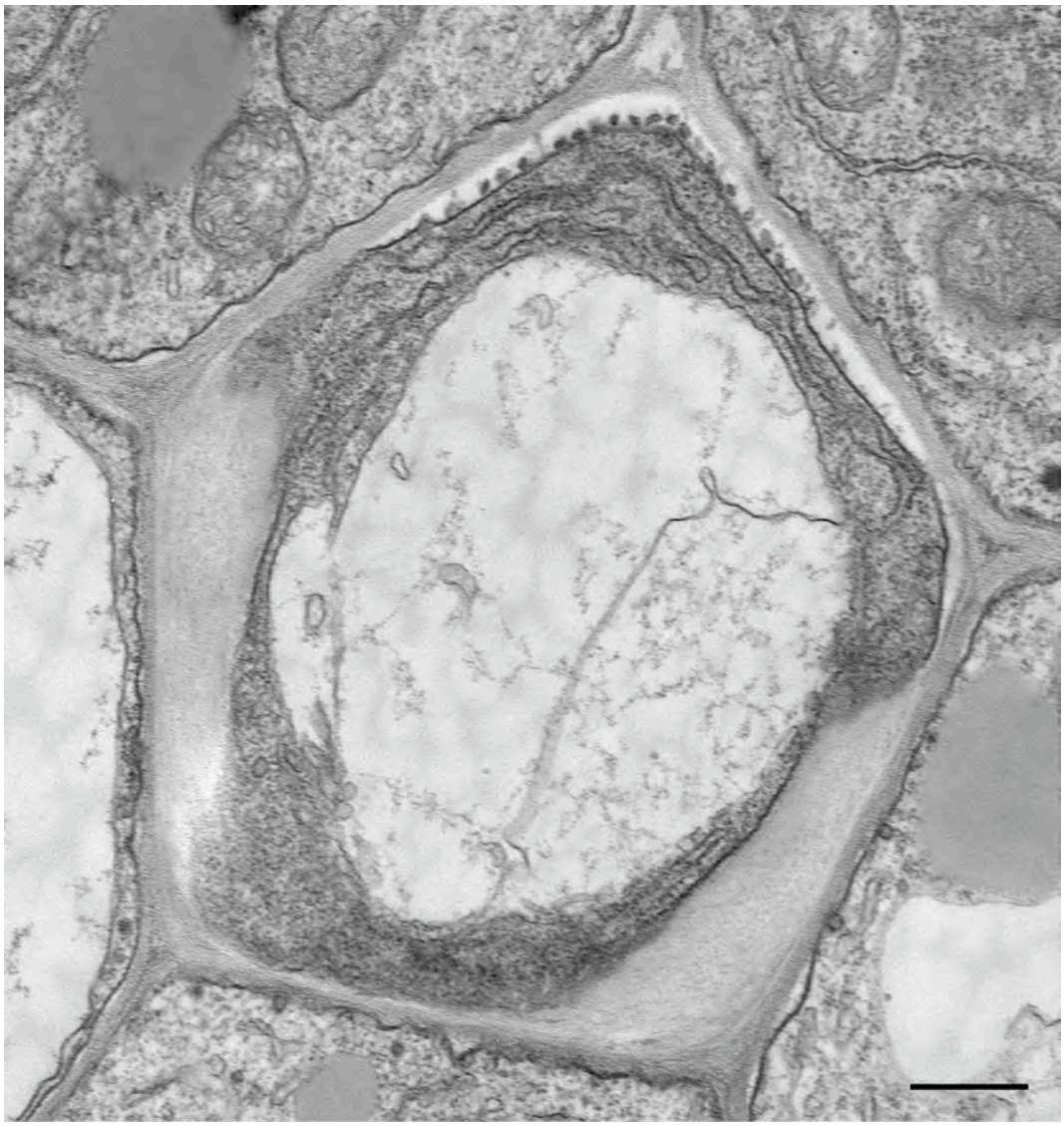

Figure 8. Implosion of the central vacuole. The tonoplast membrane collapsed inward, signifying the beginning of final bulk autolysis. Bar =500 nm.

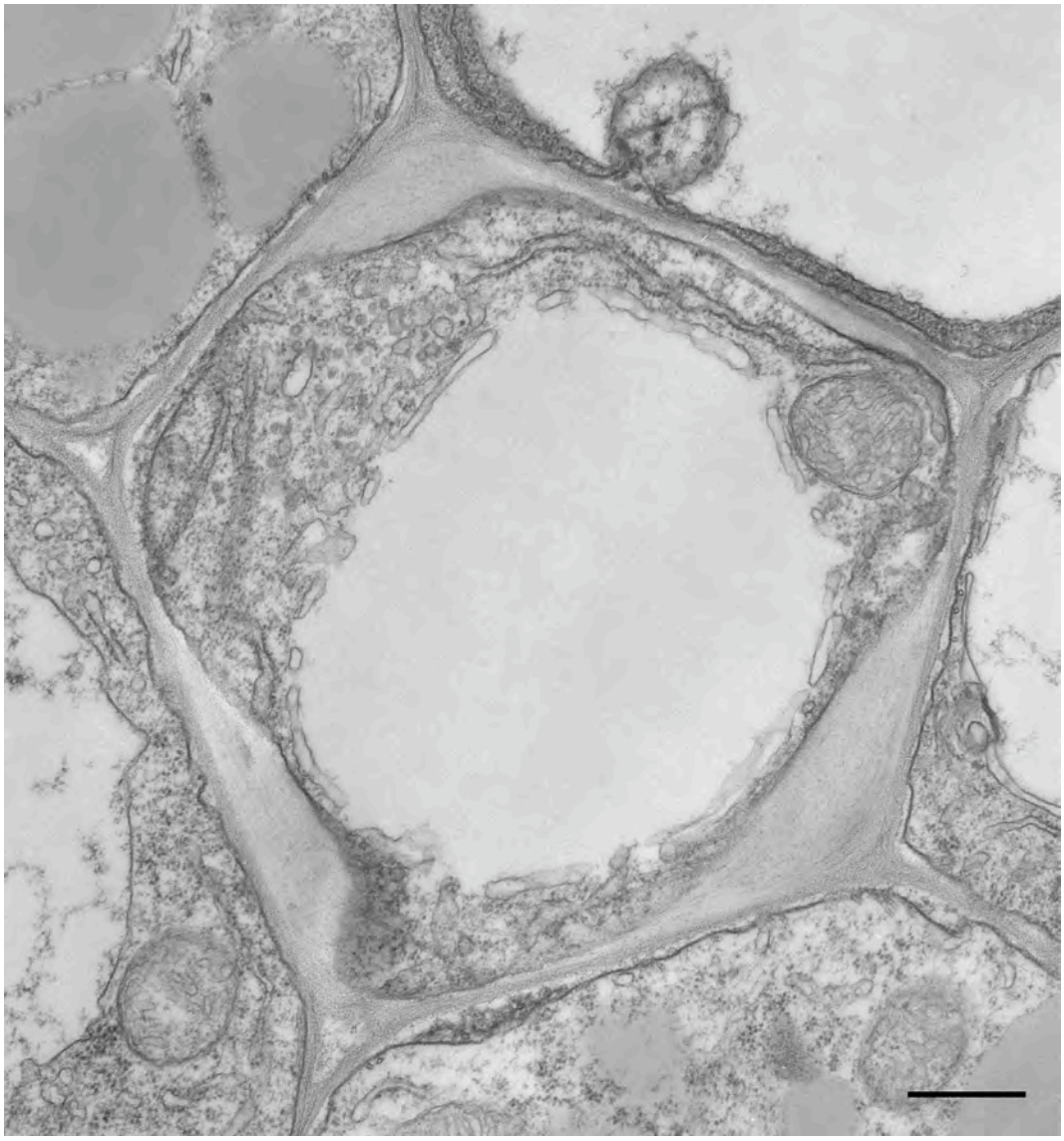

Figure 9. After vacuole breakdown. The tonoplast membrane disappeared, which indicates that cell autolysis has started. Bar = 500 nm.

Figure 10. More advanced degradation of the cell. Cell integrity was lost and organelles were disappearing. A mitochondria on the left corner still persists. Bar = 500 nm.

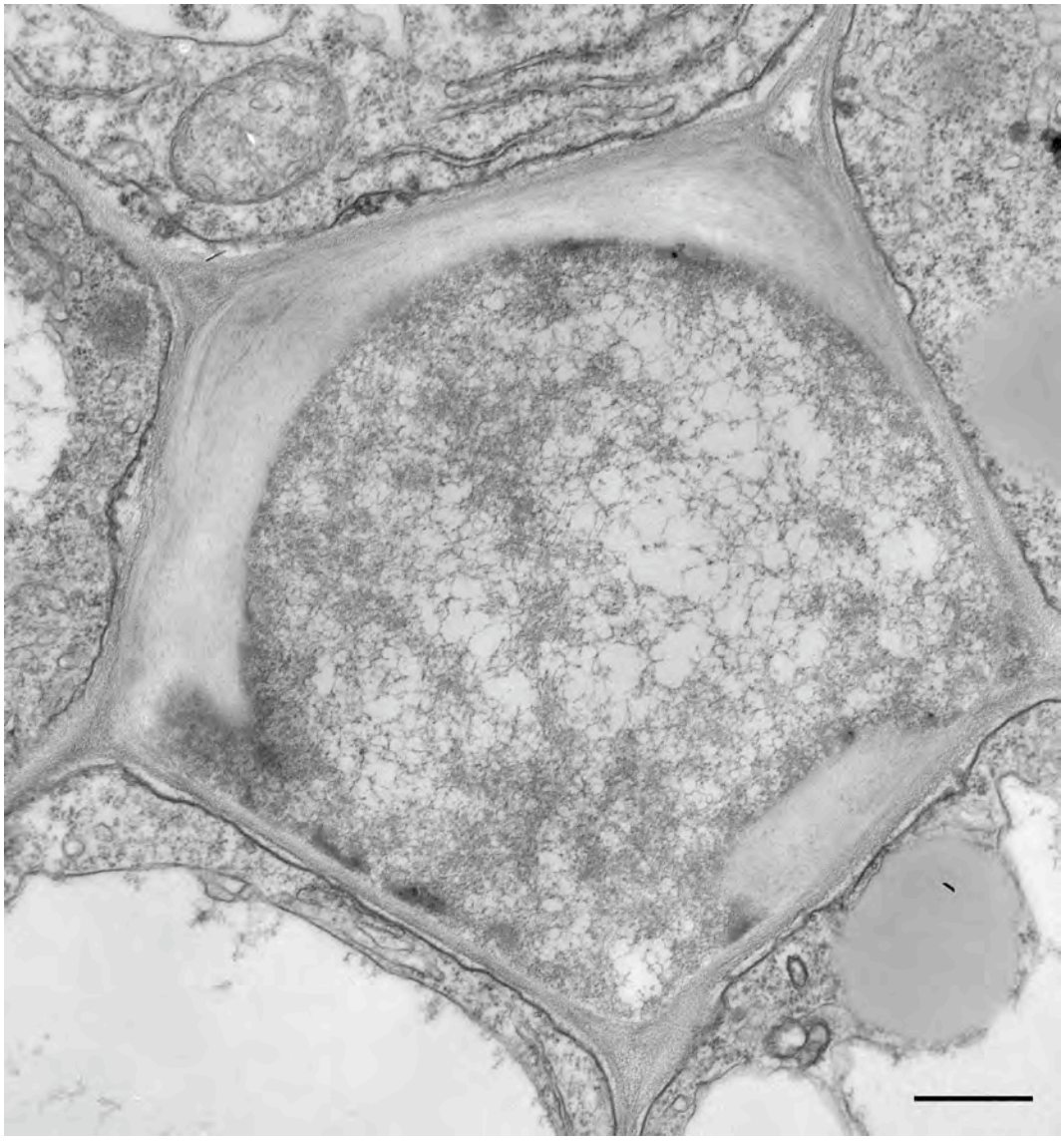

Figure 11. Just before emptying the cell to become a functional TE. Fibrous structure inside TE was a new finding of this investigation. Bar = 500 nm.

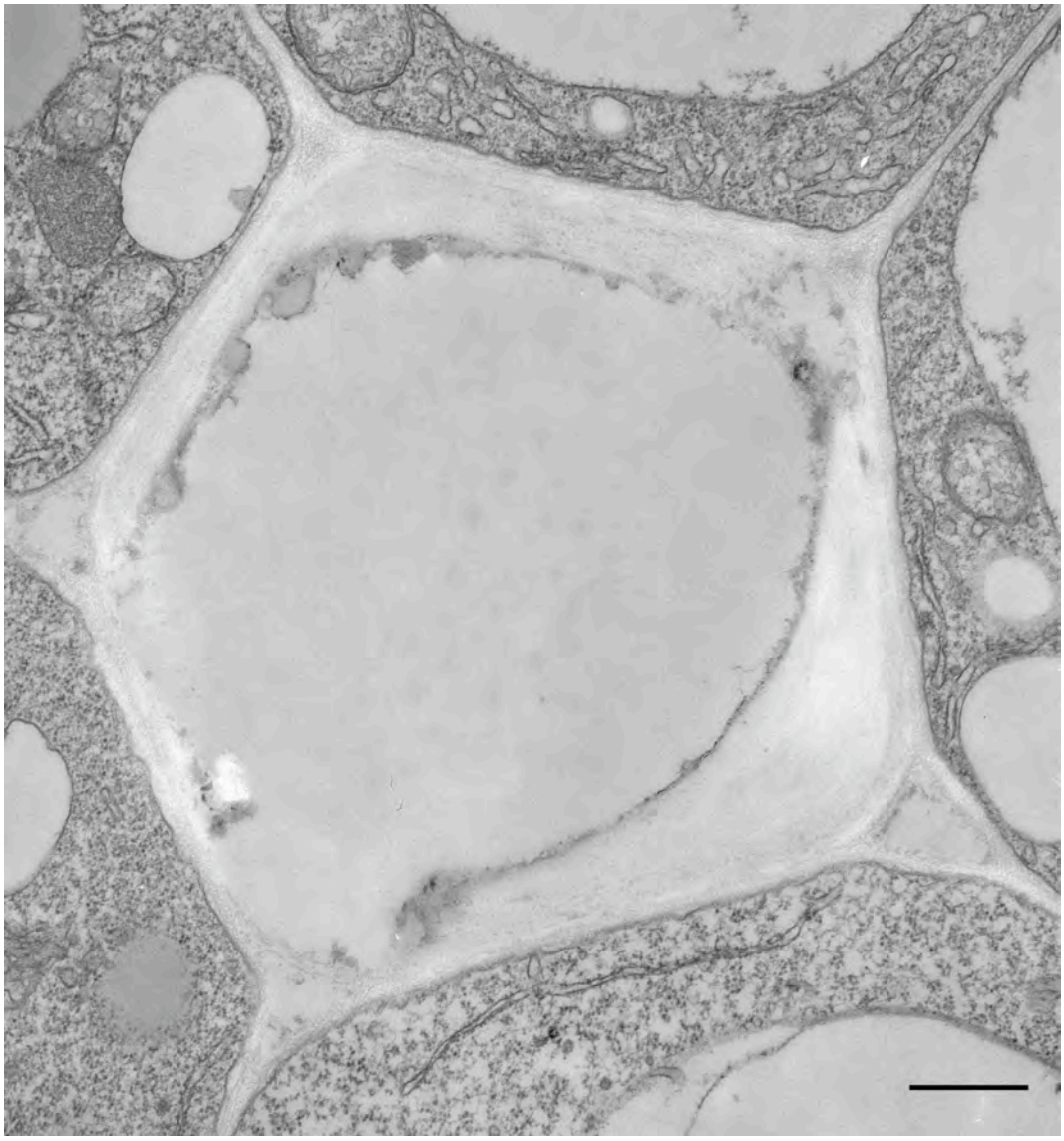

Figure 12. A dead, functional TE in the final stage. Remaining materials in close proximity to the cell walls were the last cell remnants awaiting removal. Bar = 500 nm.

CHAPTER 3

Roles of XCP1 and XCP2 Cysteine Proteases in Tracheary Element Differentiation in *Arabidopsis thaliana*

Introduction

Programmed cell death in animals

Programmed cell death (PCD) is an indispensable cell suicide process for the normal growth and development of most multicellular organisms (Ameisen, 2002). Among all organisms, PCD has been most highly investigated in animals. Three types of PCD have been found in animals (van Doorn and Woltering, 2005): (a) autophagy, in which cytoplasmic components are delivered via an autophagosome, a double membrane structure, to the lysosome for degradation in the same cell; (b) apoptosis, in which chromatin condensation and nuclear fragmentation are followed by appearance of membrane bounded apoptotic bodies that are phagocytosed by adjacent cells and degraded in lysosomes; and (c) least commonly, non-lysosomal PCD, in which cell suicide occurs by inhibiting major cellular pathways (van Doorn, 2005).

Programmed cell death in plants

Autophagy and autolytic mechanism, which is similar to non-lysosomal PCD, are distinguished as the most common types of plant PCD (Beers, 1997; van Doorn and Woltering, 2005). However, PCD in plants differs from that of animals in certain ways. A different type of autophagy, without involvement of an autophagosome, in plants is the permeabilization of vacuoles, resulting in release of stored degradative enzymes into the cytoplasm, which is subsequently cleared (Obara et al., 2001; van Doorn and Woltering, 2005). Another observation that differs from animals is that true apoptosis requiring engulfment of apoptotic bodies and phagocytosis in another cell has not been observed in plants even though DNA fragmentation and occurrence of apoptotic-like bodies, characteristic of apoptosis, were reported (Gilchrist, 1997). Absence of true apoptosis might

be explained by the presence of the plant cell wall, which makes this kind of apoptosis impractical.

Importance of understanding programmed cell death in plants

Programmed cell death is involved in plant development and defense processes such as reproduction, senescence, tracheary element (TE) differentiation (xylogenesis), and pathogenesis (Beers, 1997; Greenberg, 1996). Throughout the life cycle of plants, PCD is highly controlled by several cellular mechanisms such as signaling and gene regulation, which is less understood compared to animal systems.

There are many intriguing aspects of plant PCD worthy of study (Morgan and Drew, 2004). In most cases, certain cells die at a given time, but others do not. For example, TEs commit suicide to be functional dead cells as a part of the vascular system, but only the cells that are destined to be TEs die. How plants target specific cells and accomplish selectivity is still under investigation. Precisely how the timing of TE death is controlled during their differentiation program is also unknown but interesting.

Genetic pathways and signals directing PCD might be different between organisms (Mittler and Shulaev, 2004) and even within a single organism (Beers and McDowell, 2001). Understanding these differences are increasing with the availability of newly completed genomes. Better and new experimental systems will be needed to identify pathways and key regulators of PCD, which overall will find many applications to improve agriculture. For example, inhibition or reduction in senescence-associated PCD might result in an increase of plant biomass under stressful agricultural condition. Mittler and Shulaev (2004) discussed nine other manipulations of PCD processes in plats that might benefit agriculture: “(1) enhance resistance to obligatory pathogens by enhancing an hypersensitive response (HR) of

by engineering an HR in plants that does not activate PCD upon infection with a specific pathogen, (2) enhance the resistance of plants to necrotrophic pathogens by preventing PCD, (3) reducing disease symptoms caused by a PCD, (4) reduce or alter PCD associated with abiotic stress, (5) inhibition of PCD involved in flower, fruit or whole plant senescence, (6) inhibition of PCD in storage (seed, tuber) tissues, (7) engineering male sterility and pollen incompatibility, (8) developing new herbicides, and (9) altering the shape and size of leaves or other organs by linking specific developmental pathways to PCD genes".

Understanding the physiology and regulation of plant vascular tissue development along with the relation to PCD is an area of great economic significance because of the major role of vascular tissue in herbaceous stalks and wood as renewable resources. Therefore, understanding the basic biology of this differentiation process may ultimately lead to design of genetic engineering strategies for crop improvement.

Protease structure

Proteolytic enzymes catalyze the cleavage of peptide bonds in proteins. They are described with several terms. Peptidase is the general term for both endopeptidases and exopeptidases. While exopeptidases act only near amino and carboxyl termini of polypeptide chains, endopeptidases act preferentially in inner regions of peptide chains. Protease and proteinase are synonymous terms with peptidase and endopeptidase, respectively.

The most well known cell death proteases are endopeptidases divided into five subclasses related to their catalytic mechanism as follows (Beers et al., 2000):

- Serine endopeptidases (EC 3.4.21)
- Cysteine (Thiol) endopeptidases (EC 3.4.22)
- Aspartic endopeptidases (EC 3.4.23)

- Metalloendopeptidases (EC 3.4.24)
- Threonine endopeptidases (EC 3.4.25)

The names of serine, cysteine, aspartic and threonine endopeptidases reflect the amino acid residues required at the active site for the catalytic process. While serine endopeptidases have a serine residue in the active site, cysteine endopeptidases have a cysteine residue involved in the catalytic activity. Metalloendopeptidases involve a metal ion in catalytic activity.

Function of cysteine proteases in programmed cell death

Caspases, a family of cysteine proteases, are involved in apoptosis in animals as part of the proteolytic cascade. Once activated, caspases may activate other downstream caspases, which leads to breakdown of the cell. The idea that proteases might be participated in plant PCD initially came from the assumption of similarity in biological processes between animals and plants.

Plant cysteine proteases are involved in cell death processes, organ senescence, plant resistance to pathogens and insects, and protein degradation and mobilization during seed germination (Beers et al., 2004). In this research, the role of cysteine proteases was investigated during TE differentiation.

Tracheary element differentiation

TEs consist of vessels and tracheids functioning to deliver water throughout plant parts and to give mechanical strength to the plant body. TEs are differentiated from procambium or vascular cambium through cell changes including secondary wall synthesis, cell suicide and autolysis. TEs undergoing autolysis lose their nuclei and cell contents,

forming functional dead cells at maturity. Regulatory and molecular mechanism playing roles in TE autolysis are not well identified (Fukuda, 1997b; Kuriyama and Fukuda, 2002).

Cysteine proteases and tracheary element differentiation

Cysteine protease gene expression and enzyme activity were associated with TE differentiation in cultured cells of *Zinnia elegans* (Minami and Fukuda, 1995; Ye and Varner, 1996; Beers and Freeman, 1997). Protease activity was increased during TE differentiation, and TE autolysis was blocked by a cysteine protease inhibitor (Woffenden, 1998), resulting in the hypothesis that these enzymes were involved in degradation of cellular contents. However, direct testing of a role for any protease in TE autolysis was previously lacking.

XCP1 and XCP2, xylem-specific cysteine proteases in Arabidopsis

XCP1 and XCP2, which are papain-like enzymes with 70% amino acid identity, are synthesized as preproproteins of ~40 kDa that undergo at least two co- or post-translational proteolytic processing events: cleavage of the N-terminal signal sequence then the regulatory prodomain to yield the active mature protease (Beers et al., 2000). They were sequenced from an Arabidopsis secondary xylem cDNA library (Zhao et al., 2000), and *XCP1*- or *XCP2*- promoter:ß-glucuronidase (GUS) fusions were expressed in TEs of transgenic Arabidopsis. XCP1 was immunolabeled within TE vacuoles of whole Arabidopsis sepals and roots, but the results were not always consistent (Funk et al., 2002), perhaps due to changes induced during sample processing in standard immunofluorescence protocols (Salnikov et al., 2001). Analysis at Genevestigator® (https://www.genevestigator.ethz.ch; Zimmerman et al., 2004) showed that XCP1/XCP2 are both widely expressed in wild-type Arabidopsis, but XCP2 had a higher expression level and both genes were developmentally regulated. Strongly up-regulated XCP1 and XCP2 expression occurred in tissues with differentiating

TEs including the hypocotyl, stem, node, and root hair zone, which was analyzed further in this research.

Need for more research on XCP1 and XCP2

In TEs differentiating in suspension culture, the onset of autolysis is associated with changes in tonoplast transport capability (Kuriyama, 1999) and formation of possibly autophagic small vacuoles in correlation with reduced density of the cytoplasm (Groover and Jones, 1997). After a calcium influx, cell death is visibly initiated by rapid vacuolar implosion so that mixing occurs between vacuolar contents and the cytoplasm (Groover et al., 1997; Groover and Jones, 1999; Obara et al., 2001). Prominent models of PCD in TEs propose that cysteine proteases, along with S1-nucleases, RNAses, and acid phosphatases, are loaded into the central vacuole as they are synthesized during TE differentiation and upon vacuolar collapse, they are proposed to mix with the newly acidified cytoplasm and effect the degradation of organelles during final autolysis (Kuriyama and Fukuda, 2002). However, there was heretofore no direct evidence that cysteine proteases or other hydrolases participated in autolysis by this mechanism.

Immunofluorescence and confocal microscopy of plants expressing XCP1- and XCP2-GUS also supported the localization to the vacuole in xylem, but these results had a relatively low resolution. In the confocal study for XCP1, labeling was also detected in the cell wall in mature TEs and associated with the plasma membrane in Arabidopsis (Funk et al., 2002). In collaboration with Dr. Eric Beers at Virginia Polytechnical University, this study was conducted to better understand the function, exact cell-type where it was active, and subcellular location of each protease.

As reported here, analysis of TE autolysis *in planta* at the electron microscopic level provided evidence that XCP1 and XCP2 participate in autolysis by a somewhat different mechanism than previously hypothesized. Taking advantage of the predictable developmental file of TE differentiation behind the root tip of germinating Arabidopsis seeds (Busse and Evert, 1999), we were able to examine dozens of differentiating TEs from four genotypes, wild type and three T-DNA knockout lines, at all stages of differentiation. Good preservation of ultrastructure and antigenicity in minimally handled tissue were achieved with rapid methods for microwave-assisted processing of plant samples (methods modified from Russin and Trivett, 2001). Importantly for this study, microwave-assisted fixation reduces the incidence of vacuolar rupture during conventional fixation in plant cells (Heumann, 1992) and preserves the location of soluble antigens, including soluble proteins and small peptides (Login and Dvorak, 1988; Benhamou et al., 1991; Mizuhira et al., 2000).

Materials and Methods

To accomplish this work, I received from Dr. Beers Lab the following reagents and materials:

- *XCP1*- or *XCP2*-promoter:GUS lines
- Antibodies (anti-XCP1, anti-XCP2P, anti-XCP2, anti-XCPM)
- Wild-type and *xcp1*, *xcp2*, *xcp1xcp2* knockout lines

Full method descriptions for production of their materials are in preparation for publication (Avci et al., in preparation).

Generation and purification of antisera and immunoblot analysis

This part was conducted at Virginia Tech and included here to show the specificity of antibodies that we used in this study. Four different polyclonal antibody preparations were

used to evaluate protein extracted from isolated xylem: (1) anti-XCP1, against the XCP1 proprotein (prodomain plus mature domain); (2) anti-XCP2 against the proprotein; (3) anti-XCP2P against the prodomain only; and (4) anti-XCP2M against the mature domain only. In addition, anti-XCP2 antibody was affinity purified. To clone partial open reading frames of XCP2 in frame with a C-terminal 6xHis tag for expression of recombinant protein prior to antibody production, the following primer pairs were used. For XCP2 proprotein: sense, 5'-TACTCCATCGTTGGATACTCC-3', anti-sense, 5'-AAGATCAACCCCGCACCGC-3'. For XCP2 prodomain only: sense, 5'-TACTCCATCGTTGGATACTCC-3', anti-sense, 5-AGCGAACTCTGCGTAAGATCTT-3'. For XCP2 mature domain only: sense, 5'-GACTATGCCTTTGAGTACATT-3', antisense, 5'-TACTCCATCGTTGGATACTCC-3'. A xylem cDNA library (Zhao et al., 2000) was used as template for polymerase chain reaction (PCR) amplification using tag polymerase. T/A cloning of PCR products was performed using the pTrcHis2-TOPO vector (Invitrogen, Carlsbad, CA), which provides an initiator Met and a C-terminal poly-His tag. All clones were sequenced to confirm absence of mutations and correctness of reading frame.

To purify Poly-His tagged XCP2, *Escherichia coli* cells (100 mL) were cultured as specified by Invitrogen. Expression was induced by 1 mM isopropylthio-β-galactoside (IPTG) and cells were harvested 4 h later by centrifugation (4,000*g*, 20 min). All purification steps were performed at 4^{o}C. Cells were resuspended in lysis buffer (12 mL, 50 mM NaH_2PO_4, pH 8.0, plus 300 mM NaCl and 1 mg/mL lysozyme) and incubated on ice for 30 min. Following sonication, the pellet containing inclusion bodies was collected by centrifugation (10,000*g*, 30 min), solubilized in denaturing buffer (1 mL; 8 M urea, 100mM NaH_2PO_4, 10mM Tris-HCl, pH 8.0), and clarified by centrifugation (14,000*g*, 10 min). The

resulting supernatant was added to a column containing 300-uL bed volume of nickel-nitrilotriacetic acid- (nickel-NTA)-agarose beads equilibrated in denaturing buffer, and the poly-His tagged proteins were allowed to bind by reapplying the flow-through 3 times before discarding the unbound proteins in the final flow-through. The following washes were used to remove background proteins from the nickel-NTA-agarose beads: 5 mL of denaturing buffer, pH 6.5; 5mL of lysis buffer, without lysozyme; 2mL of lysis buffer pH 4.5. Purified protein was then released using 1 mL of elution buffer (8 M urea, 100mM NaH2PO4, 10 mM Tris-HCL, 500mM imidazole, and 10mM 2-mercapto-ethanol, pH 8.0). The elution was repeated twice and the eluates were pooled prior to examination on 12% SDS PAGE and analysis by MALDI-TOF mass spectrometry for confirmation of identity prior to polyclonal antibody preparation (Funk et al., 2002).

For immunoblot analysis, protein was extracted from secondary xylem of hypocotyls of 8 week old Arabidopsis plants (Zhao et al., 2000) by homogenizing at 4°C in a mortar and pestle with 100 mM NaH_2PO_4, pH 7.2, containing 150 mM NaCl, 20 μmol leupeptin and 14 mM 2-mercaptoethanol (4:1 buffer vol:tissue wt). After clarification by centrifugation (14,000*g*, 20 min) the supernatant was concentrated eight- to ten-fold using YM10 concentrators (Millipore, Bedford, MA) followed by immunoblot analysis as described (Woffenden et al., 1998).

Characterization of *xcp1* and *xcp2* T-DNA knockout lines, and generation of a *xcp1xcp2* double knockout line

These lines, diagrammed in Figure 1 and 2, were provided by Dr. Beers and coworkers; methods they used are described here. Arabidopsis genomic DNA was isolated as described previously (Lukowitz et al., 2000). T-DNA insertion lines SALK_084789.31.40.x

(*xcp1*) and SALK_010938 (*xcp2*) were obtained from the Arabidopsis Biological Resource Center (Alonso et al., 2003). Insertions of T-DNA in these mutant alleles were confirmed by sequencing the PCR products amplified from genomic DNA using a pROK2 T-DNA left border primer LBb1, 5'-GCGTGGACCGCTTGCTGCAACT-3', in combination with the appropriate gene-specific primers: for *XCP1*, sense 5'-ATGGCTTTTTCTGCACCATC-3' and antisense 5'-TCACTTGGTCTTGGTAGGAT-3'; for *XCP2*, sense 5'-GAATCCTCTGTTTTGCTCTTGC-3' and antisense, 5'-AAGATCAACCCCGCACCGC-3'. For *xcp2*, primer LBb1 yielded a flanking *XCP2* sequence when used with either *XCP2* sense or antisense primers, indicating that T-DNA was present as a tandem (or higher) inverted repeat. For *xcp1*, primer LBb1 yielded a flanking *XCP1* sequence only when combined with the *XCP1*sense primer. Homozygous single-gene knockouts, which were null for each transcript as demonstrated by RT-PCR (described below) were carried to at least the T3 generation, then crossed to generate *xcp1xcp2* plants which were identified by PCR as described above for single knockouts.

RT-PCR was carried out using the RETROscript Kit (Ambion, Austin, TX) using total leaf RNA isolated with the RNeasy Plant Mini Kit (Qiagen). Briefly, cDNA was synthesized from 1 μg of total RNA in 20-μl reaction. 1 μl of cDNA was used as template for PCR amplification in 25-μl reaction with following gene-specific primers: for *XCP1*, sense 5'-CCATTTCAGCATCAGCTCTC-3' and antisense 5'-TCACTTGGTCTTGGTAGGAT-3'; for *XCP2* sense, 5'-ATGGCTCTTTCTTCACCTTCAA-3', and antisense, 5'-CTTAGTTTTGGTGGGGAAAAG-3'. As a positive control actin (*ACT7*) was amplified: sense primer, 5'-GGCCGATGGTGAGGATATTC-3', and antisense primer, 5'-CTGACTCATCGTACTCACTC-3'.

Growth of Arabidopsis

Seeds of wild-type and transformed *Arabidopsis thaliana* (Columbia were cold-treated on moist filter paper in Petri dishes (24 h, 4°C) then germinated under white fluorescent light with an 16h/8h and 25°C/20°C day/night cycle. Whole Arabidopsis seedlings 2.5-3 d old (total time after imbibition) were harvested with minimal disturbance and processed as described below. Cold-treated (3-4 d, 4°C in distilled water) seeds of wild-type and transgenic plants are transferred onto soil (Pro-Mix, Premier Horticulture Inc., PA) and grown under the light intensity of approximately 200 μmol m^{-2} s^{-1} with an 16h/8h and constant temperature of 20 – 22°C for phenotypic observations.

Detection of GUS in the laser scanning confocal microscope

GUS was detected with ImaGene Green™ C_{12} FDGlcU Gene Expression Kit (I-2908; Molecular Probes, Eugene, OR), a lipophilic, fluorogenic, membrane-permeant, substrate that forms a nontoxic fluorescent product (495/540 nm excitation/emission) within viable plant cells. The use of ImaGene green on whole roots extended the manufacturer's protocol and typical uses (Fleming et al., 1996) of incubating tissue sections.

The 2.5-3 d whole seedlings transformed with the *XCP1*- or *XCP2*-promoter:GUS reporter gene (seeds provided by Dr. Eric Beers) were placed in 20mM phosphate buffer (pH 7.2) containing 50 μM ImaGene Green™. After 3-4 h incubation and washing in buffer (2 x 5min), EM-grade formaldehyde (Ladd Research, Williston, VT) was added to the final wash (1% v/v final concentration) before microwave fixation (3 x 20 sec pulse, 650 W, temperature restricted at 36.5° C, 20 inches of Hg vacuum; see below for microwave details). After washing with buffer, seedlings were mounted in phenylenediamine mountant (Salnikov

et al., 2001) prior to observation in a laser scanning confocal microscope (Leica SP, Wetzlar, Germany; 514 nm Argon-ion excitation laser; emission 490 – 540 nm).

Microwave-assisted sample processing for electron microscopy

Whole wild type and knockout seedlings were fixed and embedded for electron microscopic observation by use of a laboratory-grade microwave with integrated specimen temperature control and vacuum following the general instructions of the manufacturer (Biowave Model 34700; Pelco, Redding, CA). Microwave fixation was initiated within 2 min of placing the seedlings in microcentrifuge tubes containing fixative. Temperature was restricted at 36.5°C during fixation and did not exceed 40°C during infiltration.

For immunolabeling, fixation was in 4% (v/v) formaldehyde or 2% (v/v) formaldehyde plus 0.2% (v/v) glutaraldehyde in 20 mM sodium cacodylate buffer (pH 7.2). Low energy microwave fixation (150 W, 20 in Hg vacuum, 3 x 3 min with 1 min on ice between steps) was followed by brief fixation at 650W (with vacuum, 6 x 10 sec with 20 sec intervals). After rinsing in buffer (250 W, no vacuum, 3 x 1 min), seedlings were optionally exposed to 2% (w/v) uranyl acetate (aq) (150W, 20 in Hg vacuum, 3 x 2 min with 30 sec on intervals) in order to improve membrane contrast slightly. Then, dehydration in an ethanol series (30, 50, 70, 90, 100%; 250W, no vacuum, 40 sec each step) was followed by infiltration in LR White resin:ethanol (1:3, 1:1, 3:1) followed by 3 x 100% resin (250W with vacuum, 3 min each step).

For optimal analysis of ultrastructure, primary fixation was in 2.5% glutaraldehyde (v/v) in 50mM sodium cacodylate buffer (pH 7.2). Initial 3 x 5 min low energy microwave fixation (150 W with vacuum) was followed by brief fixation (650W with vacuum, 6 x 10 sec with 20 sec intervals). Samples were washed in buffer as described above, and secondary

fixation occurred in 1% (w/v) osmium tetroxide/ 1.5 % (w/v) potassium ferricyanide (another membrane contrasting agent) in the same buffer (150 W, with vacuum, 3 x 45 sec with 45 sec rests between steps). Dehydration and infiltration in Spurr's resin was as described for LR White except acetone was used throughout.

Fully infiltrated seedlings were flat-embedded between two glass slides (Salnikov et al., 2003). LR White resin was polymerized under UV light (360 nm; overnight, 4°C) to avoid any potential heat-induced reduction of antigenicity. Spurr's resin was polymerized overnight at 60°C. In order to obtain root cross-sections, a ~ 2 mm^2 resin section containing the whole seedling (to avoid damaging TEs of interest) was cut out with a razor blade and glued vertically to a roughened tangential face or within a slit cut into a blank Spurr's resin block. Sequential 2 µm thick sections were made with a diamond knife on an ultramicrotome (MT2-B, Sorvall). Reliable location of differentiating protoxylem TEs in 2.5 – 3d Arabidopsis seedling roots was aided by prior descriptions of their longitudinal (Busse and Evert 1999) and cross-sectional placement within the diarch stele (Dolan et al., 1993). As demonstrated in Figure 3, flat-embedded sections were used to take cross sections starting from behind the root tip region. Sections were collected as the root hair zone was approached, affixed to slides by low temperature heating, and stained with 1% aq. (w/v) Toluidine Blue (warmed 15 – 20 sec, then washed), which bound to both cytoplasm and patterned secondary wall thickenings. When the first differentiating TEs were detected with a 100x objective near the root hair region, thin sections were collected at approximately 30-50 µm intervals throughout the whole TE differentiation zone until complete TE clearing was observed in wild-type plants. Sections were collected on Formvar-coated grids, optionally immunolabeled (see below), and then stained with 2% uranyl acetate (aq. or in 70% ethanol

for immunolabeling and ultrastructure, respectively) for 15 minutes and lead citrate (Reynolds, 1963) for 4 minutes in humid Petri dishes (including sodium hydroxide pellets to trap CO_z during lead citrate staining) before observation in the transmission electron microscope (JEOL 100S). Negatives were scanned at high resolution (Epson 4870 scanner) for preparation of digital plates.

Immunocytochemical labeling

Basic solutions used were: Tris buffer (TB) 20 mM Tris-buffer, 0.02% azide, pH 8.2; Tris buffered saline (TBS; TB plus 150 mM NaCl, pH 7.5); and TBST (TBS plus 0.05% (v/v) Tween 20). TB was used to minimize gold aggregation and background. Thin sections collected on nickel grids were: (a) blocked (30 min, RT, high humidity chamber) in TBST plus 5% (w/v) normal goat serum (Sigma S-2007) and 0.1 M Glycine; (b) incubated (overnight, 4°C) in TBST with 5% goat serum and primary antibody, either 1:1200 anti-XCP2 with or without affinity purification or 1:1200 anti-XCP2M crude serum; (c) washed 3x by dipping grids in TBS; (d) incubated (1 h RT) in TB plus 0.06% (w/v) bovine serum albumin and 1:50 goat anti-rabbit secondary antibody coupled to 10 nm colloidal gold (AuroProbe, Amersham Biosciences, Piscataway, NJ); and (d) washed in TB then distilled water. When it was helpful to emphasize the colloidal gold in low magnification overviews, red dots were applied over each gold particle by use of Canvas 9.

Replication

The summary of cysteine protease location throughout the time-course of TE differentiation in wild-type plants was derived from sections of dozens of independent plants. For T-DNA lines, *xcp1*, *xcp2*, and *xcp1xcp2*, phenotypes were analyzed in a minimum of 6 independent plants along with wild-type plants grown in parallel.

Results

The XCP1 and XCP2 promoters drove GUS gene expression specifically in differentiating tracheary elements

As demonstrated by *XCP1*- and *XCP2*-promoter:GUS fusions, both cysteine proteases can be predicted to be specific to differentiating TEs of Arabidopsis roots (Fig. 4). Green fluorescence derived from GUS activity on the ImaGene Green substrate appeared only in the differentiating procambial strand, specifically in the youngest TE that also had secondary wall thickenings detectable in DIC. The green fluorescence was absent in an adjacent but more mature TE that had thicker secondary walls, presumably because autolysis had occurred and destroyed all intracellular proteins.

Demonstration of the specificity of antibodies and absence of XCP1 and XCP2 in *xcp1xcp2* plants

Immunoblotting

Neither XCP1 nor XCP2 has been N-terminally sequenced to allow exact protein cleavage sites to be determined. However, information from papain prodomain and signal sequence cleavage sites (Groves et al., 1996) and *in vitro* studies with recombinant XCP1 (Zhao et al., 2000) indicates that extracts containing XCP1 and XCP2 should yield immunoreactive polypeptides with approximate molecular masses of 40, 37 and 24 kD for prepropeptides, propeptides and mature peptides, respectively. In Figure 5, arrowheads indicate XCP1/XCP2-related bands in this size range. Two large polypeptides were observed in wild-type as predicted using affinity-purified anti-XCP2 (Fig. 5 a, lane 1), affinity-purified anti-XCP2P (Fig. 5 a, lane 3), and crude anti-XCP2M serum (Fig. 5 b, lane 1). As expected, the lower mass polypeptides detected by anti-XCP2 were not detected by anti-XCP2P,

confirming that the prodomain was absent from these proteins (compare Fig. 5 a lane 3 to lane 1). Instead of a 24 kD polypeptide, two bands at about 30 and 26kD were detected with anti-XCP2 (Fig. 5 a, lane 1) and anti-XCP2M (Fig. 5 b, lane 1). Migration patterns identical to these have been reported for cysteine proteases from several plant species (van der Hoorn et al., 2004), possibly due to accumulation of partially processed propeptides *in planta* or during sample preparation.

Still requiring explanation are other bands labeled by affinity-purified anti-XCP2 and crude anti-XCP2M (Fig. 5 a, b). In both cases, the corresponding bands persisted in the double knockout, *xcp1xcp2* (lane 2 in Fig. 5 a, b), but they were not detectable with the pre-immune serum for anti-XCP2M in either wild-type or *xcp1xcp2* (Fig. 5 b, lanes 3 and 4, respectively). Given the lack of non-specific labeling, which was also observed for the pre-immune serum of anti-XCP2 (data not shown), the bands common to both wild type and *xcp1xcp2* xylem likely represent one or more related cysteine proteases detectable by immunoblotting in secondary xylem extracts. Notably, the other polypeptides were not recognized by anti-XCP2P, and they were also not detected in electron microscopic immunocytochemistry of differentiating root TEs (see below). Anti-XCP1 labeled a barely detectable ~30 kD protein in xylem extracts from wild-type, but not from *xcp1xcp2* plants (data not shown because this antibody was not useful in immunocytochemistry).

Additional immunoblotting results showed that affinity-purified anti-XCP2 recognized both XCP2 and XCP1. The labeled polypeptides had the same molecular weight profile in wild type and *xcp1* and *xcp2* single knockouts (Fig. 5 c lanes 1, 2, 3). Similar results were obtained with anti-XCP2M and anti-XCP2P (data not shown). Therefore, anti-

XCP2 antibodies reacted with both XCP1 and XCP2, which is reasonable given the 70% amino acid identity of the proteins and the multiple epitopes recognized by polyclonal sera.

Immunocytochemical labeling in electron microscopy

Under the conditions used here for preparing tissue samples for EM, antibody binding was strictly dependent upon the presence of XCP1 or XCP2, which we refer to hereafter 'XCP1/XCP2' labeling. Positive immunocytochemical results on wild-type TEs were obtained with anti-XCP2, with and without affinity purification, and anti-XCP2M. These antibodies also labeled both *xcp1* and *xcp2* TEs, consistent with the results of immunoblotting (Fig. 6 e and f, respectively). Only *xcp1xcp2* TEs in which neither XCP1 or XCP2 transcript was present showed no labeling. The null result for *xcp1xcp2* TEs, also demonstrated that the additional polypeptides labeled in immunoblots did not confound understanding the cellular behavior of XCP1 and XCP2. In another control, only sparse, non-specific labeling distributed over all cell types was observed after labeling with the pre-immune serum of anti-XCP2M (Fig. 6 d). Despite positive results in immunoblots, anti-XCP1 or anti-XCP2P did not label TEs in immunocytochemical protocols (data not shown).

Subcellular compartmentation of XCP1/XCP2 over the time course of wild-type tracheary element differentiation

The authentic detection of XCP1 and XCP2 was supported by equivalent results obtained with 3 polyclonal antisera: anti-XCP2 with and without affinity purification and anti-XCP2M. All 3 antisera labeled only TEs, which were located reliably at various stages of differentiation by reference to prior descriptions for Arabidopsis (Busse and Evert, 1999; Dolan et al., 1993). The first TEs differentiate within the procambial zone of the diarch stele near the beginning of the root hair zone, and they are flanked by two pericycle cells, each of

which faces two endodermal cells in most cases. The progression of wild type TE differentiation (defined here in 6 stages) is indicated by the characteristics of the vacuole, the extent of wall thickening, and the nature of the cytoplasm:

Stage 1: Dense cytoplasm, initial wall thickenings at cell corners

Stage 2: Small vacuoles; more wall thickening

Stage 3: Large central vacuole formed by small vacuole fusion; patterned secondary wall deposition becomes extensive

Stage 4: Cellular contents and XCP1/XCP2 appear within the vacuolar space

Stage 5: Tonoplast disruption allows increased flow of cellular components into the vacuolar space

Stage 6: Bulk autolysis proceeds until total TE clearing is achieved

Labeling of XCP1/XCP2 in the cytoplasm began to be observed at the earliest stages of TE differentiation (stage 1) when only the cell corners showed wall thickening (data not shown). Evidence of immediate storage in the central vacuole was not seen, although we cannot rule out that XCP1/XCP2 were too highly dispersed in a large vacuolar space to be detected by immunolabeling. Instead, for a prolonged period during vacuole consolidation and secondary wall thickening (Fig. 6 stage 2-3), XCP1/XCP2 accumulation was detected only in the cytoplasm. Only at stage 4 of TE differentiation, when secondary wall thickening was advanced, was XCP1/XCP2 detected in association with electron dense aggregates within the large central vacuole (Fig 6 a). In immunolabeling preparations, these aggregates often appeared connected to the cytoplasm at a small area near the tonoplast boundary. Although late-stage Arabidopsis root TEs have other small, possibly autophagic, vacuoles as described in other TEs (Groover et al., 1997; see Fig. 9 d, arrow), XCP1/XCP2 labeling was

not enriched in association with them. At stage 5 of tonoplast disruption, XCP1/XCP2 were still detected in the cytoplasm. At stage 6, XCP1/XCP2 remained associated with cellular remnants throughout autolysis in wild type TEs (Fig. 6 c).

No dense labeling was observed over any other conspicuous membrane-bound storage compartment. Instead the labeling remained relatively dispersed throughout the cytoplasm. Labeling was observed over: (a) ER (Fig. 7 a); (b) in association with Golgi stacks (Fig. 7 b); (c) small vesicles of ~30 nm diameter with an electron dense center (Fig. 7 c-f) ; and (d) on electron dense aggregates within the intact central vacuole (Fig. 7 g). The existence of XCP1/XCP2 in small vesicles is consistent with the conventional understanding of proteins processed in the endomembrane system and targeted to the vacuole. The presence of dispersed (i.e. putatively soluble) XCP1/XCP2 within the vacuole or complete loading of XCP1/XCP2 into the vacuole were never observed.

Phenotypic characterization of *xcp1*, *xcp2*, and *xcp1xcp2* T-DNA lines

The growth and morphology of *xcp1*, *xcp2*, or *xcp1xcp2* T-DNA lines grown in a growth chamber was not detectably different from wild-type. Similarly, no differences were detected in the tissue organization of roots viewed in thick section (data not shown). In contrast, thin sections of differentiating TEs in roots fixed with osmium to optimize the ultrastructure showed differences in the autolytic process in *xcp1* and *xcp1xcp2* TEs (Fig. 8). These results were completely consistent during observation of at least 6 independent seedlings of each type. Both *xcp1* and *xcp1xcp2* TEs showed extensive electron dense remnants (Fig. 8 b, d) at the same stage of development at which wild-type and *xcp2* TEs were almost completely cleared (Fig. 8 a, c). These remnants in T-DNA lines were sometimes seen within the vacuole in ultrastructural preparations (Fig. 9 d). The remnants

were detectable over approximately a 100 μm distance above differentiating TEs, but they were absent in older TEs. Consistently, the remnants in *xcp1* TEs were more dispersed than those observed in *xcp1xcp2* TEs (compare Fig. 8 b and d). Other than the persistence of cellular remnants, no other differences were observed in the autolytic process of *xcp1* and *xcp1xcp2* compared to wild-type.

New ultrastructural observations on autolyzing TEs

In stage 3 TEs with an intact central vacuole, accumulations of vesicles near the tonoplast, invaginations of the tonoplast that contained vesicles, and an increased amount of electron dense contents within the vacuole were observed (Fig. 9 a). After tonoplast implosion (compare Fig. 9 b and e for an earlier and later stage, respectively), cytoplasmic contents diffused into the former vacuolar space. Then, confirming observations on other TEs made by others, e.g. organelle swelling and rupture occurred, with ER and double-membraned organelles persisting longest during autolysis. Just before complete TE clearing, highly dispersed cellular remnants with a fibrillar aspect filled the TE lumen of wild-type (Fig. 9 c) and *xcp1xcp2* (Fig. 9 f) plants.

Discussion

The data reported here demonstrate that XCP1/XCP2 participate in TE autolysis by a specific mechanism involving degradation of particular cellular components within the central vacuole prior to vacuolar rupture. One or both of the proteases is also likely to participate in bulk cellular clearing after vacuolar rupture. Microwave-assisted chemical fixation prior to transmission electron microscopy allowed unprecedented views throughout TE differentiation of changing vacuolar behavior and stage-specific association of XCP1/XCP2 with the central vacuole. These images showing XCP1/XCP2 involved in TE

autolysis provide one of only a few cases where cysteine proteases have been seen in locations consistent with their hydrolytic function as contrasted with their storage pre-hydrolysis. Other hydrolytic locations visualized recently include: (a) the nucleus of the dying embryo suspensor of *Picea abies*, which is the degradation target of a metacapase-type cysteine protease translocated from the cytoplasm (Bozhkov et al., 2005); and (b) electron dense granules both inside and outside cell walls of highly disrupted cells of the seed inner integument (Nakaune et al., 2005). XCP1/XCP2 carry out their degradative function by a third mechanism, demonstrating the plasticity of cysteine protease action to mediate PCD in different developmental processes.

Microwave-assisted chemical fixation revealed cellular details of XCP1/XCP2 participation in tracheary element autolysis

Microwave-assisted chemical fixation allowed rapid fixing of whole seedlings, efficient processing of multiple samples, retention of the native compartmentalization of soluble proteins, good preservation of cellular structure, and maintenance of high antigenicity. In this process, there is a synergistic effect of the microwave energy, the effects of mild heating (generally optimized in the range of 35 – 45°C), and greatly increased rates of diffusion of chemicals through tissues (Kok and Boon, 1992). Tissue blocks up to 1 cm thick can be fixed with high quality within seconds (Login and Dvorak, 1988), and washing and resin infiltration steps are similarly rapid (Giberson and Demaree, 1999; Lonsdale et al., 1999), leading to high work efficiency. The ability to preserve plant vacuolar structure, which is often difficult with conventional electron microscopic methods (Burgess and Linstead, 1984b), and minimization of diffusion of molecules was especially important to this study, as summarized in the introduction.

Several attributes of cellular structure in seedlings fixed to optimize ultrastructure were similar to cryofixation: smooth plasma membrane in close contact with the cell wall, round organelle profiles, dense cytoplasm, vacuoles with electron dense material, straight microtubules, wide ER cisternae, and (larger vesicles associated with Golgi stacks) (Kiss et al., 1990). The high quality vacuolar preservation revealed details of the process of vacuolar implosion at the end of TE cell wall deposition (Fig. 9 b and e), which had been detected via video light microscope in isolated suspension-cultured TEs of *Zinnia elegans* (Groover et al., 1997). Sections collected at 30-50 μm intervals throughout the length of the TE differentiation zone in the radicle generated confidence in conclusions about stages of differentiation. Figure 9 b and e can be interpreted as showing an earlier and a later time after tonoplast implosion. Cytoplasmic components fill the former vacuolar space gradually, which is consistent with inherent structural organization of the cytoplasm (e.g. by cytoskeletal elements) that is not affected by release of vacuolar pressure and takes some time to be destroyed through the autolytic process.

TEs that were lightly fixed to preserve antigenicity also retained good structural preservation with: (pre-implosion) rounded vacuoles indicative of minimal loss of turgidity before cellular immobilization; stage-specific electron dense contents in vacuole; and close contact between the plasma membrane and cell wall.

The role of XCP1 and XCP2 in tracheary element autolysis

Incubation of living roots with a fluorogenic GUS substrate prior to fixation and observation in the laser scanning confocal microscope showed that GUS expressed under control of the XCP1 or XCP2 promoter was restricted to differentiating TEs. Extending previous results (Funk et al., 2002), these observations showed that promoter activity

initiated along with the onset of secondary wall thickening. Consistently, immunocytochemistry at the electron microscopic level showed that XCP1/XCP2 protein synthesis began in association with the ER and Golgi at the earliest stage of TE wall thickening at the cell corners. The proteases continued to accumulate within small, ~ 30 nm diameter vesicles with an electron dense center in the cytoplasmic compartment as secondary wall thickening progressed. Vesicles with similar appearance have been reported in other differentiating TEs (Cronshaw and Bouck, 1965). During most of secondary wall thickening, we did not observe labeling of dispersed XCP1/XCP2 within an electron transparent central vacuole, although we cannot rule out the possibility that the proteases were too dilute within the large vacuolar space to be labeled. At a late stage of secondary wall deposition, XCP1/XCP2 were labeled in association with dense aggregates within the intact central vacuole, although they also remained in the cytoplasmic compartment. The vacuolar aggregates appear very similar to those observed: (a) in senescing Arabidopsis roots in which another cysteine protease, vacuolar processing enzyme-γ (VPEγ), is involved in degradation of vacuolar invertase (Rojo et al., 2003); and (b) for vacuolar accumulations of sweet potato sporamin and barley lectin (proteins with recognized vacuolar sorting signals) in transgenic Arabidopsis (Ahmed et al., 2000). Finally, XCP1/XCP2 were observed on cellular remnants near the end of TE clearing.

Transmission electron microscopy in the developmental context revealed that cellular remnants in TEs of *xcp1* and *xcp1xcp2* plants persisted longer after the onset of final autolysis than in wild type plants. These remnants together with the observation of XCP1/XCP2 within the intact central vacuole late in TE differentiation could be viewed as consistent with the hypothesis that XCP1 and XCP2, which are processed to mature proteins

at pH 5.5, are imported into the acidic vacuole for activation prior to release upon vacuolar implosion to aid total cell clearing. Alternatively, four observations support a more specific role for XCP1 and XCP2 in degrading particular cellular components that are specifically imported into the central vacuole for degradation before final autolysis. First, cellular remnants were observed within the tonoplast of *xcp1xcp2* plants before total cell clearing had begun (Fig. 9 d). Second, the morphologically distinct remnants persisted throughout the autolytic process until they were all that remained within *xcp1* or *xcp1xcp2* TEs. Third, although TE clearing was quickly completed in *xcp2* plants, XCP2 may also have a particular role in selective degradation within the vacuole because the cellular remnants in *xcp1xcp2* TEs looked different than remnants in *xcp1* TEs. Fourth, both types of remnants in *xcp1* and *xcp1xcp2* TEs were morphologically distinct from any observed in wild type TEs, indicating that they do not represent a stage in normal autolysis. The replication of these results was extensive, leading to confidence that real phenotypic differences, not random variance due to insufficient sampling, were observed. Presently, we do not know the significance for TE differentiation of small-scale degradation within the intact vacuole before final cell clearing is enacted in association with rupture of the vacuole. Contrary to results reported for suspension cultured *Zinnia* TEs (Groover et al., 1997), we did not detect noticeable cleaning of the cytoplasm before vacuolar rupture, emphasizing the small-scale nature of initial degradation within the vacuole.

In addition to a possible specific role in degrading particular cellular components within the intact vacuole, XCP1/XCP2 were labeled on highly dispersed cellular remnants until the end of autolysis in wild-type TEs. Since complete vacuolar importation of XCP1/XCP2 was never observed, perhaps residual XCP1/XCP2 in the cytoplasm became

activated upon vacuolar rupture and participated in total cell clearing as well. Activation by removal of NH_2- and COOH-terminal propeptides in the acidic pH generated after vacuolar rupture has been proposed for cysteine proteases stored in cytoplasmic ricinosomes (Greenwood, 2005).

The ability to see cellular remnants in *xcp1* and *xcp1xcp2* plants was transient in developmental time, persisting about 100 μm above the point of total clearing in wild type TEs. It is likely that the remnants were washed away by moving water in functional TEs. The normal phenotype of *xcp1* and *xcp1xcp2* plants (data not shown) was consistent with a fully functional xylem. In a test for sensitivity to water deprivation as judged by onset of plant senescence and death, no difference between wild type or any T-DNA line was observed (data not shown).

During TE differentiation, all cellular components are degraded into more reduced molecular or non-structural forms by the action of proteases, nucleases, and hydrolases. These reduced molecules are likely to be recycled for use in other metabolic pathways in the plant because, from an energetic and evolutionary perspective, this would enhance plant survival and reproduction. However, in *xcp1* and *xcp1xcp2* knockouts, some cellular remnants could not be degraded due to loss of cysteine protease activity. Some metabolic energy that had been converted into cellular molecules remained arrested in remnants that could not be used. Although no difference in plant growth in the knockout lines grown in the laboratory were observed, in nature and over long evolutionary time this deficiency could diminish individual plant competitiveness compared to others in the population that could completely recycle TE cytoplasmic molecules.

Just before final cell clearing, the residual cell components in wild type TEs and *xcp1xcp2* TEs (except for the remnants already described that persisted) appeared highly dispersed with fibrillar elements. No residual organelle structure was visible. This change was distinctive and suggestive of a new type of enzyme or enzyme mixture, e.g. for membrane and/or primary cell wall degradation (to maximize TE conduction capacity), that might be secreted from neighboring cells or become active at the last stage of autolysis.

Cell biological processes associated with XCP1/XCP2 participation in autolysis

Absence of high density storage within the cytoplasmic compartment

In immunolabeled specimens, no large aggregates of XCP1/XCP2 in the cytoplasm were observed. Similarly, in samples fixed for optimum ultrastructural observations, no electron dense vesicles or tubules consistent with high density protein storage were observed. Therefore, in contrast to many others, XCP1/XCP2 cysteine proteases were not stored at high density prior to importation into the vacuole. Other cysteine proteases in plant vegetative cells studied so far are synthesized in the rough ER and stored at high density in swollen ER cisternae or electron dense small vacuoles derived from ER prior to their degradative function. High density storage of cysteine protease within endomembrane compartments exists in various cell types including: bean cotyledons prior to protein mobilization (Toyooka, 2000); healthy Arabidopsis seed epidermal cells to prepare for defensive cell death (Hayashi, 2001); senescing Arabidopsis root parenchyma (Rojo, 2003); seed nucellar cells that die before endosperm filling in castor bean (Greenwood, 2005); and senescing leaves of Arabidopsis and soybean (Otegui, 2005). Lack of specific cytoplasmic storage mechanisms in TEs may relate to rapid differentiation that requires ~ 8 - 15 h between the first visible signs of cellular differentiation (banding of microtubules) and cell death

(Groover et al., 1997; Roberts et al., 2004) in contrast to other cell differentiation and death events involving cysteine proteases that require many days (Greenwood, 2005).

Papain-like proteases generally have signal peptides dictating either lysosomal (vacuolar) accumulation or secretion. The papain-like peptidases, XCP1, XCP2, and p48-17 (Ye and Varner, 1996) expressed in TEs all have a unique NH_2-terminal sequence, [D/E][F/Y]SI[V/L]GY of unknown function that is shared only with papaya laticifer proteases I, III, and IV. This motif occupies the same relative position as the NPIR domain involved in vacuolar targeting of aleurain (Holwerda et al., 1992) and AtALEU (Ahmed et al., 2000). Unlike complete autolysis of TEs, laticifers (the source of papain) undergo selective autolysis of cytoplasmic contents and remain alive at maturity. Immunolabeling of laticifers with a polyclonal antibody raised against chymopapain after traditional chemical fixation showed sparse labeling mainly close to the ER and within ~1 μm diameter vacuoles (Ying et al., 1994), but these did not have electron dense contents as was observed for other cysteine protease storage vacuoles (Greenwood, 2005; Otegui et al., 2005). The conclusions on cysteine protease subcellular location within laticifers must be considered preliminary because of absence of proof of specificity of the antibody, mostly low magnification images, and sparse labeling that could be non-specific in some cases (Ying et al., 1994). It would be of interest to determine if the [D/E][F/Y]SI[V/L]GY domain specifies retention of cysteine proteases in small vesicles that remain dispersed throughout the cytoplasm before final importation into the vacuole in laticifers as well as TEs.

Changes in vacuolar function

A first sign of changing function of the central vacuole to facilitate autolysis is the intrusion of cytoplasmic contents into the area of a large central vacuole that retains its

tonoplast and rounded periphery (see results described above in specimens fixed for immunolabeling). Cytoplasmic contents might become part of the central vacuole through pinching off of trans-vacuolar cytoplasmic strands as was suggested based on early electron microscopy of pine tracheids (Wodzicki and Humphreys, 1972), delivery of contents of autophagic vacuoles, and/or fusion of other cytoplasmic vesicles with the vacuole. Our data allow all of these possibilities. The vacuolar aggregates containing XCP1/XCP2 were usually associated with the tonoplast boundary and often showed continuity with the cytoplasm; therefore, they could arise from transvacuolar cytoplasmic strands. Arabidopsis TEs had double membraned structures resembling autophagic vacuoles, and accumulation of large vesicles was observed near the tonoplast. However, since XCP1/XCP2 were not ever labeled densely in the cytoplasm or in dense aggregates near the vacuole, these cysteine proteases must be imported by another mechanism, probably through fusion of small vesicles with the tonoplast. At the same developmental time as aggregates containing XCP1/XCP2 appeared in the intact central vacuole, many swollen ER cisternae were observed in the cytoplasm, which agrees with other observations of gradual cellular breakdown before final autolysis (Burgess and Linstead, 1984a; Van Doorn, 2005). The final collapse of the tonoplast occurred in a second stage to effect total TE clearing.

Overall model for cellular behavior of XCP1/XCP2 cysteine proteases

Figure 10 demonstrates a model in the light of our findings about cellular trafficking and processing of XCP1/XCP2 cysteine proteases. XCP1/XCP2 are papain-like prepropeptidases that are synthesized in rough endoplasmic reticulum (rER). The pre or N-terminal signal sequence facilitates protease transfer into the ER as commonly seen in many proteins as well as papain-like cysteine proteases (Bromme and Petanceska, 2001). After

leaving the ER, the two proteases are transferred to the Golgi. XCP1/XCP2 leave the Golgi in approximately 30 nm vesicles. In early stages of TE differentiation and during secondary wall synthesis, XCP1/XCP2 localize mainly in cytoplasm. When secondary wall synthesis is complete, some XCP1/XCP2 are loaded into vacuole through an unknown mechanism where they localize onto cytoplasmic components, which were also internalized. At low pH of vacuole, XCP1/XCP2 become active by the removal of prodomain and start degradation that occurs before vacuolar collapse. Later on in TE differentiation, vacuole implosion acidifies the cytoplasm where cytoplasmic XCP1/XCP2 become active for further degradation of the cell. XCP1/XCP2 are localized on cytoplasmic remnants until the end of TE clearing.

References

Ahmed S, Rojo E, Kovaleva V, Venkataraman S, Dombrowski J, Matsuoka K, Raikhel, N (2000) The plant vacuolar sorting receptor AtELP is involved in transport of NH(2)-terminal propeptide-containing vacuolar proteins in *Arabidopsis thaliana*. J Cell Biol 149: 1335-1344.

Ameisen JC (2002) On the origin, evolution, and nature of programmed cell death: a timeline of four billion years. Cell Death Differ 9: 367-393.

Avci U, Beers EP, Haigler CH. XCP1 and XCP2 cysteine proteases aid autolysis in differentiating tracheary elements. In preparation for publication.

Beers EP (1997) Progrrammed cell death during plant growth and development. Cell Death Differ 4: 649-661.

Beers EP, Freeman TB (1997) Proteinase activity during tracheary element differentiation in *Zinnia* mesophyll cultures. Plant Physiol 113: 873-880.

Beers EP, Woffenden BJ, Zhao C (2000) Plant proteolytic enzymes: possible roles during programmed cell death. Plant Mol Biol 44: 399-415.

Beers EP and McDowell JM (2001) Regulation and execution of programmed cell death in response to pathogens, stress and developmental cues. Curr Opin Plant Biol 4: 561-567.

Beers EP, Jones AM, Dickerman AW. (2004) The S8 serine, C1A cysteine and A1 aspartic protease families in Arabidopsis. Phytochemistry 65: 43-58.

Benhamou, N., Noel, S., Grenier, J., and Asselin, A (1991) Microwave energy fixation of plant tissue: an alternative approach that provides excellent preservation of ultrastructure and antigenicity. J Electron Microsc. Tech. 17: 81-94.

Bozhkov PV, Suarez MF, Filonova LH, Daniel G, Zamyatnin AA Jr, Rodriguez-Nieto S, Zhivotovsky G, Smertenko A (2005) Cysteine protease mcII-Pa executes programmed cell death during plant embryogenesis. PNAS 102: 14463-14468.

Bromme D, Petanceska S (2001) Papain-like cysteine proteases and their implications in neurodegenerative diseases. In: Role of proteases in the pathophysiology of neurodegenerative diseases. New York, Kluwer, 47-61 pp.

Burgess J, Linstead P (1984a) *In-vitro* tracheary element formation: structural studies and the effect of tri-iodobenzoic acid. Planta 160: 481-489.

Burgess J, Linstead P (1984b) Comparison of tracheary element differentiation in intact leaves and isolated mesophyll cells if Zinnia elegans. Micron Microscopia Acta 15: 153-160.

Busse JS, Evert RF (1999) Pattern of differentiation of the first vascular elements in the embryo and seedling of Arabidopsis thaliana. Int J Plant Sci 160: 1-13.

Cronshaw J, and Bouck GB (1965) The fine structure of differentiating xylem elements. J. Cell Biol. 24: 415-431.

Dolan L, Janmaat K, Willemsen V, Linstead P, Poethig S, Roberts K, Scheres B (1993) Cellular organization of the *Arabidopsis thaliana* root. Development 119:71-84.

Fleming AJ, Manzara T, Gruissem W, Kuhlemeier C (1996) Fluorescent visualization of GUS activity and RT-PCR analysis of gene expression in the shoot apical meristem. Plant J 10: 745 – 754.

Fukuda H (1997b) Programmed cell death during vascular system formation. Cell Death Differ 4:684–688.

Fukuda H (2000) Programmed cell death of tracheary elements as a paradigm in plants. Plant Mol Biol 44: 245-53.

Funk V, Kositsup B, Zhao C, Beers EP (2002) The Arabidopsis xylem peptidase XCP1 is a tracheary element vacuolar protein that may be a papain ortholog. Plant Physiol. 128: 84-94.

Giberson RT and Demaree RS (1999) Microwave processing technique for electron microscopy: A four-hour protocol. Methods in Molecular Biology 117: Electron Microscopy Methods and Protocols, 145 – 158.

Gilchrist D (1997) Mycotoxins reveal connections between plants and animals in apoptosis and ceramide signaling. Cell Death Differ 4: 689-698.

Greenberg JT (1996) Programmed cell death: A way of life for plants. PNAS 93: 12094-12097.

Greenwood JS, Helm M, Gietl C (2005) Ricinosomes and endosperm transfer cell structure in programmed cell death of the nucellus during Ricinus seed development. Proc Natl Acad Sci U S A. 8; 102(6): 2238-43. Epub 2005 Jan 31.

Groover A, DeWitt N, Heidel A, Jones A (1997) Programmed cell death of plant tracheary elements differentiating in vitro. Protoplasma 196: 197-211.

Groover A, Jones AM (1999) Tracheary element differentiation uses a novel mechanism coordinating programmed cell death and secondary wall synthesis. Plant Physiol 119: 375-384.

Groves MR, Taylor MA, Scott M, Cummings NJ, Pickersgill RW, Jenkins JA (1996) The prosequence of procaricain forms an alpha-helical domain that prevents access to the substrate-binding cleft. Structure 4: 1193-1203.

Hayashi Y, Yamada K, Shimada T, Matsushima R, Nishizawa NK, Nishimura M, Hara-Nishimura I (2001) A proteinase-storing body that prepares for cell death or stresses in the epidermal cells of Arabidopsis. Plant Cell Physiol. 42(9): 894-899.

Heumann HG (1992) Microwave-stimulated glutaraldehyde and osmium tetroxide fixation of plant tissue: ultrastructural preservation in seconds. Histochem 97: 241-347.

Holwerda BC, Padgett HS, Rogers JC (1992) Proaleurain vacuolar targeting is mediated by short contiguous peptide interactions. Plant Cell 4: 307-318.

Kiss JZ, Giddings ThH Jr, Staehelin LA, Sack FD (1990) Comparison of the ultrastructure of conventionally fixed and high pressure frozen/freeze substituted root tips of *Nicotiana* and *Arabidopsis*. Protoplasma 157: 64-74.

Kok LP and Boon ME (1992) Microwave cookbook for microscopists: Art and Science of Visualization, 3rd edition. Coulomb Press Leyden: Leiden. 432 pp.

Kuriyama H (1999) Loss of tonoplast integrity programmed in tracheary element differentiation. Plant Physiol 121: 763-774.

Kuriyama H and Fukuda H (2002) Developmental programmed cell death in plants. Curr Opin Plant Biol 5:568-573.

Login GR and Dvorak AM (1988) Microwave fixation provides excellent preservation of tissue, cells, and antigens for light and electron microscopy. Histochem. J. 20: 373-387.

Lonsdale JE, McDonald KL and Jones RL (1999) High pressure freezing and freeze substitution reveal new aspects of fine structure and maintain protein antigenicity in barley aleurone cells. Plant J 17: 221 – 229.

Lukowitz W, Gillmor CS, and Scheible WR (2000) Positional cloning in Arabidopsis. Why it feels good to have a genome initiative working for you. Plant Physiol 123: 795-805.

Minami A, Fukuda H (1995) Transient and specific expression of a cysteine endoproteinase associated with autolysis during differentiation of Zinnia mesophyll cells into tracheary elements. Plant Cell Physiol 36: 1599-1606.

Mittler R and Shulaev V (2004) Programmed cell death in plants: future perspectives, applications and methods. In: Programmed Cell Death in Plants, J. Gray (ed.) Blackwell Publishing. Oxford, UK pp. 251-264.

Mizuhira V, Hasegawa H, and Notoya, M (2000) Fixation and imaging of biological elements: heavy metals, diffusible substances, ions, peptides, and lipids. Prog Histochem Cytochem 35: 67-183.

Morgan PW and Drew MC (2004) Plant cell death and differentiation. In: Programmed Cell Death and Related Processes, Nooden LD (ed.), Academic Press. pp. 19-36.

Nakaune S, Yamada K, Kondo M, Kato T, Tabata S, Nishimura M, Hara-Nishimura I (2005) A vacuolar processing enzyme, gammaVPE, is involved in seed coat formation at the early stage of seed development. Plant Cell 17: 876-887.

Obara K, Kuriyama H, Fukuda H (2001) Direct evidence of active and rapid nuclear degradation triggered by vacuole rupture during programmed cell death in Zinnia. Plant Physiol 125: 615-626.

Otegui MS, Noh YS, Martinez DE, Vila Petroff MG, Staehelin LA, Amasino RM, Guiamet JJ (2005) Senescence-associated vacuoles with intense proteolytic activity develop in leaves of Arabidopsis and soybean. Plant J 41(6): 831-44.

Reynolds ES (1963) The use of lead citrate at high pH as an electron-opaque stain in electron microscopy. J Cell Biol 17: 208-212.

Roberts AW, Frost AO, Roberts EM and Haigler CH (2004) Roles of microtubules and cellulose microfibril assembly in the localization of secondary cell wall synthesis in developing tracheary elements. Protoplasma 224: 217-229.

Rojo E, Zouhar J, Carter C, Kovaleva V, Raikhel NV (2003) A unique mechanism for protein processing and degradation in *Arabidopsis thaliana*. Proc Natl Acad Sci USA 100: 7389 – 7394.

Russin WA, Trivett CL (2001) Vacuum-Microwave combination for processing plant tissues for electron microscopy. In: Microwave Techniques and Protocols, Giberson RT and Demaree RS, Jr, eds, Humana Press, Totowa, JH, pp 25-35.

Salnikov VV, Grimson MJ, Delmer DP, Haigler CH (2001) Sucrose synthase localizes to cellulose synthesis sites in tracheary elements. Phytochemistry 57: 823-833.

Salnikov V, Grimson MJ, Seagull RW and Haigler CH (2003) Localization of sucrose synthase and callose in freeze substituted, secondary wall stage, cotton fibers. Protoplasma 221: 175-184.

Tooyoka K, Okamoto T, Minamikawa T (2000) Mass transport of a proform of a KDEL-tailed cysteine proteinase (SH-EP) to protein storage vacuoles by endoplasmic reticulum-derived vesicle is involved in protein moblization in germinating seeds. J Cell Biol 148: 453-463.

van der Hoorn RA, Leeuwenburgh MA, Bogyo M, Joosten MH, Peck SC (2004) Activity profiling of papain-like cysteine proteases in plants. Plant Physiol 135:1170-1178.

van Doorn WG, Woltering EJ (2005) Many ways to exit. Cell death categories in plants. Trends in Plant Science 10: 117-122.

van Doorn WG (2005) Plant programmed cell death and the point of no return. Trends in Plant Science 10: 478-483.

Wodzicki TJ, Humphreys WJ (1972) Cytodifferentiation of maturing pine tracheids: the final stage. Tissue and Cell 4: 525-528.

Ye ZH, Varner JR (1996) Induction of cysteine and serine proteinases during xylogenesis in *Zinnia elegans*. Plant Mol Biol 30: 1233-1246.

Woffenden BJ, Freeman TB, Beers EP (1998) Proteasome inhibitors prevent tracheary element differentiation in Zinnia mesophyll cultures. Plant Physiol 118: 419-430.

Ying Z, Ben-ren J, Bing Y (1994) Laticifer ultrastructural and immunochemical studies of papain in *Carica papaya*. Acta Botanica Sinica 36: 497-501.

Zhao C, Johnson BJ, Kositsup B, Beers EP (2000) Exploiting secondary growth in Arabidopsis: Construction of xylem and bark cDNA libraries and cloning of three xylem endopeptidases. Plant Physiol 123: 1185-1196.

Zimmermann P, Hirsch-Hoffmann M, Hennig L, Gruissem W (2004) GENEVESTIGATOR. Arabidopsis microarray database and analysis toolbox. Plant Physiol 136: 2621-2632.

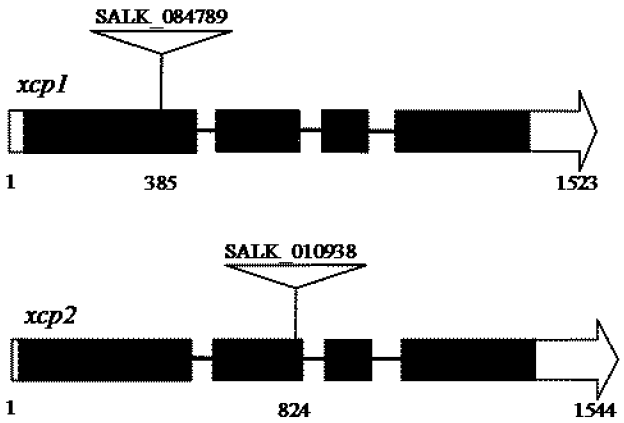

Figure 1. T-DNA insertion sites in SALK_084789 (*xcp1*) and SALK_010938 *(xcp2)* lines used for this study. Exons are represented by black boxes, untranslated regions by white boxes; introns by lines, T-DNA insertions by triangles. Numbers beneath each diagram indicate the lengths of full length genomic sequences and positions of T-DNA inserts. Figure provided by Dr. Eric Beers.

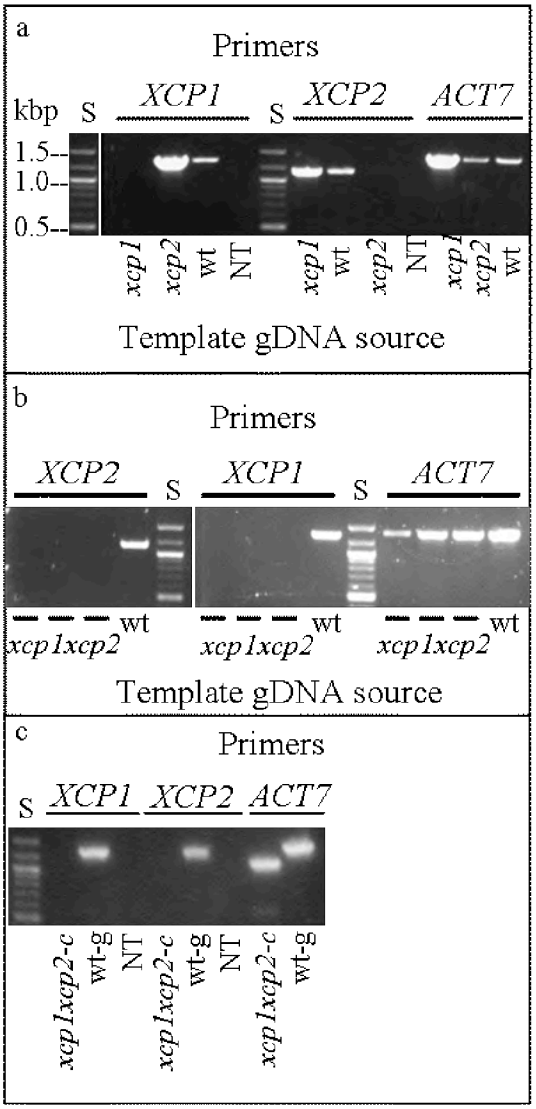

Figure 2. Genotyping and detection of transcript for *XCP1* and *XCP2* T-DNA insertion lines. (a) and (b). Ethidium bromide-stained gels show PCR-based confirmation of homozygosity of *xcp1*, *xcp2* (a) and *xcp1xcp2* lines (b) used for this study. All T-DNA insertion lines used tested positive for PCR product amplified from T-DNA-specific/gene-specific primer combinations (data not shown) and negative for amplification of wild type genes (a and b). Gene-specific primers used are shown above the gel images. Sources of template genomic (g) DNA are shown below the gel images. *ACT7* primers were used for positive controls with each source of gDNA template. Negative controls were primer-only, no-template (NT) reactions. Three plants from a single *xcp1xcp2* line were tested (b). (c) Ethidium bromide-stained gel showing that RT-PCR using RNA from *xcp1xcp2* plants yielded no product corresponding to *XCP1* and *XCP2*. PCR positive controls were performed with wild type gDNA (wt-g) or *xcp1xcp2* cDNA (*xcp1xcp2-c*) and primers as indicated above the gel image. Sizes of three benchmark rungs of 100-bp DNA ladder (a, lane S) apply to standards used in all gels. Figure provided by Dr. Eric Beers.

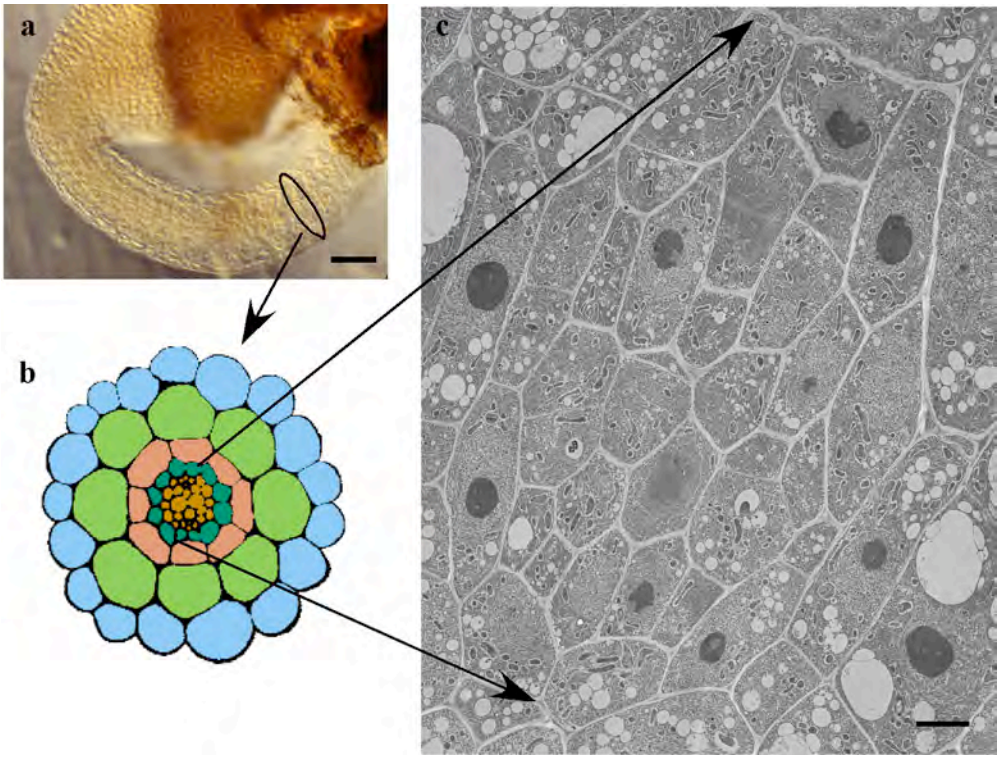

Figure 3. Illustration of the root stele in Arabidopsis; (a) 2.5 day-old Arabidopsis seedling flat-embedded and ready for sectioning (photographed with DIC optics in the light microscope)**.** (b) Diagram showing a corresponding cross section of the root region circled in (a) (Dolan et al., 1993). Starting from the center, each colored cell layer in b corresponds to stele, pericycle, endodermis, cortex and epidermis, respectively. (c) Transmission electron micrograph showing cells that would have differentiated into vascular tissue within the stele. Bar in (a) = 100 μm, and bar in (c) = 2 μm.

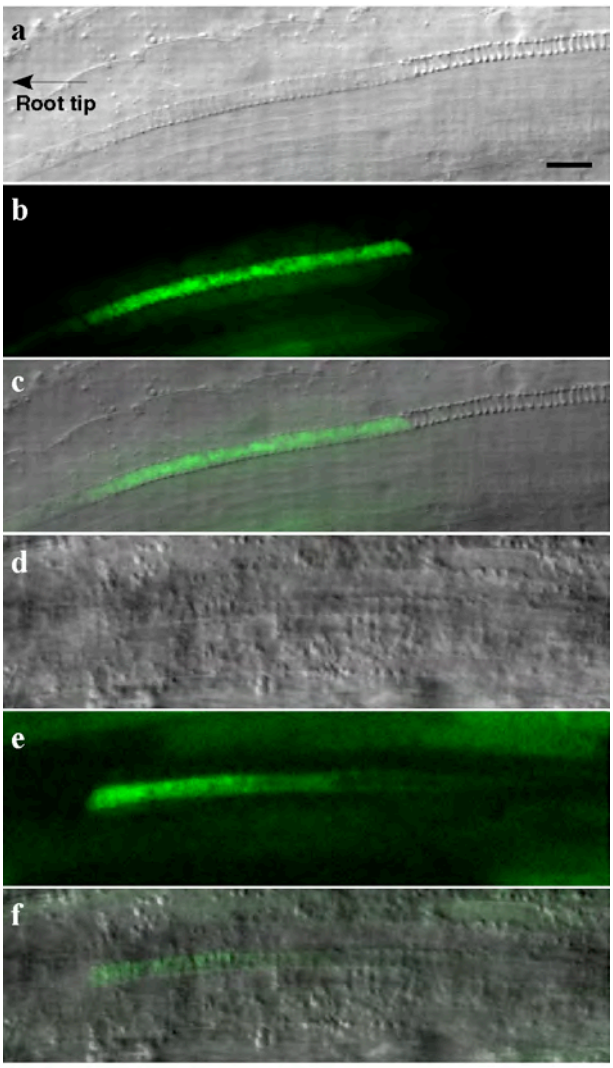

Figure 4. Light micrographs of differentiating roots of Arabidopsis seedlings transformed with XCP1 (a-c) or XCP2 (d-f) promoter/GUS fusions. DIC (a, d) shows the first differentiating TEs behind the root tip (arrow). The green fluorescent GUS signal (with Imagene Green substrate) was detected specifically in TEs (b, e), along with the first patterned secondary wall thickenings visualized in DIC (overlay in c, f). Bar in (a) = 10 μm for all micrographs.

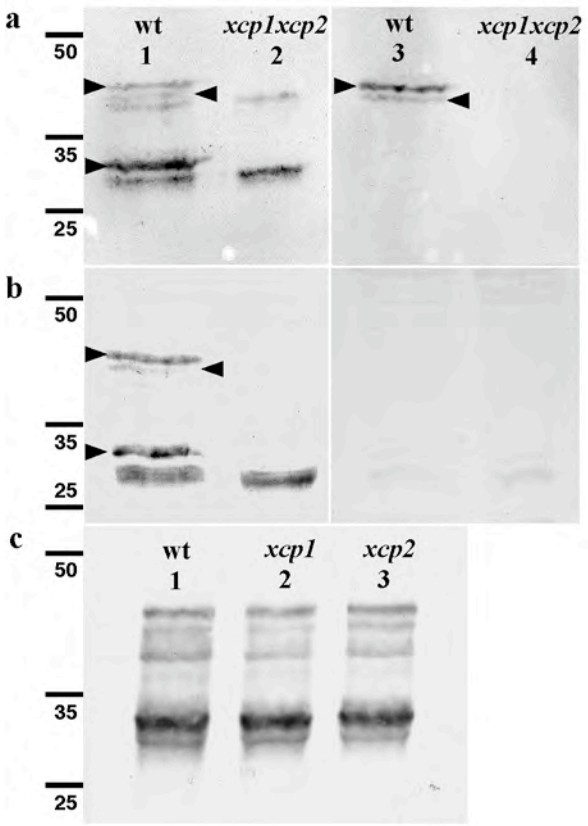

Figure 5. Immunoblot analysis of xylem protein extracts with anti-XCP1 and anti-XCP2 antibodies. The data identified mature and proproteins and confirmed the lack of XCP1 and XCP2 expression in *xcp1xcp2* plants. (a) Affinity-purified anti-XCP2 labeled five bands in wild type, three of which (lane 1, arrowheads) are attributable to XCP2 and XCP1 based on their absence from *xcp1xcp2* plants (lane 2). The two slowest migrating polypeptides (lane 1, upper arrowheads) were identified as the XCP2 and XCP1 proprotein by labeling with affinity-purified anti-XCP2P in wild type (lane 3, arrowheads), but not in *xcp1xcp2* extracts (lane 4). (b) Anti-XCP2M (crude serum) labeled the same five polypeptides in wild-type (lane 1; compare to b) and, again, the same three bands were absent from *xcp1xcp2* extracts (lane 2). The preimmune serum for anti-XCP2M gave barely detectable labeling of several polypeptides, none of which comigrated with XCP1 or XCP2, in both wild type (lane 3) and *xcp1xcp2* extracts (lane 4). (c) Affinity purified anti-XCP2 antibodies recognized XCP2 and XCP1. Identical banding patterns were detected in xylem protein extracts from wild type (lane1) and two single T-DNA insertion lines, *xcp1* (lane 2) and *xcp2* (lane 3).

Figure 6. Immunolabeling through several sequential stages of TE differentiation, labeled 2-6 as judged from the thickness of the secondary wall and the characteristics of the central vacuole. In each case, the upper TE in the pair is more advanced than the one below. XCP1/XCP2 accumulate in the cytoplasm at the earliest stage of secondary wall thickening, while initially being excluded from the merging small vacuoles (a2). Cytoplasmic accumulation continues through the stage of forming a unified central vacuole and thicker secondary walls (b2, c3). When the walls are quite thick, XCP1/XCP2 co-localized with apparent cytoplasmic elements within the central vacuole (a4, b5). After vacuolar rupture, XCP1/XCP2 proteins persisted on cytoplasmic remnants throughout the TE clearing process (c6). Labeling was achieved with either anti-XCP2M (a, c) or affinity purified anti-XCP2 (b). All colloidal gold particles are highlighted with red dots. Several controls for electron microscopic immunolabeling further demonstrated that the antisera used were cross-reactive with XCP1 and XCP2, but not with other proteins in differentiating xylem elements. (d) Sparse labeling with the preimmune serum to anti-XCP2M including a parenchyma cell (upper right); (e) TEs in *xcp1* single knockout plants retained sparse labeling with affinity purified anti-XCP2; (f) TEs in *xcp2* single knockout plants retained sparse labeling with anti-XCP2M; (g) TEs in *xcp1xcp2* double knockout plants did not show labeling with anti-XCP2M. Gold particles were highlighted by red dots. Bar in a = 1 μm for (a-d). Bar in (e) = 1 μm for (e-f).

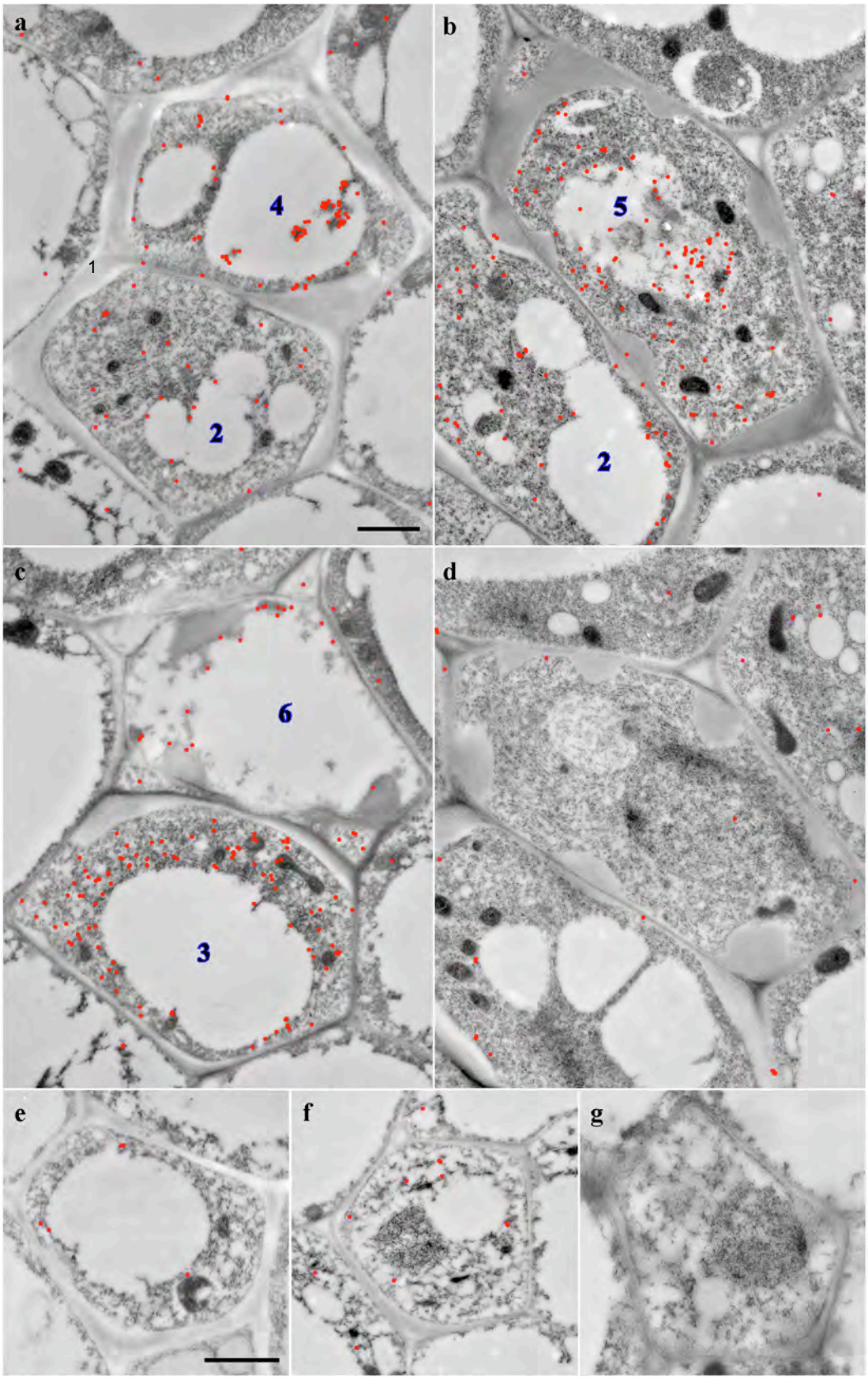
a
4
1
2
b
5
2
c
6
3
d
e
f
g

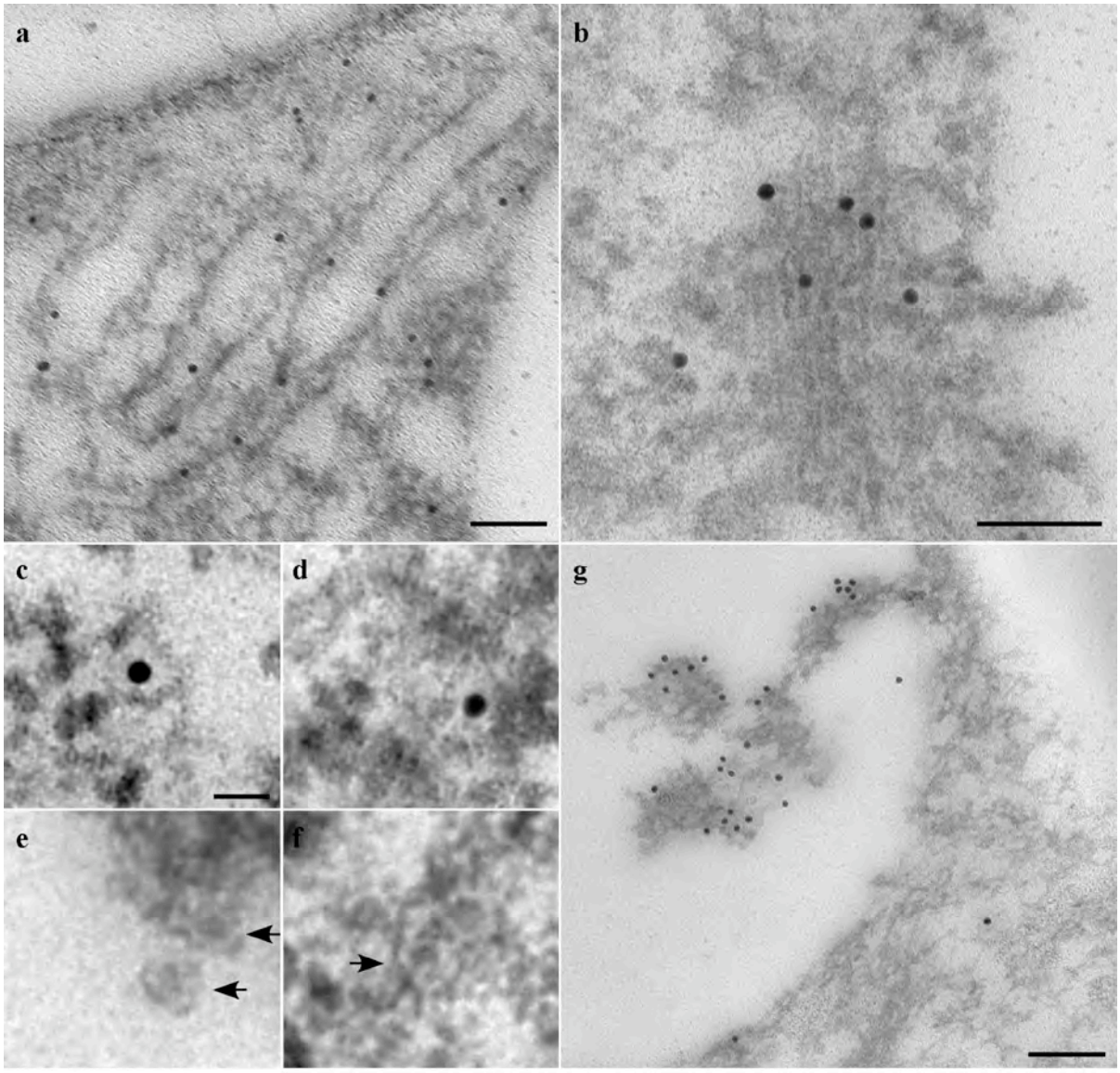

Figure 7. Immunolabeling with affinity purified anti-XCP2 of particular cell structures in wild-type TEs. (a) Swollen cisternae of endoplasmic reticulum. There was a large secondary wall thickening visible on the other side of the cell (data not shown), although the vacuole was still turgid; (b) Golgi apparatus; (c-f) Immunogold labeled and non-labeled vesicles (arrows) involved in the trafficking of cysteine proteases in TEs; (g) Apparent cytoplasmic contents imported into the vacuole. Bars = 100 nm for (a, b, g) and 20 nm in (c) for (c-f).

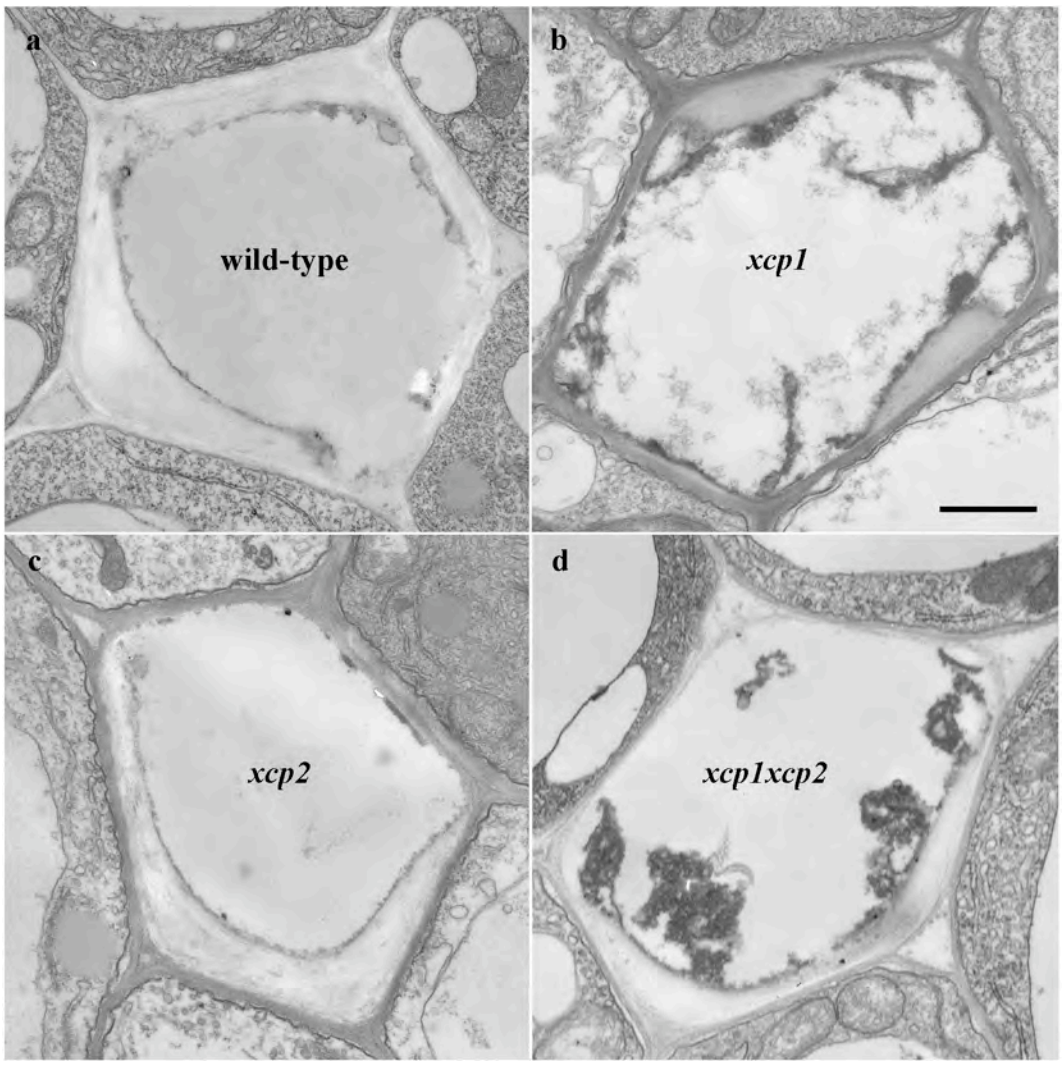

Figure 8. Electron micrographs of TEs fixed for optimal ultrastructure revealed that deficiency in XCP1 caused delayed clearing during autolysis. (a) Completely-cleared wild-type TE; (b) Incomplete clearing in a *xcp1* TE; (c) Complete clearing in a *xcp2* TE; (d) Incomplete clearing in an *xcp1xcp2* TE. The different morphology of remnants in B and D was consistent, suggesting that XCP2 had a specific effect on autolysis even though its absence did not delay clearing in a detectable manner if XCP1 was present. Bar in b = 1 μm for (a-d).

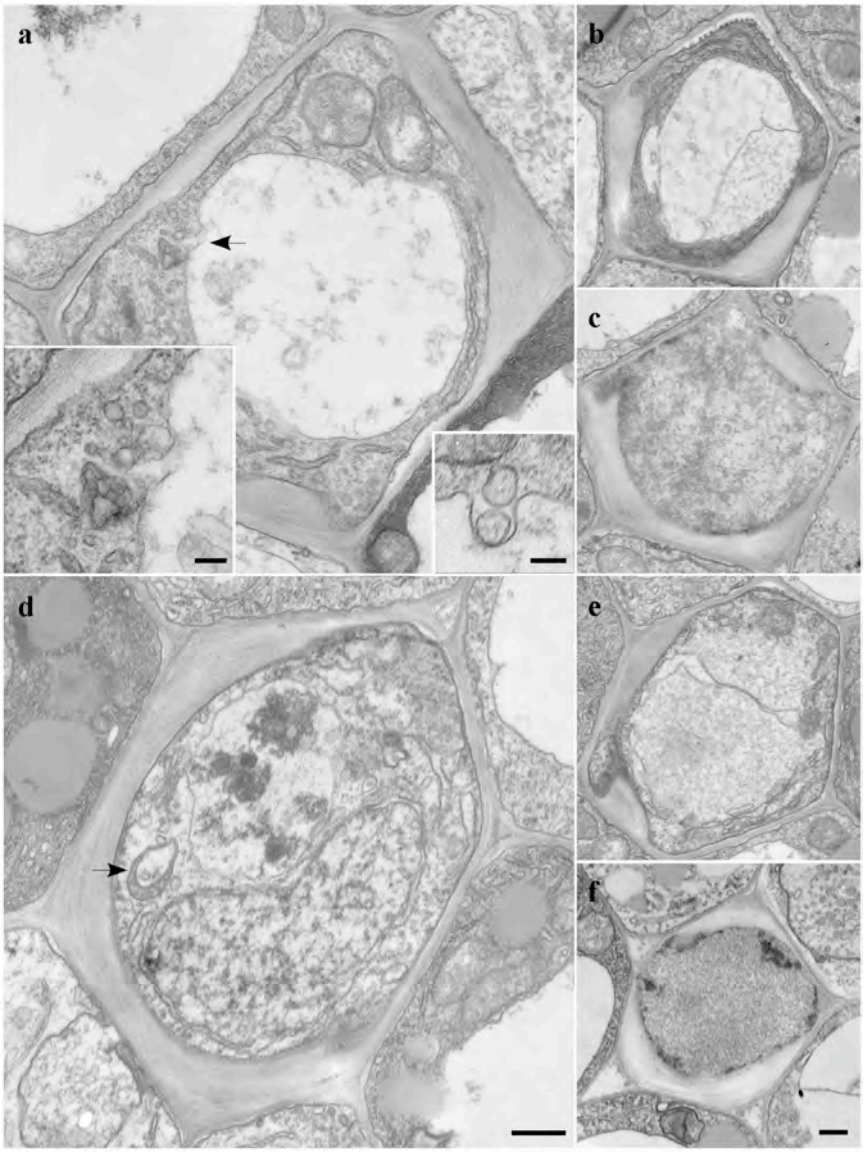

Figure 9. New ultrastructural features of TE autolysis. Vesicles in close proximity to tonoplast were identified as indicated by an arrow in (a) with the magnified image inset at the left bottom corner. The inset at the bottom right shows an image from another TE (overview not shown): here two vesicles may have been about to fuse with or be taken into the vacuole. The collapse of the central vacuole along with diffusion of the cytoplasm into the former vacuolar space was observed in TEs of wild-type (b) and *xcp1xcp2* (e) plants. Near the end of autolysis, a distinct phase of extreme dispersion of remaining cytoplasmic remnants was seen in TEs of wild-type (c) and *xcp1xcp2* (f) plants, except that the undigested components in *xcp1xcp2* plants were present as a darkly-staining residue. These remnants can also be observed inside the vacuole in an earlier stage as shown in (d). The arrow in (d) pointed an autophagic vacuole. Bar in (f) = 1 μm for (b, c, e, f). Bar in (d) = 1 μm for (a, d). Bars shown in bottom images in (a) are equal to 100 nm.

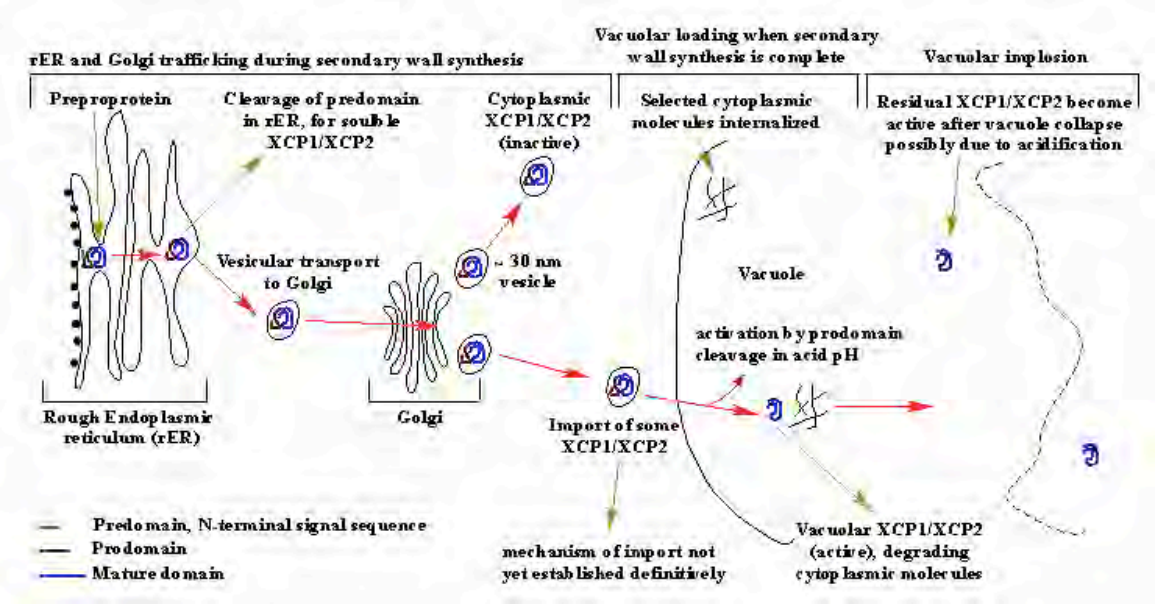

Figure 10. Overall model for cellular behavior of XCP1/XCP2 cysteine proteases. Cleavage of the predomain occurred in rER, and proteases with their prodomain plus mature domain were transferred to the Golgi. After processing in the Golgi, XCP1/XCP2 first appeared dispersed in the cytoplasm. The evidence suggested that the proteases were stored in vesicles with the diameter of approximately 30 nm. Later, near the completion of secondary wall synthesis, some of the XCP1/XCP2 molecules were transported into the vacuole. Within the still-intact vacuole, the proteases were localized on internalized cytoplasmic components. Based on undegraded remnants appearing in *xcp1* and *xcp1xcp2* knockouts, we hypothesize that proteolytic degradation occurred in the vacuole after XCP1/XCP2 became actived by prodomain cleavage in acidic pH. Subsequently, the central vacuole collapsed, and at this time the acidification of cytoplasm would activate residual XCP1/XCP2 in the cytoplasm to eventually degrade all their targets until the end of the clearing of TEs.

CHAPTER 4

Role of the NAC Transcription Factor XND1 in tracheary element differentiation in *Arabidopsis thaliana*

Introduction

Transcription factors

Development and differentiation in plants are continuous processes due to action of meristematic cells throughout the plant life cycle. Meristems contain totipotent stem cells that allow plants to generate new organs or a new plant, which is one of the main differences compared to animals. In this scheme, transcription factors (TFs) and phytohormones are main regulators of meristematic growth and development (Long and Benfey, 2006).

Regulation of gene expression in response to developmental programs and environmental changes is often controlled by TFs. Since TFs are very important in determination of cellular activities, alteration in gene expression of TFs causes dramatic changes to plants (Liu et al., 1999).

Over 5% of Arabidopsis genome codes more than 1500 TFs (Riechmann et al., 2000). Most plant TFs contains 4 domains: (1) a DNA-binding region, by which TFs specifically bind to *cis*-acting elements of the gene; (2) an oligomerization site, which determines the specificity and affinity of TFs; (3) a transcription regulation domain, the domain that functions as either repressor or activator; and (4) a nuclear localization signal, which determines selectivity for entering the nucleus (Liu et al., 1999).

The main methods used in plant studies to identify the role of TFs are over-expression and antisense technology. As in the study reported here, over-expression involves high level expression of a target gene under control of either a constitutive or tissue-specific promoter in transgenic plants. This strategy may result in plants with a higher level of TFs or plants with a lower level of the manipulated TF due to co-suppression (Schwechheimer et al., 1998).

How do NACs fit into overall scheme of transcription factors affecting xylem?

The NAC family transcription factors, with 110 members in Arabidopsis, are plant specific and involved in cell elongation, apical meristem development, lateral root growth and stress responses (Ooka et al., 2003; Olsen et al., 2005). All NAC transcription factors have a NAC domain in the N-terminal region, a domain initially identified in the petunia NO APICAL MERISTEM (NAM) gene, and the Arabidopsis ATAF1, ATAF2, and CUC2 genes (Aida et al., 1997).

In primary roots of Arabidopsis, VND6 (VASCULAR RELATED NAC DOMAIN) and VND7 are suggested to be involved in differentiation of metaxylem and protoxylem, respectively (Kubo et al., 2005). Over-expression of NST1 and NST2 (NAC SECONDARY WALL THICKENING PROMOTING FACTOR) caused the promotion of secondary wall thickening, and these TFs were required for anther dehiscence in Arabidopsis (Mitsuda et al., 2005). Recent research in Arabidopsis revealed that NST1 and NST3 together are redundant key regulators of the formation of secondary walls in woody tissues (Mitsuda et al., 2007). NAC transcription factors were also proposed to be possible regulators of secondary wall thickening in TEs since ectopic expression of NST1 and NST2 resulted in TE-like structures in epidermal cells (Mitsuda et al., 2005). Another study showed that simultaneous inhibition of NST1 and SND1 (SECONDARY WALL-ASSOCIATED NAC DOMAIN PROTEIN) by RNA interference (RNAi) or T-DNA knockouts resulted into loss of secondary wall formation in fiber of *Arabidopsis thaliana* (Zhong et al., 2007). Overall, these findings suggest that these NAC domain TFs are master regulators and switches of secondary wall formation in plants. Identification of all NAC TFs is very important, perhaps eventually leading to manipulation of wood quality and production.

Xylem NAC Domain1 (XND1)

In collaboration with Dr. Eric Beers and his lab at Virginia Tech, who provided the genetically altered lines, microscopic observations were made of the effects of over-expression of XND1 in Arabidopsis. XND1 was previously reported as highly expressed in xylem (Zhao et al., 2005). Over-expression of XND1 resulted in dwarf plants with blocked xylem differentiation that die prematurely (Beers Lab, unpublished data). XND1 loss-of-function mutants showed an approximately one-third reduction in height compared to wild type Arabidopsis, ecotype Landsberg. Fiber and vessel member length was also shortened in similar degree (Beers Lab, unpublished data). In this study, we examined the T-DNA and over-expressor lines to allow more detailed characterization of phenotypes at the cellular level.

Materials and Methods

To accomplish this work, I received from Dr. Beers Lab the following reagents and materials:

- Wild-type and *XND1* T-DNA knockout line (9 week-old)
- XND1 over-expressor and wild-type like plants

Full method descriptions for production of their materials are in preparation for publication (Zhao et al., in preparation).

T2 plants segregating for WT and dwarf phenotypes were obtained from WT-like, herbicide-resistant T1 plants transformed with *Pro$_{35S}$:XND1-HAStrep* and grown under a 14/10 h day/night cycle at 21 – 22°C until harvest at 24 days old. Over-expressors were extremely stunted, and normally growing plants used as WT controls were selected based on death of individual leaves painted with 18.19% Glufosinate-ammonium (Ignite Herbicide;

Bayer CropScience). At least three independent plants were examined in each case, and images shown are representative. The GT_5_12667 *Ds* null line for *XND1* was grown to maturity (~ 9 weeks) along with WT plants as controls.

All samples were fixed and embedded for light and electron microscopy by use of a laboratory-grade microwave with integrated specimen temperature control and vacuum (Biowave Model 34700; Pelco, Redding, CA). Primary fixation (2.5 % glutaraldehyde (v/v) in 100 mM sodium cacodylate buffer, pH 7.2) occurred in two phases, both under vacuum (20 in Hg) and with sample temperature restricted to 36.5°C throughout the processing: (a) 3 x 5 min, 150 W, with 1 min on ice between pulses; and (b) 6 x 10 seconds, 250 W, with 20 second intervals. After rinsing in buffer (3 x 1 min, 250 W, no vacuum), secondary fixation [1% osmium tetroxide/1.5% potassium ferricyanide (w/v) in 100 mM sodium cacodylate buffer, pH 7.2] occurred (3 x 1 min, 150 W, with vacuum). Samples were dehydrated in acetone (30, 50, 70, 90, 100%; 250W, 40 sec each step, no vacuum), and infiltrated in Spurr's resin: acetone (1:3, 1:1, 3:1) followed by 3 x 100% resin (250 W, 3 min each step, with vacuum). Infiltrated samples were flat-embedded in fresh 100% resin as previously described (Salnikov et al., 2003), followed by polymerization overnight at 60°C.

For sectioning, a ~2 mm^2 resin sector containing a hypocotyl region adjacent to the root was cut out with a razor blade and glued (QuickTite SuperGlue, Manco Inc., Avon, OH) vertically to the side of a blank Spurr's resin block. Thick or thin sections were made with glass or diamond knife, respectively, on an ultramicrotome (MT2-B, Sorvall). For light or fluorescence microscopy, thick sections were affixed to slides by low temperature heating, stained to provide general contrast with 0.05% (w/v) Toluidine Blue (1 min) or, to highlight various ß-1,4-linked cell wall polysaccharides including cellulose (Taylor et al., 1996), with

0.005% (w/v) Tinopal LPW (10 min; dark) and washed briefly in water. Tinopal-stained sections were mounted in anti-fade solution [0.1% o-phenylenediamine in 90% glycerol/10% Tris buffered saline (v/v, pH 8.6)], and all sections were photographed under identical conditions with a Q-Color 5 digital camera (Olympus) on an upright microscope (BH2, Olympus) equipped with fluorescence optics and Violet filter set (excitation, 20 nm BP at 405 nm; emission > 455 nm) (Olympus Corporation, Center Valley, PA). Thin sections for electron microscopy were collected on Formvar-coated grids and stained with 2% uranyl acetate (in 70% ethanol (v/v)) for 15 minutes and lead citrate (Reynolds, 1963) for 4 minutes in humid Petri dishes (including sodium hydroxide pellets to trap CO_2 during lead citrate staining). Micrographs taken on a JEOL 100S transmission electron microscope were scanned at high resolution (Epson 4870 scanner) for compilation of digital plates.

Results

Comparison of approximately 9-week old *XND1* T-DNA knockout and wild-type plants showed that xylem differentiation had proceeded similarly in both cases, including deposition of patterned secondary walls followed by autolysis of mature cells at the electron microscopy level (Fig. 1) even though T-DNA knockout plants had shorter internodes morphologically compared to control plants.

Comparison in the light microscope of the central stele in cross-sections of dwarfed XND1 over-expressors vs. wild-type-like, herbicide-sensitive, plants growing in the same pots showed that cell number continued to increase within the stele despite the extreme dwarfing (Fig. 2). In the central zone of control plants, there were xylem cells, including protoxylem and larger metaxylem elements, with visible secondary wall thickenings (Fig. 2 a). In contrast, the center of the stele of XND1 over-expressors was occupied with

protoxylem-sized cells with larger diameter than most of the surrounding regular parenchyma cells, but lacking apparent secondary wall thickening (Fig. 2 b). Like the control plants, the XND1 over-expressors had two visible phloem poles, but the width of each phloem pole appeared greater. These finding were confirmed by staining nearby sections from the same plants with Tinopal LPW. In XND1 over-expressors, an abnormally large zone of cells with bright walls occupied both phloem poles, but, unlike the control (Fig. 2 c), cells in the xylem zone had walls with width and fluorescence approximately like the surrounding parenchyma (Fig 2 d). Other differences in XND1 over-expressors compared to controls were more frequent and less oriented patterns of cell division with the stele, particularly surrounding the aberrant phloem zone, and unusual cellular inclusions that were most frequently seen in the cortex. Transmission electron micrographs showed these cellular inclusions to be small (about 0.25 – 0.33 x the size of normal chloroplasts), poorly developed, and contorted plastids highly filled with (putative) starch (data not shown).

Electron microscopy showed that the central cells in XND1 over-expressors had only thin, unpatterned, cell walls (Fig. 3 and 4). They also retained cytoplasmic contents (Fig. 3 b) in contrast to normally autolysed TEs found in wild-type-like plants. In the absence of normal xylem differentiation, electron micrographs confirmed that phloem-like cells had proliferated in XND1 over-expressors (Fig. 3 d). The images were also consistent with the continuation of frequent cell division in the aberrant phloem up until the time of plant harvest, as judged by separation of large cells with thin dividing walls. More cell walls in the older part of the extended phloem zone were extremely thick with an undulatory appearance that appeared as an exaggeration of morphological aspects sometimes seen in the control phloem (Fig. 4 c and d). A light-staining inner cell wall layer in control phloem was not seen

in XND1 over-expressors. The cortical cells in the XND1 over-expressors had irregularly shaped plastids and more stored starch (Fig. 4 f, arrow) compared to cortical chloroplasts of wild-type-like plants (inset in Fig. 4 e).

Discussion

The extreme dwarfing typical of XND1 over-expressors is likely due to the absence of functional water-conducting xylem. The incipient xylem cells fail to deposit patterned secondary walls, and they do not undergo autolysis, rendering them non-functional for water conduction. Cells in the potential xylem zone enlarge in diameter similarly to protoxylem, but larger cells typical of metaxylem were never seen. Perhaps this reflected negative feed-back from the absence of normal organ growth; in this case, larger diameter metaxylem cells to facilitate more water conduction would not have any advantage. Data from the xylogenic suspension cultures supports the possibility of chemical signals from nearby parenchyma coordinating the protoxylem to metaxylem transition by relaying information on the rate of organ expansion (Roberts et al., 1994). The failure to complete xylem differentiation in the XND1 over-expressors was correlated with increased cell division and a proliferation of phloem-like cells in the same two locations where they normally occur. In general, the polarity of the stele was maintained in the presence of XND1 over-expression, but cell division within and surrounding the phloem poles was over-stimulated. Increased frequency and less controlled orientation of cell division also extended into the pericycle adjacent to the aberrant phloem poles of the XND1 over-expressors, but such changes were not observed in the cortex (Fig 4).

The phloem cells in XND1 over-expressors have highly thickened cell walls that can be at least partly interpreted as an exaggeration and partial disorganization of the phloem

wall structure seen in the control plants. In the XND1 over-expressors, double walls between cells often were about 1 μm thick, whereas in the control such walls rarely reached 0.5 μm thick. Some of the cells with greatly thickened walls were highly cleared of cytoplasmic contents, which would be consistent with completion of the developmental program for sieve elements. However, we cannot know based on these data if they are functioning in this way, or if a few cells within the phloem zone with thinner walls and dense cytoplasmic contents were differentiated companion cells. Some of the latter type may have been recent derivatives of the hyper-division within the aberrant phloem still in the process of depositing thicker walls.

Brighter staining with Tinopal LPW of phloem in XND1 over-expressors is consistent with thicker walls that contained ß-linked polysaccharides, but specific conclusions about wall chemistry are not possible because of the non-specificity of the stain (Hughes and McCully, 1975; Taylor et al., 1992). An aspect of the normal phloem wall structure—the inner light-staining layer (Evert, 1990a)—was not seen in the aberrant phloem. Biphasic walls in primary phloem of dicots typically form, if at all, as cells approach maturity (Evert, 1990a), and this might not occur developmentally in the aberrant phloem if continuing division reflects a perpetual "juvenile" state. Because the epidermal cell walls also look similar to those of aberrant phloem, it can be hypothesized that over-expression of XND1 ectopically stimulates one aspect of phloem wall thickening while at the same time suppressing xylem secondary wall formation. [Note that the thick walls of dicot sieve tubes are typically classified as primary walls (Evert, 1990a), but in the context of more unusual walls, the primary/secondary wall classification has little meaning.] However, since all cell walls in the XND1 over-expressors were not overly-thickened (for example parenchyma

walls in the cortex remain thin), this effect was only observed in cells destined to deposit thick cell walls.

Notably, the cell walls in the altered phloem are morphologically highly similar, both in thickness and undulatory appearance of darkly staining walls, to those in sieve elements of earlier-evolved land plants, *Equisetum hyemale* (Evert, 1990b) and *Abies alba* (silver fir) (Schulz 1990). It would be interesting in further work to determine if plants more primitive than angiosperms have a higher level of expression of an XND1 ortholog.

Summary

There are three main steps for the formation of TEs and fibers in plants: (1) cambial cell division; (2) cell expansion; and (3) differentiation and secondary wall thickening. It is known that all the steps above are highly regulated. TEM data showed that cell division was established in both XND1 over-expressor and null lines. However, cell expansion in these particular lines was not complete as observed in plant height as well as in the length of TEs and fibers (Beers Lab, unpublished data). As a result xylem differentiation was blocked and no secondary wall was formed. This indicates that XND1 may act as a repressor of differentiation along with cell wall thickening since cell expansion was not properly achieved. XND1 might be a part of transcriptional switch mechanism, which assures proper progression from cell division to cell differentiation in programmed cell death of xylem differentiation.

References

Aida M, Ishida T, Fukaki H, Fujisawa H and Tasaka M (1997) Genes involved in organ separation in Arabidopsis: an analysis of the cup-shaped cotyledon mutant. Plant Cell 9: 841-857.

Evert RF (1990a) Dicotyledons, In: H.-D. Behnke and R.D. Sjolund, eds., *Sieve Elements: Comparative Structure, Induction, and Development*. Springer Verlag: NY, pp. 103-138.

Evert RF (1990b) Seedless vascular plants, In: H.-D. Behnke and R.D. Sjolund, eds., *Sieve Elements: Comparative Structure, Induction, and Development*. Springer Verlag: NY, pp. 35-62.

Hughes J, McCully ME (1975) The use of an optical brightener in the study of plant structure. *Stain Technol* 50: 319-329.

Kubo M, Udagawa M, Nishikubo N, Horiguchi G, Yamaguchi M, Ito J, Mimura T, Fukuda H and Demura T (2005) Transcription switches for protoxylem and metaxylem vessel formation. Genes Dev 19: 1855-1860.

Liu L, White MJ, MacRae TH (1999) Transcription factors and their genes in higher plants functional domains, evolution and regulation. Eur J Biochem 262, 247–257.

Long TA, Benfey PN (2006) Transcription factors and hormones: new insights into plant cell differentiation. Curr Opin Cell Biol 18: 710-714.

Mitsuda N, Seki M, Shinozaki K, Ohme-Takagi M (2005) NAC Transcription Factors, NST1 and NST3, Are Key Regulators of the Formation of Secondary Walls in Woody Tissues of Arabidopsis. Plant Cell 17: 2993-3006.

Mitsuda N, Iwase A, Yamamoto H, Yoshida M, Seki M, Shinozaki K, Ohme-Takagi M (2007) NAC Transcription Factors, NST1 and NST3, Are Key Regulators of the Formation of Secondary Walls in Woody Tissues of Arabidopsis. Plant Cell 19: 270-80.

Olsen AN, Ernst HA, Leggio LL, Skriver K (2005) NAC transcription factors: structurally distinct, functionally diverse. Trends Plant Sci 10: 79-87.

Ooka H, Satoh K, Doi K, Nagata T, Otomo Y, Murakami K, Matsubara K, Osato N, Kawai J, Carninci P, Hayashizaki Y, Suzuki K, Kojima K, Takahara Y, Yamamoto K, Kikuchi S (2003) Comprehensive analysis of NAC family genes in Oryza sativa and Arabidopsis thaliana. DNA Res 10: 239–247.

Reynolds ES (1963) The use of lead citrate at high pH as an electron-opaque stain in electron microscopy. J Cell Biol.17: 208.

Riechmann JL, Heard J, Martin G, Reuber L, Jiang C, Keddie J, Adam L, Pineda O, Ratcliffe OJ, Samaha RR, Creelman R, Pilgrim M, Broun P, Zhang JZ, Ghandehari D, Sherman BK, Yu G (2000) Arabidopsis transcription factors: genome-wide comparative analysis among eukaryotes. Science 290: 2105-2110.

Roberts AW, and Haigler CH (1994) Cell expansion and tracheary element differentiation are regulated by extracellular pH in mesophyll cultures of zinnia elegans L. Plant Physiol 105: 699-706.

Salnikov V, Grimson MJ, Seagull RW and Haigler CH (2003) Localization of sucrose synthase and callose in freeze substituted, secondary wall stage, cotton fibers. *Protoplasma* 221: 175-184.

Schulz A (1990) Conifers. In: HD Behnke and RD Sjolund, eds., *Sieve Elements: Comparative Structure, Induction, and Development*. Springer Verlag: NY, pp. 63-88.

Schwechheimer C, Zourelidou M, Bevan MW (1998) Plant transcription factor studies. Annu Rev Plant Physiol Plant Mol Biol 49:127-150.

Taylor JG, Haigler CH, Kilburn DG, Blanton RL (1992) Detection of cellulose with improved specificity using laser-based instruments. *Biotechnic and Histochemistry* 71: 215 – 223.

Zhao C, Craig JC, Petzold HE, Dickerman AW, Beers EP (2005) The xylem and phloem transcriptomes from secondary tissues of the Arabidopsis root-hypocotyl. Plant Physiol 138: 803-818.

Zhao C, Avci U, Grant EH, Haigler CH, Beers EP. XND1, a member of the NAC domain family in Arabidopsis thaliana, negatively regulates lignocellulose synthesis and programmed cell death in xylem. In preparation for publication.

Zhong R, Richardson EA, Ye ZH (2007) Two NAC domain transcription factors, SND1 and NST1, function redundantly in regulation of secondary wall synthesis in fibers of Arabidopsis. Planta early pub.

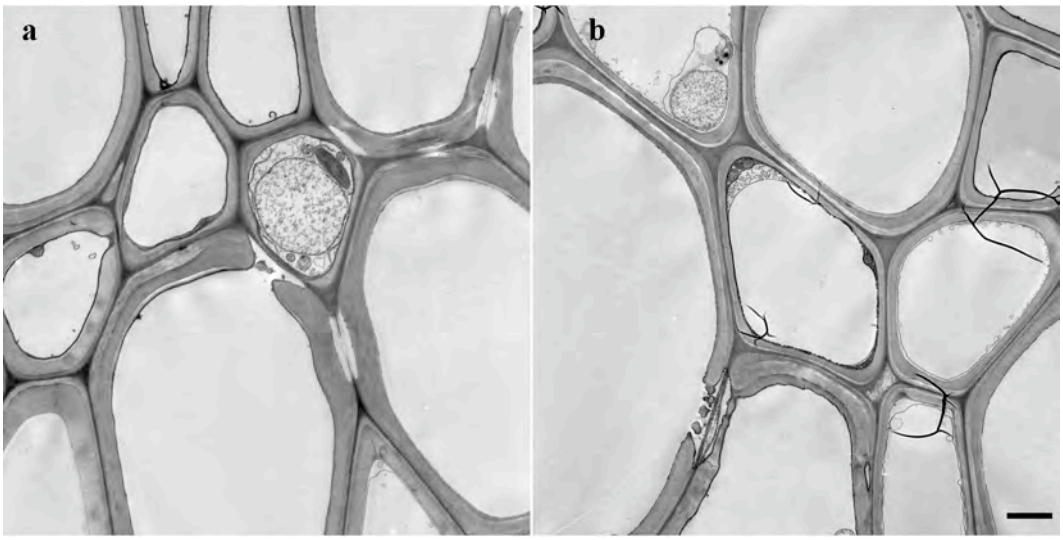

Figure 1 Transmission electron micrographs of cross-sections within the xylem zone of the first stem internode of WT (a) and the shorter plants of GT_5_12667, the *Ds* null line for *XND1* (b). Xylem differentiation had proceeded similarly in both cases, including deposition of patterned secondary walls followed by autolysis of mature cells. The bar in (b) for both micrographs equals 1 μm.

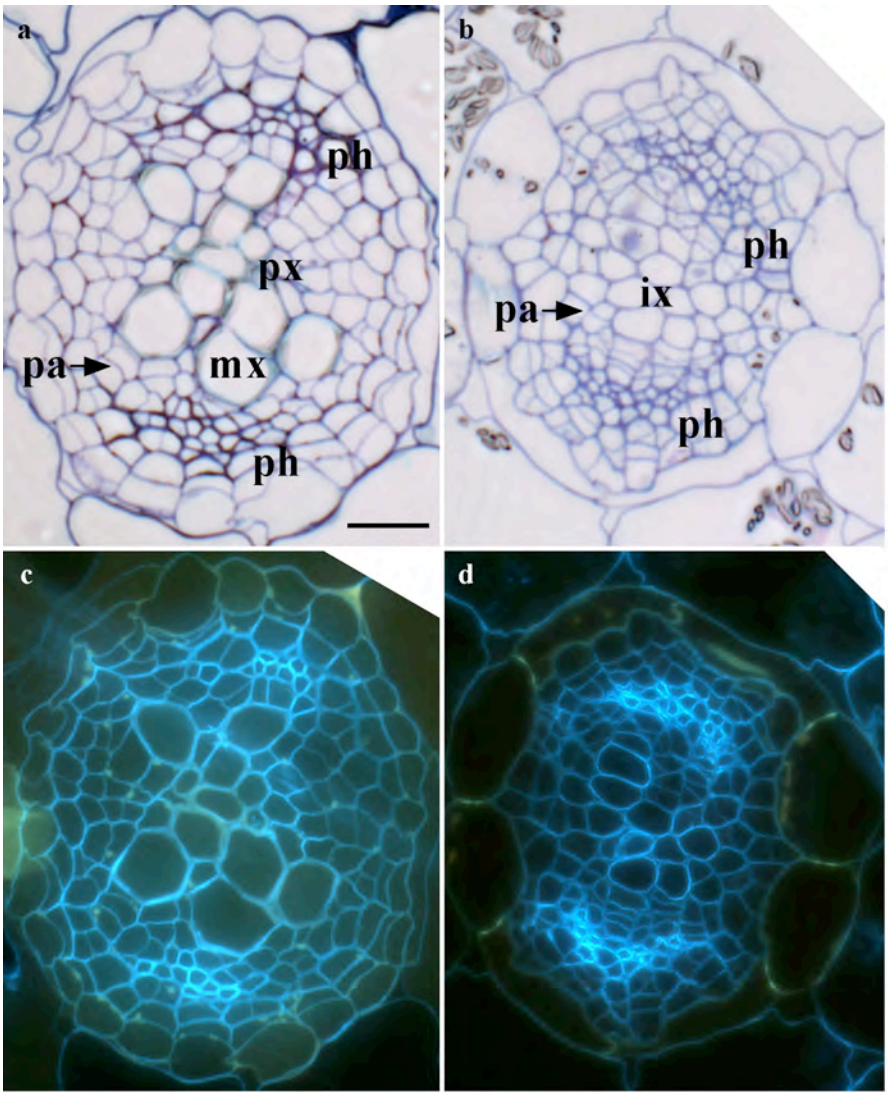

Figure 2: Light micrographs of hypocotyl cross-sections from 24 day old plants of wild type controls (a, c) and dwarf XND1 over-expressors (b, d) viewed with brightfield optics after Toluidine Blue staining (a, b) or fluorescence optics after Tinopal LPW staining (c, d). In the brightfield micrographs, labels indicate: pa, parenchyma cells; ph, the right edge of two phloem poles of each stele; px, protoxylem in the center of the normal stele; mx, larger mextaxylem cells in the normal stele; and ix, the approximate center of the incipient xylem zone of dwarf XND1 over-expressors. The bar in (a) for all micrographs equals 20 μm.

Figure 3: Transmission electron micrographs of the hypocotyl stele of a representative wild-type-like plant (a, c) and a XND1 over-expressor (b, d). For both xylem (a, b) and phloem (c, d) image pairs, equivalent regions of the stele are shown in the same orientation. Cells in the xylem zone of the XND1 over-expressor (b) had diameters similar to normal protoxylem, but they lacked secondary wall thickenings and had not autolyzed. Cell enlargement equivalent to metaxylem cells in the wild-type plants (upper cell in a) did not occur in the XND1 overexpressor (b). Within the phloem pole of the XND1 over-expressor (d), cells had proliferated and deposited abnormally thick cell walls compared to the wild-type-like plants (c). The walls shown in (c and d) are among the thickest seen in both genotypes. Unlike the control micrograph (upper left corner of c), a prospective xylem cell is not visible in the XND1 over-expressor (d) because of the increased number of dividing cells between the phloem and xylem zones. The bar in (d) for all micrographs equals 1 μm.

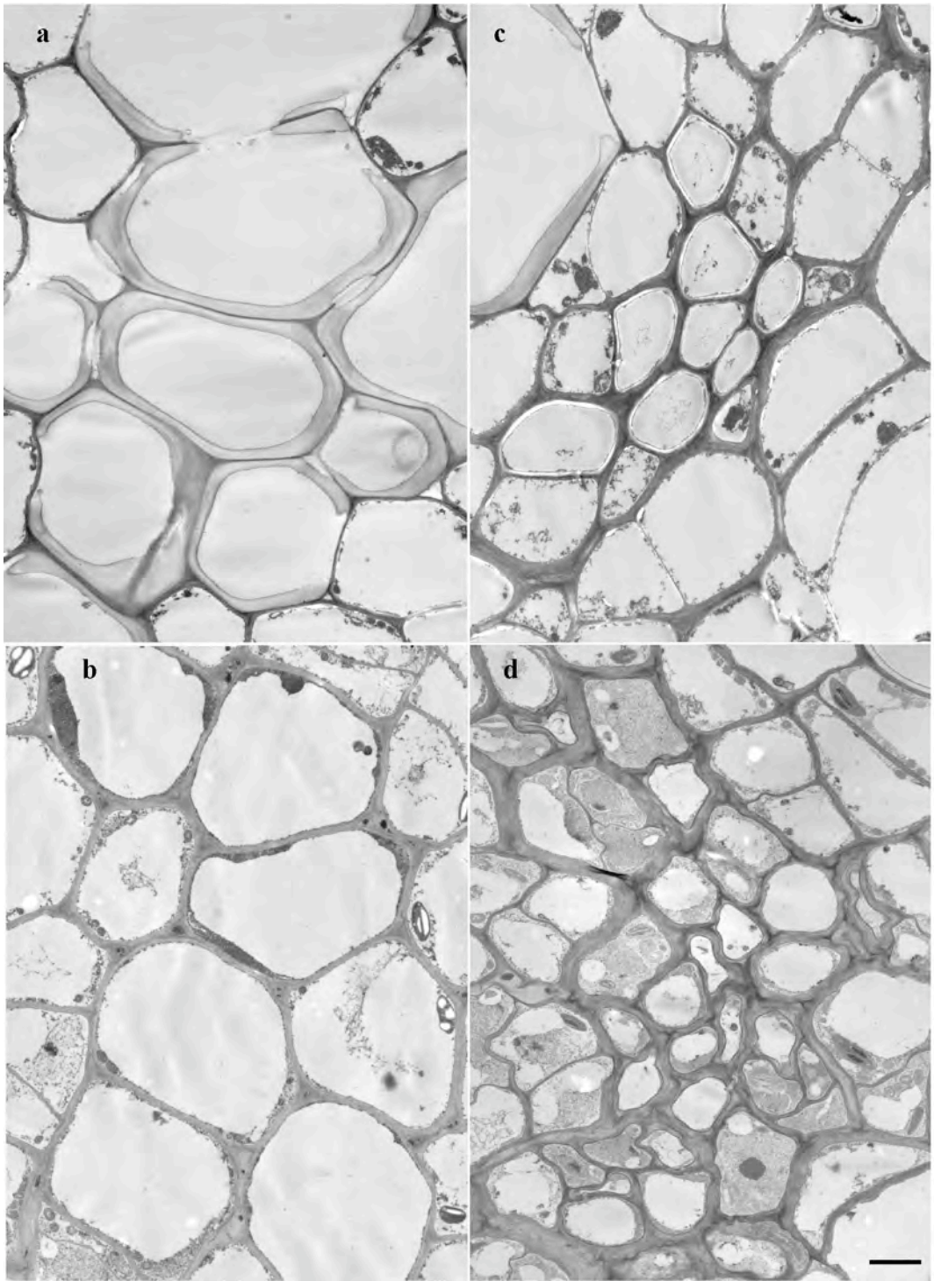
a
c
b
d

Figure 4: Transmission electron micrographs comparing the structure of xylem (a, b), phloem (c, d), and cortical (e, f) cells of wild-type-like plants (a, c, e) and a XND1 over-expressors (b, d, f). In contrast to dead xylem cells with thick, patterned, secondary walls in wild-type-like plants (a), cells in the xylem zone of XND1 over-expressors (b) had only thin cell walls and retained their cytoplasmic contents. Amyloplasts in the xylem zone were uniquely found in XND1 over-expressors (b, arrow). In the phloem (d) of XND1 over-expressors, many cell walls were thicker and more irregularly organized than in wild-type-like plants (c). Cortical cell walls appeared similar in both types of plants (e, f), except that dark-staining material at cell junctures bordering lacunae did not appear well-integrated into the overall wall structure in the XND1 over-expressor (f). The cortical cells in the XND1 over-expressors had irregularly shaped plastids with less interior membranes and more stored starch (arrow indicates one of six such organelles in (f) compared to cortical chloroplasts of wild-type-like plants (inset in e). All bars equal 0.5 μm and also apply to the images paired with (a, c, e).

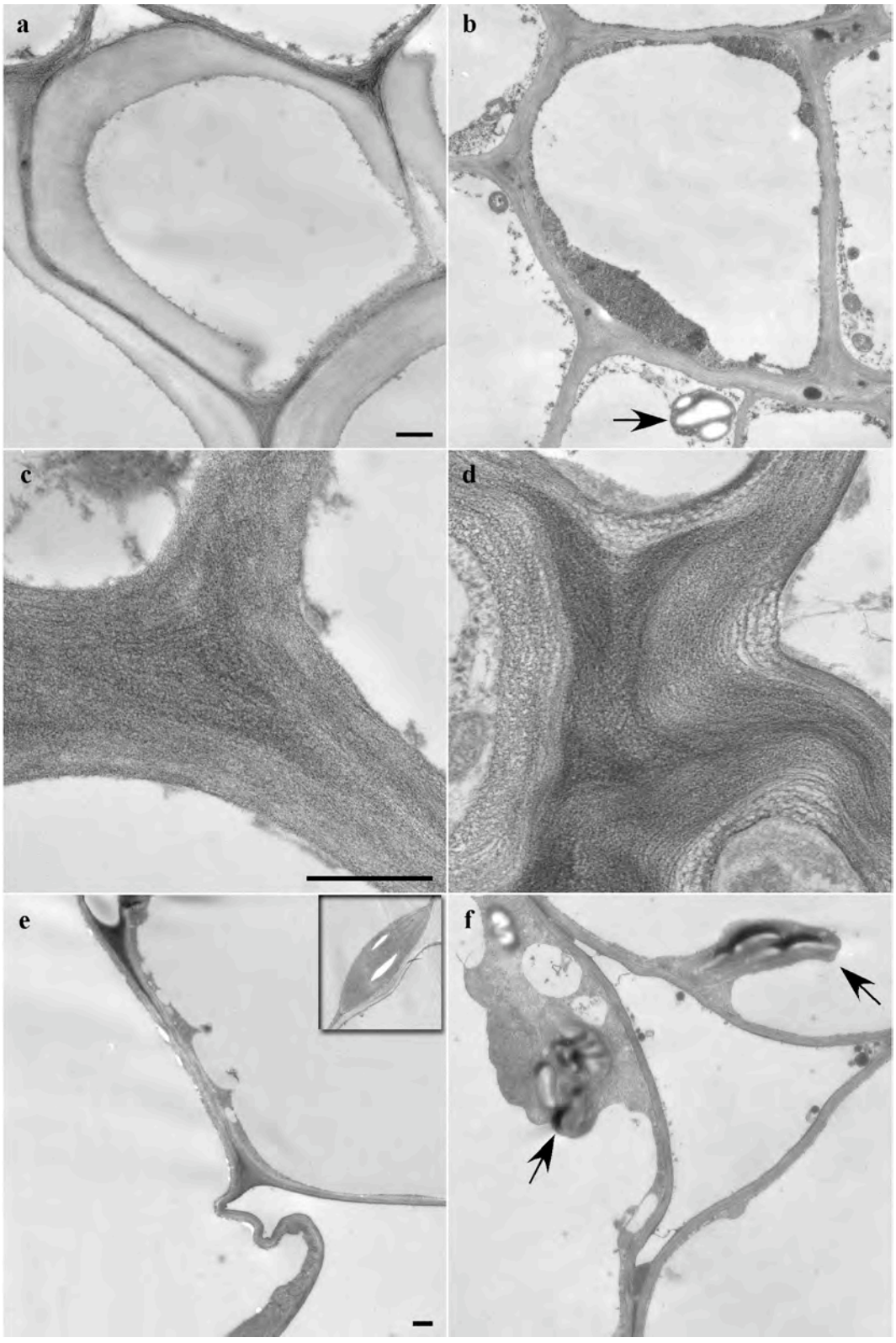
a
b
c
d
e
f

CHAPTER 5

Microscopic observations on effects of ectopic expression of a native cellulose synthase gene in transgenic poplar

Introduction

Cellulose synthase genes

Secondary xylem or wood accounts for most of the biomass in trees, 42% to 50% of which is cellulose. Other main components are hemicellulose (25-30%) and lignin (20-25%) (Suzuki et al., 2006). This biomass is one of the major carbon sink on Earth, which provides renewable material that can be used for manufacturing or as an energy source. The latter, in the context of conversion to biofuels, has received increased attention recently, with cellulose being the most abundant and valuable material for conversion processes. Therefore, understanding the biosynthesis of cellulose along with the other cell wall components is very important.

Cellulose synthase (CesA) genes are presumed to encode catalytic subunits of cellulose synthase, which is part of the enzyme complex that is responsible for the synthesis of cellulose. Freeze fracture electron microscopy of plasma membranes allowed visualization of cellulose synthases within rosettes of six intramembrane protein aggregates (Kimura et al., 1999). Each subunit synthesizes β-1,4-glucan chains, which then crystallize to form cellulose microfibrils. These microfibrils provide the main strengthening components of plant cell walls to help maintain turgor pressure and control the extension direction of a plant cell (Somerville, 2006).

The first plant CesA gene was identified in cotton (*Gossypium hirsutum*) fiber by shape similarity to a bacterial gene with low sequence similarity, and CesA proteins were predicted to be membrane-bounded proteins (Pear et al., 1996). Availability of a genomic database and mutant collections in Arabidopsis allowed further genetic identification and characterization of CesA genes (Arioli et al., 1998; Somerville et al., 2004). Arabidopsis has

10 CesA genes (Richmond, 2000), some of which are required for primary wall cellulose synthesis (AtCesA1, AtCesA3 and AtCesA6) and some of which are required for secondary wall (AtCesA4, AtCesA7, AtCesA8) cellulose synthesis (Doblin et al., 2002). Although they are ß-1,4-glucosyl transferases, the precise biochemical functions and activity of CesA genes in what may be a multi-step cellulose synthetic process still remain to be identified (Doblin et al., 2002).

Cellulose synthase genes from poplar

The genus of *Populus* is known as poplar and includes aspen and cottonwood. Completion of its genome sequence has made poplar a preferred model system to compare genes between organisms and to better understand wood formation in trees. Eighteen CesA genes were identified in the black cottonwood (*Populus trichocarpa)* genome (Djerbi et al., 2005; Suzuki et al., 2006). Studies on these CesA genes from tree species are also limited (Wu et al., 2000; Samuga and Joshi, 2004; Liang and Joshi, 2004), and there is a need to know which CesA genes control wood formation and whether genetic manipulation of them could change wood characteristics.

Providing another important characteristic of angiosperm trees to support dissection of cellulose biosynthesis, a special wood called tension wood is formed as a gravitational response in stems and branches. Tension wood contains fibers with thick cell walls where the cells are enriched in crystalline cellulose while hemicellulose and lignin are deficient compared to normal wood (Andersson-Gunneras et al., 2006). Three aspen CesA genes, of interest to our study, were also coordinately expressed and up-regulated during tension wood production (Bhandari et al., 2006). In addition, recent microarray data showed the expression patterns of CesA genes and proteins involved in cellulose biosynthesis during formation of

tension wood (Andersson-Gunneras et al., 2006). However, there is still limited information available on the mechanisms for this special wood formation.

Over-expression of cellulose synthase genes in aspen

In collaboration with Dr. Chandrashekhar Joshi and his lab (Michigan Technological University), microscopic examinations were conducted on control and transgenic aspen plants; the latter with one of the CesA genes (PtrCesA1) over-expressed.

Seven CesA cDNAs (PtrCesA1 to PtrCesA7) in aspen (*Populus tremuloides*) have been already cloned and sequenced (Wu et al., 2000; Samuga and Joshi, 2002; Kalluri and Joshi, 2003; Samuga and Joshi, 2004). Among these CesA genes, PtrCesA1, PtrCesA2, and PtrCesA3 showed high degree of similarity (over 85%) with AtCesA8, AtCesA7, and AtCesA4 respectively (Joshi et al., 2004), which are proved to be involved in secondary wall development in Arabidopsis (Doblin et al., 2002). These three CesA genes in Arabidopsis were shown to interact with each other (Taylor et al., 2003). The same result proved to be true for PtrCesAs as well as a result of yeast-two hybrid assays (Xu and Joshi, unpublished). In addition, PtrCesA1, 2, and 3 were also coordinately up-regulated in the xylem cells during formation of tension wood in aspen (Bhandari et al., 2006). Supporting results led our collaborators to wonder whether or not simultaneous up-regulation of three CesAs is required for increased cellulose production in tree xylem. As a kind of control, transgenic aspen trees were produced with only one xylem CesA, PtrCesA1, over-expressed. The expression level of PtrCesA1 was 0.5-fold lower in secondary xylem due to co-suppression, but, surprisingly, expression of PtrCesA2 and PtrCesA3 increased about 1200-1900 times. Transgenic lines 59 and 52 had 10.46% and 4.98% glucose content in cellulose, respectively (Joshi Lab, unpublished), in contrast to 40 – 50 % in controls. In order to better determine changes on

cell walls and other cellular features in transgenic plants, light and electron microscopic observations were carried out.

Material and Methods

To accomplish this work, I received from Dr. Joshi's Lab the following materials:

- Approximately 4-month old control and transgenic aspen plants from which stem samples (~2 mm diameter) were excised were: (a) wild type (WT); (b) transgenic null lines (nL57) carried in parallel through transformation procedures; and (c) transgenic aspen plants over-expressing PtrCesA1 (tL52, tL59).

Full method descriptions for production of their materials are in preparation for publication (Joshi et al, in preparation).

All samples were cut with a razor blade into 1-2 mm wood specimens. Primary fixation for TEM was in 3% glutaraldehyde/0.05% Ruthenium Red (v/w), 10 mM sodium cacodylate buffer, pH 7.2 (30 min room temperature, then 4°C, 1 h). After buffer rinses (3 x 5 min), secondary fixation occurred in 1% OsO_4/0.05% Ruthenium Red (v/w) in the same buffer (30 min, 4°C), followed by 3 rinses. Dehydration in acetone (30, 50, 70, 90, and 100% (v/v); 15 min each) was followed by infiltration in Spurr's Resin:acetone (1:1; overnight) then 100% resin (6 h). Samples were polymerized in fresh 100% resin within flat embedding molds (60°C; overnight). Alternatively and with equivalent results for light microscopy, samples were fixed in 4% formaldehyde (v/v), 50 mM phosphate buffer, pH 7.2, dehydrated in an EtOH series, and embedded in LR White resin, hard grade.

Sections (2 μm thick) were made with an old diamond knife (to avoid damage to a new one by highly lignified tissue) on an ultramicrotome (MT2-B, Sorvall) and affixed to slides by low temperature heating. For comparisons of birefringence intensity, section

thickness was held constant and an optimal exposure time determined for the wild type sample was held constant along with unchanged optical parameters (BH2 polarizing microscope, Olympus). Slides were subsequently stained with 1% (w/v) Toluidine Blue, briefly washed (1 minute), and observed with brightfield optics. Images were recorded digitally (Q-Color 5, Olympus), and processed in Adobe Photoshop, avoiding any digital changes in comparative brightness for micrographs to be compared for birefringence intensity.

For TEM, gold thin sections were collected on Formvar-coated grids, and, in a humid chamber, they were: (a) stained with uranyl acetate (for LR White resin, 2% w/v, aq. or for Spurr's resin, 2% w/v, saturated, in 70% EtOH, both 15 min); (b) washed by 10 dips in 3 changes of H_20 then dried by wicking; (c) stained with Reynold's lead citrate (Reynolds 1963), pH 12 with two NaOH pellets as CO_2 traps in the chamber, 4 min for LR White resin and 15 min for Spurr's resin); and (d) washed and dried as above. Micrographs were recorded on film in a TEM (JEOL 100S) and the negatives were scanned and processed in Adobe Photoshop and Canvas 9 for preparation of the image plates.

At least 3 repetitions of all samples were made. Results were similar. Figures shown in this chapter represent one repetition.

Results and Discussion

For all observations, the wild-type and the null transgenic line were equivalent. All micrographs were taken near the middle of the ring of secondary xylem and in a location that was verified as typical for the sample.

Figure 1 shows that co-suppression of PtrCesA1 was associated with tendency of cells to collapse (more intensely in line 52), which in turn induces distortions in the overall

tissue of the secondary xylem compared to null line (Fig. 1 a-f). This cellular collapse was due to lack of cell wall strength arising from the deficiency in ordered secondary wall cellulose in fibers and vessel elements in secondary xylem.

Polarization microscopy was used to compare lines by their cell wall birefringence, which typically arises from ordered crystalline cellulose. Ability to compare the intensity of the birefringence signals was ensured by: (a) rotating the stage to orient cellular structure equivalently relative to the polarized light axis; (b) taking micrographs of the mutant under identical optical conditions and exposure time as used for the null line; and (c) identical image processing of the digital images of each sample. As shown in Figure 1, co-supppression of PtrCesA1 caused a deficiency in ordered secondary wall cellulose in fibers and vessel elements in secondary xylem (Fig. 1 g, h and i). In the most-altered transgenic plants (Line 52, Fig. 1 i), birefringence in the bulk of the secondary xylem was greatly reduced, which indicates a very low level or no highly oriented crystalline cellulose in the cell walls. The birefringence defining the edges of rays, which likely arises normally from adjacent secondary cell walls, was also absent, and the rays are more crooked than normal. Line 52 exhibited frequent bright birefringent spots associated with contorted cell walls (Fig. 1 i). These spots were more numerous than in line 59. The birefringent spots might be cellulose or another anisotropic wall component.

Notably, the walls in the secondary xylem region were substantially thickened compared to those in the pith or inner cortex of either null or CesA transgenic lines. This suggests that more extensive cell wall synthesis than is typical of parenchyma cells occurred in the altered secondary xylem region. There was no apparent difference in the thickness of cell walls of all lines. This result might be due to the fact that less cellulose was compensated

by other cell wall components such as lignin and xylan. The walls in the secondary xylem region lacking normal secondary wall cellulose were susceptible to compression and shape distortion. It is possible that cutting disks of branches with a razor blade before fixation induced collapse of weak cell walls. An “irregular xylem” phenotype, which was similar to that observed in the primary xylem of Arabidopsis when secondary-wall-expressed CesA genes are mutated (Turner and Somerville, 1997), was also observed in transgenic line 52, but to a much lesser extent in line 59 (Fig. 1 e).

As shown in Figure 1, the reduction in cellulose content was dependent on foreign gene dosage, with transgenic line 59 with the fewest number of foreign gene copies (Joshi and coworkers, unpublished) showing a less severe phenotype than transgenic lines 52. The birefringence in the secondary xylem in this line was faint compared to the wild-type, but cell shape in the primary and secondary xylem were nearly normal with only occasional distortion. The extra 5% cellulose in Line 59 compared to Line 52 is correlated with more ability of xylem cells in Line 59 to remain uncollapsed, which also manifests in straighter rays. Collapse of some vessels is still observed in Line 59. The evidence that even 5% extra cellulose can help to resist cellular collapse provides a morphological illustration of the importance of cellulose to conferring cell wall strength.

In TEM of the transgenics, an inner electron translucent secondary cell wall layer observed in some cells in null Line 57 (Fig. 2 a, arrow) was never observed in the mutant lines. This occurs on some fibers but not others in the null. It is likely that this is a cellulose-rich layer since cellulose (and xylan also) does not pick up electron microscopic stains well, whereas lignin is highly stainable. The middle lamella is disturbed, especially at the cell corners as judged by frequent lack of electron density at that location in the mutant (Fig. 3 c).

Note that in Line 59 with 10.46% cellulose compared to 4.98% cellulose in Line 52, the appearance of the middle lamellae more closely approaches the null (Fig. 3 b and c). Ruthenium Red that was used in the fixation procedure can stain acidic/de-esterified pectin that can be found in the middle lamella, but is a cationic dye that non-specifically enhances contrast of diverse molecules (Gahan, 1984).

Evidence of layering in the secondary cell wall, which is founded on the differential orientation of cellulose microfibrils, is largely missing in the mutants. An uneven inner layer of the secondary wall, along with electron dense bulges, is typical of the mutants and never found in the null (Fig. 3). This could be interpreted as evidence of localized secretion of stainable wall components that cannot become integrated into the wall structure as usual because of the depletion in secondary wall cellulose. The messy appearance of the cell wall staining in the mutants, with more severity in Line 52, is consistent despite the fact that grids of mutant and null were processed in parallel (Fig. 3). Therefore, this is not a staining artefact, and it likely indicates the disorganization of the cell wall components that are picking up the stain in the mutants.

Despite extreme reduction or elimination of secondary wall cellulose synthesis in the secondary xylem, vascular cambium activity and patterning and differential cell enlargement of its derivatives, for example to form ray cells, vessels, or fibers, proceed as usual. In the severely affected transgenic lines, the concentric stem organization of pith, primary xylem, secondary xylem, cambium, phloem, phloem fibers, cortex, and epidermis are not changed. There is differential enlargement between vessels (bigger) and fibers (smaller). The radial organization of rays is not changed. Autolysis of xylem cells continues. Phloem fibers are filled similarly to the null line. The preservation of tissue patterning and cell enlargement is

consistent with the dependence of these processes on primary wall formation via primary wall-specific CesAs not including PtrCesA1.

Interestingly, co-suppression of PtrCesA1 does not prevent all deposition of oriented secondary wall cellulose in vascular cells. The first-formed large vessel elements typical of secondary xylem and the first-formed fibers showed detectable birefringence and normal cell shape (Fig. 1 c, vessels close to pith, center region), indicating that they contain some ordered cellulose. This observation was repeatable. Later-formed vessels and fibers showed more severe effects of co-suppression as can be seen in all TEM images. In the controls, these vessels have more highly patterned secondary walls than those appearing in later-formed secondary xylem, but the extent of patterned wall deposition in the transgenics appeared to be reduced. The fact that first-formed vessels and fibers were not affected as severely as the ones later formed might be due to developmental control or switch mechanisms and should be studied in more detail in the future.

References

Andersson-Gunneras S, Mellerowicz EJ, Love J, Segerman B, Ohmiya Y, Coutinho PM, Nilsson P, Henrissat B, Moritz T, Sundberg B (2006) Biosynthesis of cellulose-enriched tension wood in Populus: global analysis of transcripts and metabolites identifies biochemical and developmental regulators in secondary wall biosynthesis. Plant J 45: 144-165.

Arioli T, Peng LC, Betzner AS, Burn J, Wittke W, Herth W, Camilleri CH, Plazinski J, Birch R, Cork A, Glover J, Redmond J and Williamson RE (1998) Molecular analysis of cellulose biosynthesis in Arabidopsis. Science 279: 717–720.

Bhandari S, Fujino T, Thammanagowda S, Zhang D, Xu F, Joshi CP (2006) Xylem-specific and tension stress-responsive coexpression of KORRIGAN endoglucanase and three secondary wall-associated cellulose synthase genes in aspen trees. Planta 224: 828-37.

Djerbi S, Lindskog M, Arvestad L, Sterky F, Teeri TT (2005) The genome sequence of black cottonwood (Populus trichocarpa) reveals 18 conserved cellulose synthase (CesA) genes. Planta 45: 144-165.

Doblin MS, Kurek I, Jacob-Wilk D, Delmer DP (2002) Cellulose biosynthesis in plants: from genes to rosettes. Plant Cell Physiol 43: 1407-20.

Gahan PB (1984) Plant Histochemistry and Cytochemistry: An Introduction. Academic Press: New York, 301 pp.

Joshi CP, Bhandari S, Ranjan P, Kalluri UC, Liang X, Fujino T, Samuga A (2004) Genomics of cellulose biosynthesis in poplars. New Phytol 164: 53-61.

Joshi and coworkers, Avci U and Haigler CH. Cellulose-deficient Wood: Ectopic expression of a native cellulose synthase gene in transgenic poplar trees results in perturbation of cellulose synthesis during wood formation. In preparation for publication:

Kalluri U and Joshi CP (2003) Isolation and Characterization of a New, Full-Length Cellulose Synthase cDNA from Developing Xylem of Aspen Trees. Journal of Experimental Botany 54: 2187-2188.

Kimura S, Laosinchai W, Itoh T, Cui XJ, Linder CR, Brown RM (1999) Immunogold labeling of rosette terminal cellulose-synthesizing complexes in the vascular plant *Vigna angularis*. Plant Cell 11: 2075-2085.

Liang X and Joshi CP (2004) Molecular cloning of ten distinct hypervariable regions from cellulose synthase gene superfamily in aspen trees. Tree Physiology 24: 543-550.

Pear JR, Kawagoe Y, Schreckengost WE, Delmer DP, Stalker DM (1996) Higher plants contain homologs of the bacterial celA genes encoding the catalytic subunit of cellulose synthase. Proc Natl Acad Sci USA 93: 12637–12642.

Reynolds ES (1963) The use of lead citrate at high pH as an electron-opaque stain in electron microscopy. J Cell Biol17: 208-212.

Richmond T (2000) Higher plant cellulose synthases. Genome Biol 4: 30011-30016.

Samuga A and Joshi CP (2002) A new cellulose synthase gene (PtrCesA2) from aspen xylem is orthologous to Arabidopsis AtCesA7 (irx3) gene associated with secondary cell wall synthesis. Gene 296: 37-44.

Samuga A and Joshi CP (2004) Expression patterns of two primary cell wall-related cellulose synthase cDNAs, PtrCesA6 and PtrCesA7 from aspen. Gene 334: 73-82.

Somerville C, Bauer S, Brininstool G, Facette M, Hamann T, Milne J, Osborne E, Paredez A, Persson S, Raab T, Vorwerk S, Youngs H (2004) Towards a systems approach to understanding plant cell walls. Science 306: 2206-2211.

Somerville CR (2006) Cellulose synthesis in higher plants. Annu Rev Cell Dev Biol 22: 53-78.

Suzuki S, Li L, Sun YH, Chiang VL (2006) The cellulose synthase gene superfamily and biochemical functions of xylem-specific cellulose synthase-like genes in Populus trichocarpa. Plant Physiol 142: 1233-1245.

Taylor NG, Howells RM, Huttly AK, Vickers K, Turner SR (2003) Interactions among three distinct CesA proteins essential for cellulose synthesis. Proc Natl Acad Sci 100: 1450-1455.

Turner SR and Somerville CR (1997) Collapsed xylem phenotype of *Arabidopsis* identifies mutants deficient in cellulose deposition in the secondary cell wall. Plant Cell 9: 689–701.

Wu L, Joshi CP, Chiang VL (2000) A xylem-specific cellulose synthase gene from aspen (*Populus tremuloides*) is responsive to mechanical stress. The Plant Journal 22: 495–502.

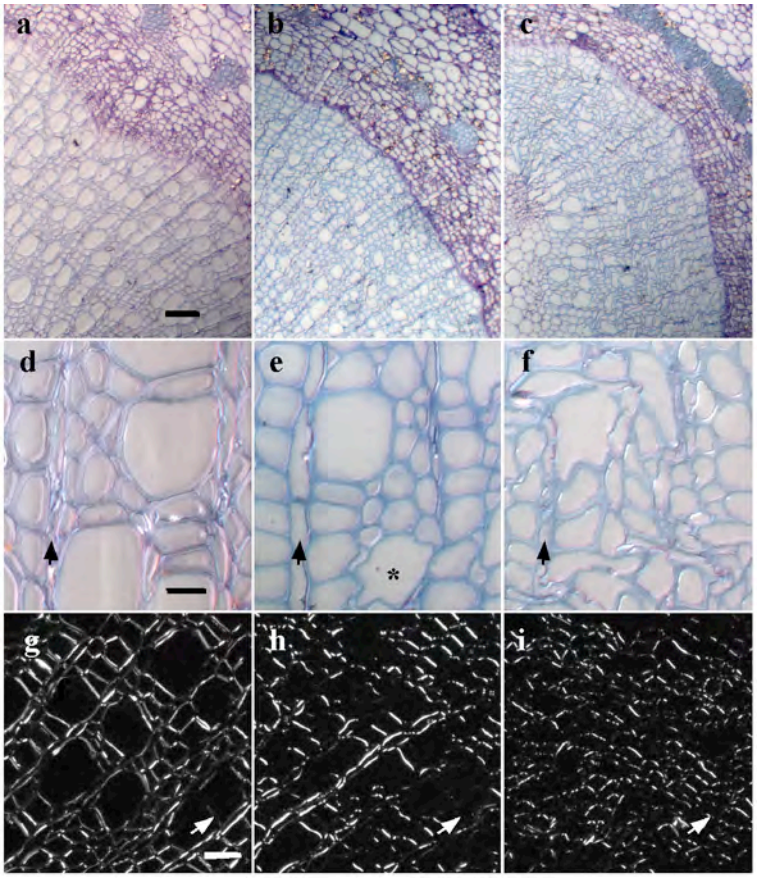

Figure 1: Light micrographs of null Line57 (a, d, g), transgenic Line59 (b, e, h), and transgenic Line 52 (c, f, i) viewed in Toluidine-Blue-stained sections with DIC optics (a, b, c, d, e, f) or in unstained sections with polarization optics (g, h, i). Line 52 (c, f) with the lowest cellulose content had extensively collapsed secondary xylem compared to the null (a, d), whereas Line 59 (b, e) with 5.48% more cellulose than Line 52 showed substantially less cellular collapse even though some vessels still had a distorted shape (e, asterisk). Analysis of birefringence in micrographs taken under identical optical conditions and exposure time confirmed that null Line 57 had the highest ordered cellulose content and cellular rigidity in the secondary xylem (g). In contrast, Line 52 (i) did not show substantial ordered cellulose within typical aligned cell walls; instead it exhibited frequent bright birefringent spots associated with contorted cell walls. Line 59 (h) was intermediate in phenotype with more ordered cellulose detected within linear cell walls and fewer isolated birefringent spots. In (d, e, f) black arrows are superimposed on one ray in the micrograph; in (g, h, i) white arrows indicate the orientation of the ray system relative to the optical axis. Bars: in (a) equals 50 µm for (a, b, c); in (d) 10 µm for (d, e, f); in (g) 20 µm for (g, h, i).

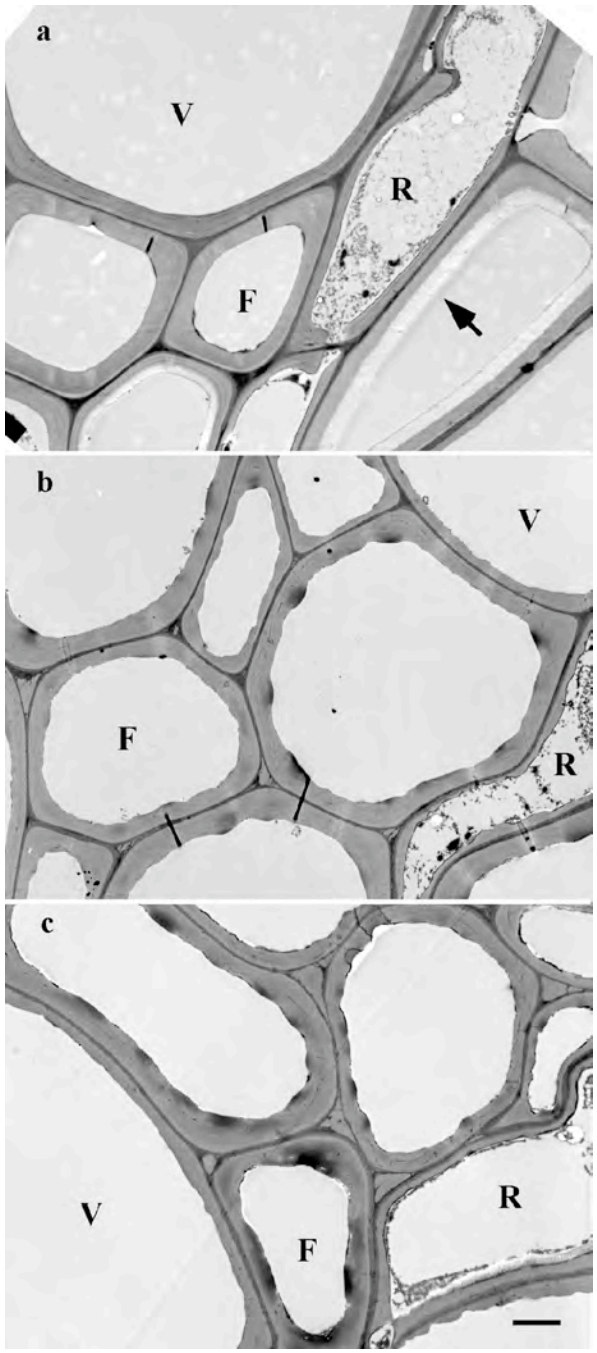

Figure 2: Transmission electron micrographs of null Line57 (a), transgenic Line59 (b), and transgenic Line 52 (c). The smooth cell walls in the null contrast with irregular cell walls in the mutants. An inner electron translucent secondary cell wall layer observed in some cells in null Line 57 (a, arrow) was never observed in the mutant lines. V, highly enlarged vessel element; F, an example of a fiber, of which there are several in each micrograph; R, ray cell with cytoplasmic contents, indicative of its living state before fixation. Bar in (c) equals 2 μm and also applies to (a) and (b).

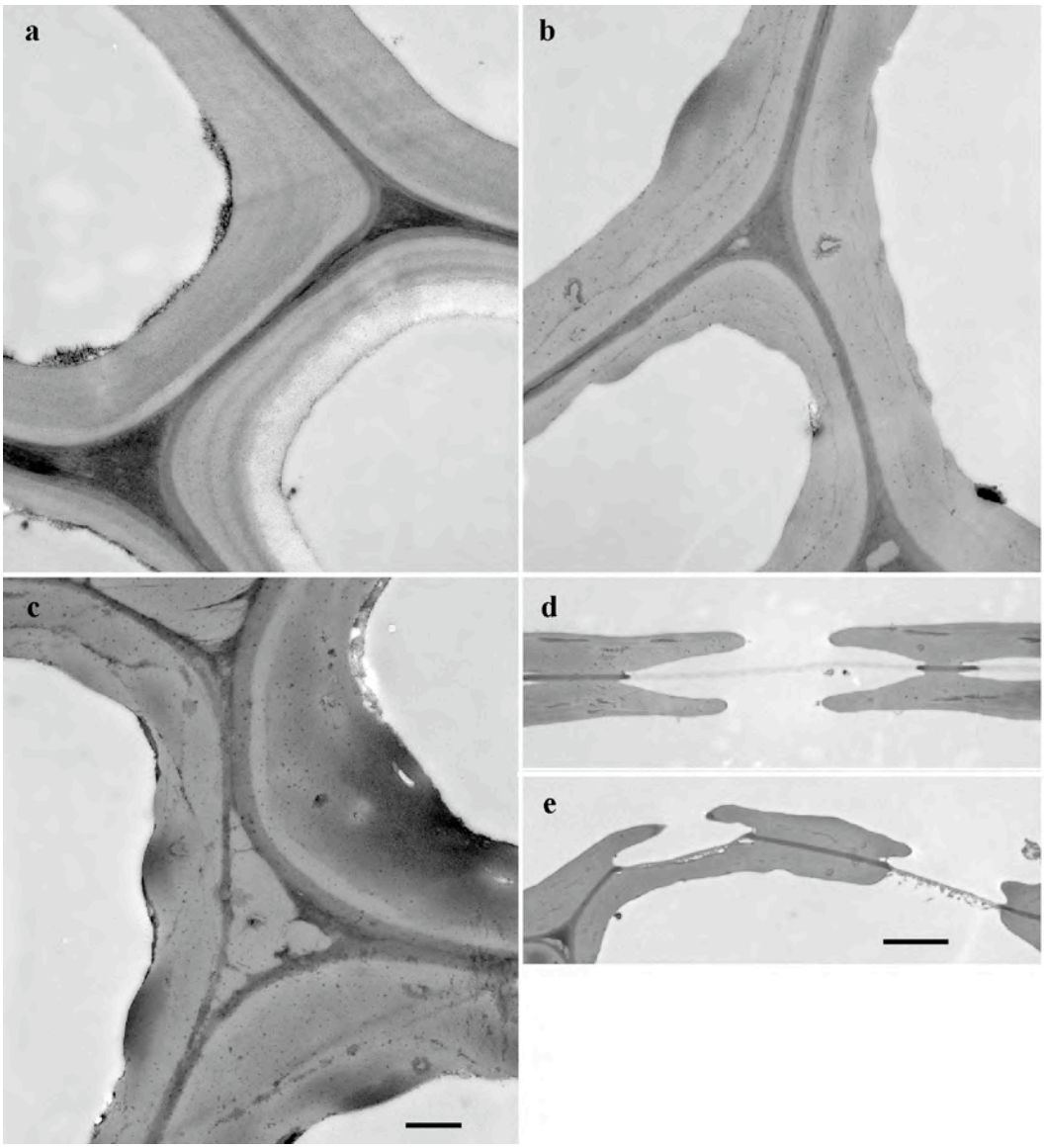

Figure 3: Transmission electron micrographs of null Line57 (a, d), transgenic Line59 (b), and transgenic Line 52 (c, e). Images were processed equivalently, so staining intensity differences are representative of reality observed in the sample. Staining irregularities observed in the bulk of the secondary wall in Line 59 (b) and to a greater extent in Line 52 (c) are typical of the transgenic lines. The cell corners are consistently depleted of electron dense material in transgenic line 52 (c) with the lowest cellulose content. Cell corners are often intermediate in appearance in Line 59 (b), although some that look like those in Line 52 do exist as well (see Fig. 2 b, center of micrograph). Compared to the pits in null line 57 (d), pits in mutant line 52 (d) and 59 (data not shown) were similar, having borders and hydrolyzed pit membranes. Bar in (c) equals 0.5 μm for (a, b, c) and bar in (e) equals 2 μm for (d, e).

CHAPTER 6

New Findings and Future Prospects

New Findings

The research reported in this dissertation proved that microscopy is very crucial and key to many findings. Microscopy could reveal phenotypes that cannot be observed otherwise. This technique should definitely be combined with the other molecular techniques in the genomic era towards identifying roles of genes, eventually the roles of proteins.

With the use of microwave-assisted methods, a newly-emerged tissue processing technique for microscopy, good ultrastructural and antigenic preservation of Arabidopsis were obtained. Increased diffusion rates of chemicals during brief microwave exposure resulted in quick processing of samples, which can take much longer in the conventional methods for electron microscopy. Therefore, several sequential tests could be tried in a short time in order to find the optimum results.

Localization and knockout studies of cysteine proteases in differentiating TEs of *Arabidopsis thaliana* revealed the real phenotype, which could be observed only at the electron microscopic level. Analysis of TE autolysis *in planta* at the electron microscopic level provided evidence that two cysteine proteases participate in autolysis by a somewhat different mechanism than previously hypothesized. In addition, a new final stage that was not previously reported to our knowledge during TE differentiation was revealed. The failure to complete xylem differentiation in XND1 over-expressor lines created extreme dwarf plants due to the absence of functional water-conducting xylem. No autolysis occurred and secondary cell walls were missing. In contrast to normal xylem, these cells had thin, unpatterned cell walls and retained cytoplasmic contents. Phloem cells had highly thickened cell walls with unknown composition.

Reduced cellulose content (5%) gave rise to collapsed vessels and fibers in transgenic aspen upon over-expression of one of the secondary cell wall specific CesA genes that were regulated simultaneously. Approximately 5% extra cellulose in one of the transgenic lines compared to the most severe line remarkably helped to resist cellular collapse, which was microscopic proof of the importance of cellulose in terms of conferring cell wall strength in plants.

Future Prospects

Microwave-assisted methods should be the choice over conventional methods for processing plant samples for microscopy when cryofixation is not suitable or practible for the purpose. Currently, I am using and optimizing microwave-assisted protocols towards unveiling an interesting developmental mechanism of cotton fibers. I will continue to seek collaborations in which power of this technique can ease and solve tissue related problems. Increased utilization of electron microscopy techniques in the new post-genomic era of identifying protein function and analyzing mutant phenotypes will help reveal key data required to understand gene and protein function in the cellular and developmental context.

Determining the nature of remnants that were seen in the T-DNA knockouts of cysteine proteases will help find characteristics of targets to be degraded in TEs by XCP1 and XCP2. Gene complementation study for knockouts and further microscopic analysis, including separate localization of the two proteins, will also strengthen the data.

Immunolabeling on exaggerated cell walls of phloem cell walls in XND1 over-expressors will help to provide information about the composition of this interesting cell wall. Overly thickened phloem walls may arise as an attempted compensation by the mutant

plants, although it is not sufficient to restore normal growth since the plants remain severely dwarfed.

More studies as in aspen are necessary to identify which genes control the wood formation in trees and what kind of regulation mechanisms are involved since there is very limited knowledge currently. Examination and elucidation of changes on cell wall composition altered by genetic manipulation of CesA genes will provide better understanding of functions of each CesA gene and their relationship. In the light of this information, improvement of cellulose in transgenic plants could be benefited industrially.

Overall, unique observations I made in the light of microscopic techniques added invaluable information and insights the study of our collaborators, which proves that microscopy should always be an indispensable part of phenotypic observations of mutants or transgenic plants to unveil more intriguing results and to give strength the study undertaken.